NATIONAL TECHNICAL UNIVERSITY OF ATHENS
SCHOOL OF NAVAL ARCHITECTURE AND MARINE ENGINEERING
DIVISION OF SHIP DESIGN & MARITIME TRANSPORT

DIPLOMA THESIS

CONCEPTUAL HYBRIDIZATION OF A BULK CARRIER'S POWER PLANT UTILIZING A LITHIUM-ION BATTERY PACK

EFSTRATIOS K. KARAVANIS

SUPERVISOR: ASSOCIATE PROFESSOR NIKOLAOS P. VENTIKOS

ATHENS
FEBRUARY 2020

Acknowledgments

I would like to thank Associate Professor Nikolaos Ventikos for supervising this thesis and for providing his guidance while allowing this research to be my own work. Furthermore, I wish to thank Ph.D. students Dimitrios Drivas and Eirini Stamatopoulou for all the time and energy they dedicated as well as for their useful input. I would also like to acknowledge and thank Assistant Professor Nikolaos Themelis for providing the necessary for this study data, for his advice and suggestions. Finally, I wish to express my gratitude to my family and friends for all the support they provided throughout my studies.

Abstract

In this work, one of the three diesel generators installed on board a 171,000 DWT bulk carrier was replaced with a lithium-ion battery pack. An extended reference on battery technology and characteristics was made and an equivalent circuit model was utilized for the accurate representation of the battery's dynamic behavior. Furthermore, the effects of the battery size and minimum allowable State of Charge (SOC) on the system's performance were investigated, and a rule-based Energy Management System (EMS) was developed for distributing the power between the gensets and the battery pack. The hybridization of the vessel's electricity generation system resulted in a 3.74% fuel consumption and emissions reduction and a 29.69% decrease in the generator sets' operating hours on average. Finally, a feasibility study was conducted, specifying the costs and savings of the proposed hybrid solution throughout the remaining lifetime of the vessel.

Σύνοψη

Στη παρούσα εργασία μια από τις τρεις γεννήτριες ενός bulk carrier μεταφορικής ικανότητας 171,000 DWT αντικαταστάθηκε από μία μπαταρία ιόντων λιθίου. Έγινε μια εκτεταμένη αναφορά στις τεχνολογίες και στα γνωρίσματα των μπαταριών και χρησιμοποιήθηκε ένα μοντέλο ισοδύναμου κυκλώματος για την ακριβή αναπαράσταση της δυναμικής συμπεριφοράς της μπαταρίας. Επιπροσθέτως, ερευνήθηκε η επίδραση του μεγέθους και της ελάχιστης επιτρεπόμενης κατάστασης φόρτισης της μπαταρίας στην συμπεριφορά του συστήματος, και αναπτύχθηκε ένα σύστημα διαχείρισης ενέργειας, το οποίο μέσα από ένα σύνολο κανόνων διανέμει την ενέργεια στις γεννήτριες και τη μπαταρία. Η μετατροπή του συστήματος παραγωγής ηλεκτρικής ενέργειας του πλοίου σε υβριδικό είχε σαν αποτέλεσμα τη μείωση της κατανάλωσης καυσίμου και των εκπομπών κατά 3.74% και του χρόνου λειτουργίας των γεννητριών κατά 29.69% κατά μέσο όρο. Τέλος, πραγματοποιήθηκε μία μελέτη εφικτότητας, μέσω της οποίας προσδιορίστηκαν τα χρήματα που θα δαπανούνταν και θα εξοικονομούνταν στη υπολειπόμενη διάρκεια ζωής του πλοίου, μέσω της προτεινόμενης υβριδικής λύσης.

Table of Contents

List of Tables

List of Figures

List of Abbreviations

AC	Alternating Current
AES	All Electric Ship
CH_4	Methane
CO	Carbon Monoxide
CO_2	Carbon Dioxide
DC	Direct Current
DCS	Data Collection System
DG	Diesel Generator
DM	Distillate Marine
DOD	Depth of Discharge
ECA	Emission Control Areas
EEDI	Energy Efficiency Design Index
EGR	Exhaust Gas Recirculation
EIAPP	Engine International Air Pollution Prevention
EMF	Electromotive Force
EMS	Energy Management System
ESS	Energy Storage System
EV	Electric Vehicle
GHG	Greenhouse Gas
HC	Hydrocarbons
HFO	Heavy Fuel Oil
HPS	Hybrid Power System
IWS	In-water Survey
IMO	International Maritime Organization
LCO	Lithium Cobalt Oxide
LFP	Lithium Iron Phosphate
Li-ion	Lithium-ion
Li-metal	Lithium-metal
Li-S	Lithium-Sulphur
LMO	Lithium Manganese Oxide Spinel
LNG	Liquefied Natural Gas
LTO	Lithium Titanate Oxide
MCR	Maximum Continuous Rating
MDO	Marine Diesel Oil
MGO	Marine Gas Oil
MRV	Monitoring, Reporting, Verification
N_2	Molecular Nitrogen
N_2O	Nitrous Oxide
Na-ion	Sodium-ion
NCA	Lithium Nickel Cobalt Aluminum Oxide
NMC	Lithium Nickel Manganese Cobalt Oxide
NMVOC	Non-methane Volatile Organic Compounds
NO	Nitrogen Monoxide
NO_2	Nitrogen Dioxide
NO_x	Nitrogen Oxides

OPS	Original Power System
OSV	Offshore Supply Vessel
PM	Particulate Matter
PTI/PTO	Power Take-In/Power Take-Out
Ro-Pax	Roll-On/Roll-Off Passenger
RO-RO	Roll-On/Roll-Off
SCR	Selective Catalytic Reduction
SEEMP	Ship Energy Efficiency Management Plan
SFOC	Specific Fuel Oil Consumption
SO_2	Sulphur Dioxide
SO_3	Sulphur Trioxide
SOC	State of Charge
SO_x	Sulphur Oxides
VOC	Volatile Organic Compounds

1 Introduction

In a hybrid power system, the cooperation of various energy sources and storage devices has as an outcome a more efficient supply of the load demand than if the same components were operating separately. Employing more than one energy sources provides the benefit of running each of them closer to their optimum operation region, which results in fuel efficiency and therefore, emissions reduction. Energy storage systems can enable this concept by storing excess energy during periods of light loading and provide it later when a deficit condition occurs. In a vessel, it is quite often for both the main engine and the diesel generators to run in the low-load range, which leads to increased fuel consumption, emissions and maintenance. The utilization of a battery has the potential of significant cost reduction, via the decrease of the required fuel and the operating hours of the diesel engines.

1.1 Objectives

The main goal of the current study is to investigate whether the replacement of a diesel generator with a lithium-ion battery pack would improve the efficiency of a bulk carrier's electricity generation system and to specify the change in fuel consumption, emissions and operating hours of the gensets due to the hybridization of the system. Since the battery's behavior is characterized by dynamic phenomena, their accurate representation via a high fidelity battery model is deemed a necessity and an objective, in order to assure the validity of the research's findings. Moreover, the examination of the impact that the battery size and the minimum permitted SOC has on the overall performance of the system is aimed. For that purpose 42 simulations of the hybrid system were conducted, utilizing actual measurements of the three originally installed generators. The determination of the optimum values of these parameters and the development of a control strategy that manages the operation of the gensets and the battery pack is important as well. Finally, the investigation of whether such a hybridization project would be economically viable is also an objective, in order to have completed a comprehensive study of the proposed hybrid solution.

1.2 Structure

The outline of the current thesis is the following: Initially, a brief reference on the emissions from shipping activity, related IMO regulations and abatement methods is made in Chapter 2. In Chapter 3 the parts of the proposed hybrid system are analyzed, as an extended description of the basic battery characteristics, current and future battery technology and fundamental principles of the marine diesel generators is conducted. In Chapter 4 the case study is presented, which includes the hybrid power system's topology, the determination of the genset that is being replaced, the selection process of the battery module and the battery modeling. In Chapter 5 the developed Energy Management System (EMS) and the rules that govern its operation are presented. In Chapter 6 the results of the hybrid system simulations are exhibited and discussed; seven battery sizes, two minimum allowable SOC values and three voyages are examined. Additionally, a feasibility study is conducted both for the selected module and another one, which has a much longer higher cycle life. Conclusions and recommendations for future research are presented in the last part of this work.

2 Emissions from Maritime Activity

Shipping is the major carrier of world trade, as almost 90% of merchandise is transferred with more than 50,000 vessels that are currently in operation [1], [2]. Engines and boilers utilized on board produce great amounts of emissions, which have detrimental effects on human health and climate change. Marine engines' exhaust gases include several substances, whose effects vary. The most significant ones as well as the methodology for estimating their amount are described in this chapter.

2.1 Emissions types

2.1.1 Carbon Dioxide (CO_2)

A combustion process which utilizes hydrocarbon fuel has as an outcome carbon dioxide formation. Its production depends on the amount of fuel burnt, which in turn, is a function of the engine's power output. CO_2 constitutes more than 5% of a diesel engine's total exhaust gases and 13% of a water-tube boiler, while being colorless, odorless and non-toxic in concentrations below 5%. Furthermore, it constitutes one of the major greenhouse gases, together with methane (CH_4), nitrous oxide (N_2O) and some hydroflorocarbons [3]. This characterization is because these substances act as a greenhouse, as they trap the reflected on earth's surface infrared radiation, resulting in global warming. Shipping doesn't contribute dramatically in the total global anthropogenic CO_2 emissions, as in 2012 only about 2.2% of the total CO2 emissions came from vessels [1]. Nevertheless, these emissions have the potential of growing between 50% and 250% by 2050, as the world trade is growing.

For this reason, the International Maritime Organization (IMO) has set the aim of reducing total annual GHG emissions from international shipping at least by 50% by 2050. To achieve this extremely difficult task, IMO introduced energy-efficiency oriented legislation that all vessels are required to comply with. Requirements adopted as amendments to MARPOL Annex VI in 2011 make mandatory the Energy Efficiency Design Index (EEDI) for newbuildings and the Ship Energy Efficiency Management Plan (SEEMP) for all vessels. Ships need to achieve a minimum required EEDI value, which is expressed in grams of carbon dioxide per ship's capacity-mile and is a function of the ship's type and size. This level is expected to be tightened every five years, to motivate technological advancements [4]. SEEMP is a mechanism that intends to improve the vessel's energy efficiency via the implementation of a management plan. Its objectives are organizing tasks like voyage planning and cleaning of the underwater parts of the hull.

Lastly, since 2018 shipowners are obliged by EU's MRV (Monitoring, Reporting, Verification) regulation to monitor and report the total CO_2 that their vessels emit annually. In 2019 IMO's DCS (Data Collection System) came online, making mandatory the reporting of data, including the total distance traveled and the amount of fuel burnt.

2.1.2 Nitrogen Oxides (NO_x)

An internal combustion engine in order to operate requires oxygen, which is found in the ambient air. The main component of air is nitrogen, the largest percentage of which doesn't react during the combustion process. However, a very small portion of it oxidizes and forms nitrogen oxides. This term is used to describe two compounds; nitrogen monoxide (NO) and nitrogen dioxide (NO_2). The formation of NO is strongly influenced by the combustion chamber's conditions, as higher temperatures result in increased production of nitric oxide [5]. NO is a colorless gas, which oxidizes to NO_2 both during combustion and after is been emitted in the air, while NO_2 is brown and more toxic. NO_x can also be formed due to the oxidation of organic nitrogen found in the fuel. Nitrogen oxides have significant effects on human health and vegetation, while NO_2, in particular, contributes greatly to acid deposition.

The maximum permitted NO_x emissions from a marine engine are described in MARPOL Annex VI, where three levels or tiers are introduced, Tier I, II and III, based on the ship's construction date. Engine's rated speed is also a parameter, as the higher the speed the stricter the regulation's limit, Table 2.1. It should be noted that Tier III applies only to vessels while operating in Emission Control Areas (ECA), where more stringent controls on sulphur and nitrogen oxides are in place. After surveying and confirmation of compliance with the regulations the Engine International Air Pollution Prevention (EIAPP) Certificate is issued [6].

Table 2.1: The maximum permitted NOx emissions from a marine diesel engine (source: IMO)

Tier	Ship construction date on or after	Total weighted cycle emission limit (g/kWh) n = engine's rated speed (rpm)		
		n < 130	n = 130 - 1999	n ≥ 2000
I	1 January 2000	17.0	$45 \cdot n^{(-0.2)}$ e.g., 720 rpm – 12.1	9.8
II	1 January 2011	14.4	$44 \cdot n^{(-0.23)}$ e.g., 720 rpm – 9.7	7.7
III	1 January 2016	3.4	$9 \cdot n^{(-0.2)}$ e.g., 720 rpm – 2.4	2.0

Measures that decrease the total amount of nitrogen oxides include dry low NO_x technologies, like late fuel injection timing, 2-stage turbocharging and variable valve timing, and wet low NO_x technologies, which aim at lowering the peak combustion temperature through the introduction of water [3].

Moreover, Selective Catalytic Reduction (SCR) systems diminish nitrogen oxide emission via catalyst elements and a reducing agent. A urea water solution is added to the exhaust gas stream, resulting in the transformation of NO_x into molecular nitrogen (N_2) and water [7]. Through this technique up to 90% NO_x reduction can be achieved.

Finally, in the Exhaust Gas Recirculation (EGR) systems a portion of the exhaust gases are mixed with the scavenge air. As a result, lower combustion temperatures are achieved due to high specific heat of CO_2 and H_2O, with the potential of decreasing NO_x emissions up to 70%.

2.1.3 Sulphur Oxides (SO_x)

Sulphur dioxide (SO_2) and, in smaller portions, sulphur trioxide (SO_3) are the result of the oxidization of sulphur, which is found in large amounts in marine fuels. Similar to NO_x, sulphur dioxide emissions have detrimental effects on human respiration, vegetation and cause acid rain. Shipping produces 10% of the global anthropogenic SO_2 emissions.

Since the amount of sulphur oxides formed is related to the composition of the fuel burnt, IMO has imposed upper limits in the sulphur content. The MARPOL Annex VI legislation set this limit to 3.5% in 2012 and on January 1st, 2020 it was further reduced to 0.5%. Inside ECAs, the applied limits are even tighter, as since 2016 the higher allowable sulphur content is 0.1%. This regulation leads to the utilization of fuels with low sulphur content, like Marine Gas Oil (MGO), Very Low Sulphur Fuel Oil (VLSFO) and Ultra Low Sulphur Fuel Oil (ULSFO) or the employment of a scrubber is required. Scrubber systems are used to clean exhaust gases and they are capable of removing up to 90% of SO_2 [3]. Their operation principle is that SO_x react with water that is sprayed into the exhaust gases and sulphuric acid is formed. Three types of scrubbers are available; open loop, closed loop and hybrid.

2.1.4 Carbon Monoxide (CO)

Incomplete combustion in diesel engines has as a consequence carbon monoxide production, the amount of which is determined by parameters like the combustion chamber's temperature and the uniformity of the air/fuel mixture. Moreover, low load operation and poor maintenance are typical causes of extended CO emissions. Carbon monoxide has a relatively small effect on climate change, although, prolonged exposure to this gas can lead to respiratory failure and death.

2.1.5 Hydrocarbons (HC)

Hydrocarbon emissions are also the outcome of incomplete combustion, thus their amount depends on the load and the general condition of the engine. Their composition consists of unburnt fuel and various organic compounds. Their effects range from eye irritation to carcinogenicity, while Volatile Organic Compounds (VOC) are of concern due to their ability to create photochemical smog in the atmosphere.

2.1.6 Particulate Matter (PM)

Particulates comprise a mixture of inorganic and organic substances, mostly consisting of elemental carbon and heavy metals, as well as un-burnt or partially-combusted fuel's hydrocarbon components. Their diameter is usually less than μm and they can have toxic and carcinogenic effects. The amount of particulate emissions depends on the quality of the combustion and the fuel burnt, with distillate fuel operation diminishing the emissions [8].

2.2 Emissions estimation

The estimation of the emissions of a ship can be achieved via two methods; the activity-based and the fuel-based approach. The first one is a bottom-up method that employs data like the vessel's speed and the engine's output, and is often considered to provide higher accuracy [9]. The second technique is a top-down method that requires fuel consumption or energy consumption measurements [10] and makes use of emissions factors.

The emissions factors may be either fuel-based, which relate the weight of the emitted pollutant to the weight of the consumed fuel (g of emissions/g of fuel), or power-based, which relate the weight of the emitted pollutant to the engine's energy output (g of emissions/kWh). Examples of the fuel-based and power-based emissions factors are presented in Table 2.2 and Table 2.3, respectively. Their value depends on the type of the engine (main or auxiliary), its speed (slow speed, medium speed or high speed) and whether the engine under study meets the IMO Tier I or II requirements. Additionally, the emissions factors vary depending on the type (HFO, MDO, MGO or LNG) and the sulphur content of the fuel.

In this work, the fuel-based method is employed and the main maritime emissions are estimated by multiplying the fuel consumption of the vessel with the emission factor proposed in the IMO's third Greenhouse Gas study [1], Table 2.3.

Table 2.2: Power-based emissions factors for auxiliary engines [11]

Engine type / Fuel type	NO_x pre-2000 engine	NO_x post-2000 engine	NO_x fleet average	SO_2	CO_2	VOC	PM	sfc
				(g/kWh)				
M/H SD / MGO	13.9	11.5	13.0	0.9	690	0.4	0.3	217
M/H SD / MDO	13.9	11.5	13.0	6.5	690	0.4	0.4	217
M/H SD / RO	14.7	12.2	13.8	12.3	722	0.4	0.8	227

Table 2.3: Fuel-based emissions factors for MGO fuel [1]

Emissions substance	Emissions factor (g/g fuel)
CO_2	3.20600
CH_4	0.00006
N_20	0.00015
NO_x	0.08725
CO	0.00277
NMVOC	0.00308
SO_x	0.00264
PM	0.00102

Due to the severe effects of the aforementioned emissions, the maritime industry is working on new ideas and solutions, including the utilization of renewable energy sources (e.g. sails, photovoltaic arrays), fuels with less or zero-emissions (e.g. LNG,

hydrogen) and concepts like the All Electric Ship (AES) and hybrid power systems, that employ batteries, generator sets, super-capacitors, etc.

3 Marine Hybrid Power Systems

The benefits that hybrid power systems offer have drawn the attention of the marine industry and both retrofits and new buildings have implemented different kinds of hybrid solutions. This trend is expected to grow as technology advances and environmental concerns are translated into strict regulations. Bearing in mind that the load demand shall always be met, it's common for the marine diesel engines to operate at low-load conditions, where they are not efficient. With the employment of an ESS the engines can be operated optimally, storing the energy surplus for later utilization.

This concept is usually referred to as load leveling and aims at relevant constant loading of the engines, Figure 3.1. Similar to this, peak shaving operation is mainly targeting peak demand reduction rather than economic efficiency, like load leveling does, resulting in a decrease of the required installed engine power [12]. The fast response and emission-free operation of ESS make them a great fit for the above purposes. Another significant utility of hybrid systems is the "spinning reserve" feature. It provides an alternative power source, which can cover the load during malfunctions of the primary source. This may prove very critical, as a fifteen-minute time period is adequate to restart an auxiliary engine and to reach full load [13].

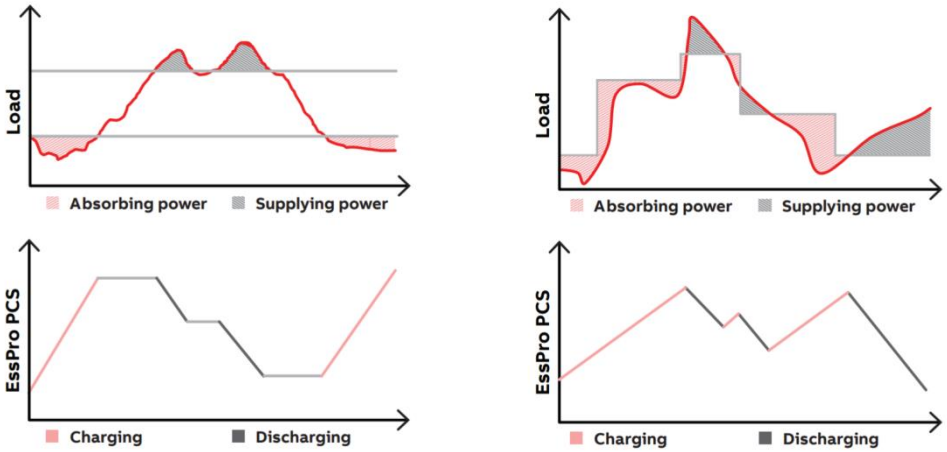

Figure 3.1: Load leveling (left) and peak shaving (right) operations of a battery system [14]

Marine hybrid power systems have employed several energy sources; batteries, fuel cells, wind-related technologies like soft-sails and Flettner rotors, the conventional marine internal combustion engines and others. Since this study investigates the implementation of a lithium-ion (Li-ion) battery into a bulk carrier's power plant, an extensive demonstration of battery characteristics and technologies, as well as a brief reference on generator sets and vessels that incorporate batteries in their power systems are presented in this chapter.

3.1 Generator sets

Generator sets (gensets) are the typical suppliers of electrical power on a marine application. They consist of a diesel pistol engine coupled via a shaft with an alternator. The engine, also referred to as the prime mover, being fed with fuel produces mechanical energy in the form of torque, which is then converted to electrical energy in the alternator. The operation of the gensets is based on the principle of electromagnetic

induction discovered by Michael Faraday; a varying magnetic field around a conductor produces an electromotive force (EMF) across the conductor. An alternator consists of a stator, which contains conductors wound in coils, and a rotor, which produces a rotating magnetic field due to its rotation, by the coupled engine, inside the stator. This magnetic field induces voltage difference between the windings of the stator and in this way alternating current (AC) is produced. Marine gensets employ a medium speed diesel engine and have as an output three-phase alternating current.

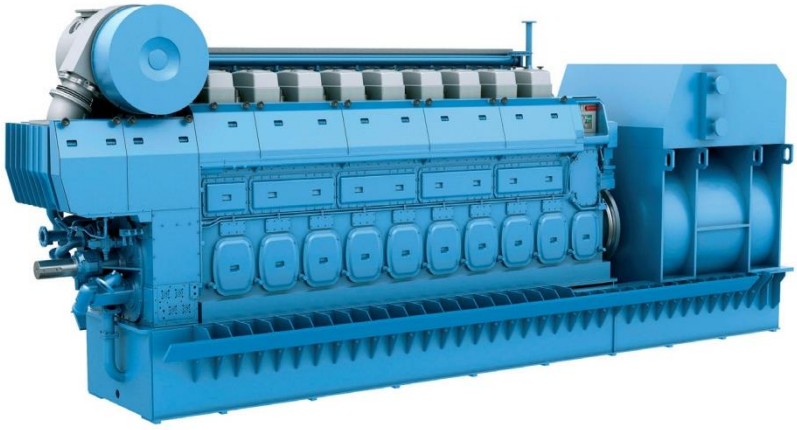

Figure 3.2: A marine generator set (source: Rolls-Royce)

The diesel generators installed on ships can operate on both residual and distillate fuel and recent models offer dual-fuel operation with LNG. Distillate marine (DM) fuel oil does not require any pre-heating for usage. Due to the introduction of 0.50% global sulphur cap by IMO, from now on most gensets will be running on MGO. It is composed of lighter distillate fractions than residual fuel and has much lower sulphur content. MGO's kinematic viscosity at 40°C is between 2 and 6 cSt and its specifications generally conform with that of DMA, ISO 8217:2017 [15].

3.1.1 Fuel consumption

The operation of diesel engines, regardless of their indented use as propulsion or auxiliary engines, is accompanied by considerable fuel expenditure, which constitutes one of the greatest expenses in a vessel. As a measure of how fuel-efficient an engine is, the Specific Fuel Oil Consumption (SFOC) is utilized. It represents the quantity of fuel needed to generate one unit of power for a specific time period. Thus, its unit of measurement is usually g/kWh. The SFOC of a prime mover varies depending on its loading condition and displays a minimum value at a certain load that lays in the 60% - 100% of the Maximum Continuous Rating (MCR) range [16]. A typical SFOC curve is presented in Figure 3.3. As a result, it's prudent to operate the engine as close as possible to their optimum loading condition, i.e. in high loads, in order to achieve the highest fuel efficiency.

Marine electrical systems need to supply power in various circumstances, where the power demand is dynamic and frequently far away from the optimum operating point. That has as an outcome increased maintenance and fuel consumption, which leads to higher costs and emissions. Due to this setback, the functionality of hybrid power systems becomes perceptible. For instance, the employment of a battery pack as a subsidiary power source to the diesel engine can reduce the fuel consumed, as the engine will be used in high loads, where it is efficient, and the lower loads can be

handled by the battery. This concept was extensively researched in Chapter 4 of this study, where the power plant of a bulk carrier was retrofitted with the installation of a Li-ion battery pack.

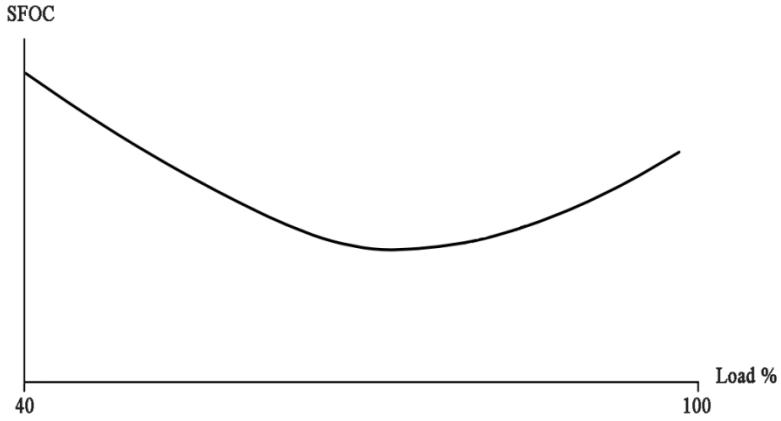

Figure 3.3: A typical SFOC curve of a diesel engine

3.2 Batteries

3.2.1 Basic concepts and electrochemical principles

The basic electrochemical unit of a battery pack is called a "cell". Inside a battery cell, chemical energy is converted into electric energy, through the reduction-oxidation (redox) reaction [17]. Cells are connected with each other composing battery modules and modules are connected either in series or in parallel, forming the battery pack, Figure 3.4. With the series configuration the designer can achieve the desired output voltage and with the parallel to reach the required capacity and DC output. The battery modules are stacked in specially designed racks, inside a designated space with cooling and venting installations.

The main components of a battery cell are the anode and the cathode, which are called the negative and positive electrodes, respectively and the electrolyte, which allows the transfer of charged ions from the anode to the cathode, through a nonconductive material, called a separator. The electrolyte is usually an acid, salt or alkaline solution.

When the battery discharges, electrons flow from the negative electrode to the positive. Simultaneously, in the electrolyte, there is a flow of anions and cations to the anode and cathode, respectively, Figure 3.5. The flow of electrons has as a result electrical current.

The reduction-oxidation reaction, as its name indicates, consists of two half-reactions; reduction, during which the cathode gains m electrons and oxidation, during which a reductant (R_1) loses m electrons, Equation (3.1), [18]. These reactions happen concurrently.

$$\begin{aligned} R_1 &\rightarrow O_1 + me^-, \quad \text{at the anode} \\ O_2 + me^- &\rightarrow R_2\,, \quad \text{at the cathode} \end{aligned} \tag{3.1}$$

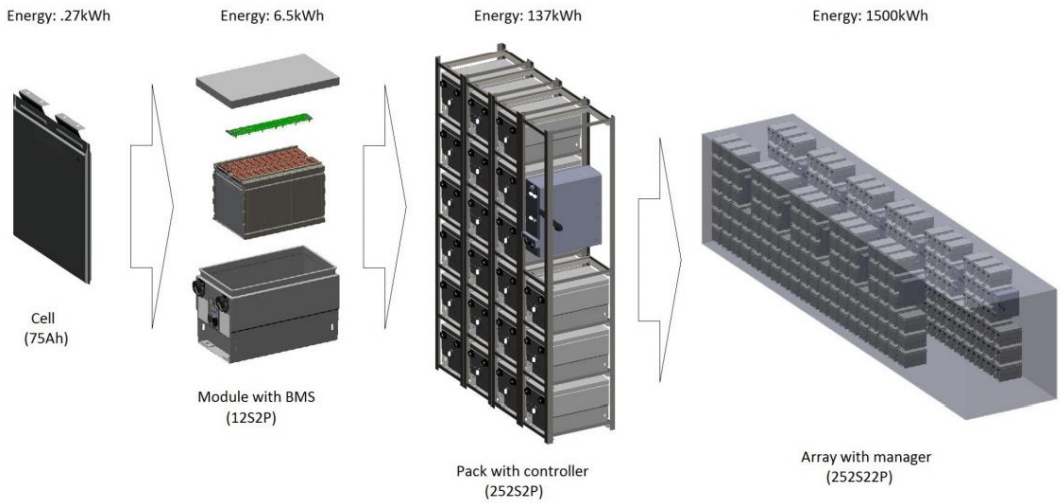

Figure 3.4: Battery cell, module and pack (source: DNV GL)

Rechargeable batteries can regain their charge by reversing the above reactions when electrical energy is provided from an outside source.

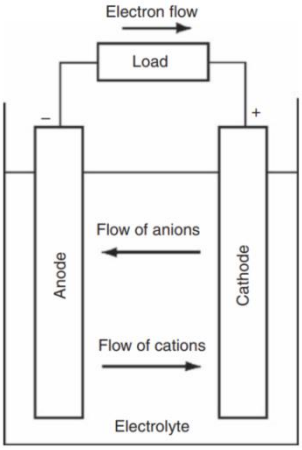

Figure 3.5: The electrochemical cell during discharge [17]

3.2.2 Terms and definitions

In this paragraph, the basic battery-related terminology is presented. Terms like the state of charge, C-rate and open-circuit voltage are defined, as they are referred later in this work.

State of Charge - SOC: The available capacity in a battery, expressed as a percentage of the rated capacity. 100% SOC equals to a fully charged battery and 0% SOC to a fully discharged one. It's one of the most important battery parameters, as it's used for its monitoring. SOC is usually calculated by integrating the battery's current over time.

Depth of Discharge - DOD: The ratio of the quantity of charge removed from the battery to its rated capacity. It's the numerical complement of the SOC.

C-rate: It is a measure of the discharging rate relative to the battery's maximum capacity. For example, the 1C rate results in a fully discharged battery in 1 hour. If the maximum capacity is 50 Ah, the 1C rate is 50 A current, while the C/5 rate is 10 A.

Capacity (or Nominal capacity) (Amperè–hours, Ah): It's the amount of current that a battery can deliver for 1 hour before it's fully discharged.

Energy (or Nominal Energy) (Watt-Hours, Wh): The total energy the battery can provide during the discharge from the maximum voltage (at 100% SOC) to the cut-off voltage. It is dependent on the discharge current, decreasing with increasing C-rate.

Internal Resistance (Ohms, Ω): The opposition to the flow of the electric current within the battery. It is affected by the physical characteristics of the electrolyte and the state of charge [19]. When the temperature raises internal resistance decreases and the battery efficiency increases. Most cell chemistries display an internal resistance increase at the end of discharge. Aging has as an outcome resistance augmentation.

Open-circuit voltage (Volts, V): The voltage between the battery terminals when no load is applied. It depends on the battery's SOC, decreasing with discharging.

Terminal Voltage (V): The voltage between the battery terminals when the load is applied. It's related to the SOC and the battery current.

Nominal Voltage (V): The characteristic operating voltage or rated voltage of the battery. It can be considered as the "normal" voltage of the battery.

Cut-off Voltage (V): The voltage at the end of the discharge. It is also referred to as the end voltage.

Cycle Life: The number of charge-discharge cycles the battery can provide before it fails to meet specific performance criteria. Usually, it's defined as the number of cycles before the capacity drops to 80% of the initial. It's calculated for specific charge and discharge conditions and depends on the current rate, the depth of cycles and temperature, both operating and storage. As the depth of discharge increases, cycle life drops.

Specific Energy (Wh/kg): Also known as the gravimetric energy density. It is the ratio of the available energy of the battery to its weight.

Specific Power (W/kg): The maximum available power per unit mass.

Energy Density (Wh/l): Also known as the volumetric energy density. It is the ratio of the battery's available energy to its volume.

Power Density (W/l): The maximum available power per unit volume.

State of Health – SOH: A subjective indication, as there is no universal agreement on how it's defined, that reflects the degradation of the battery. It takes into account the voltage, the internal resistance and the self-discharge. It signifies at which point in its life the battery is and measures its condition relative to a new battery.

3.2.3 Lithium-ion batteries

Lithium-ion batteries currently dominate the energy storage field, as they power form laptops, to electric vehicles and industrial applications and this isn't expected to change earlier than 2025 [20]. In the last decade, there have been important developments in lithium-ion battery technologies, due to the intensive research & development of the automotive industry. This made them a viable option for maritime use, as they offer high power and energy density and good cyclability [21], [22], [23]. More specifically, they have up to eight times higher energy density compared to lead-acid and nickel-cadmium batteries [24], Figure 3.6. Lithium-ion polymer batteries and lithium iron phosphate batteries can offer high capacity at high discharge currents, features that made them appropriate for hybrid marine applications, like ferries [25], RO-RO's [26], bulk carriers [27] and other ship types. Finally, the significant reduction of lithium-based cell prices in the last years made them even more appealing. In particular, between 2011 and 2015 their cost dropped 60-70% [28] and this trend is expected to be continued in the years to come.

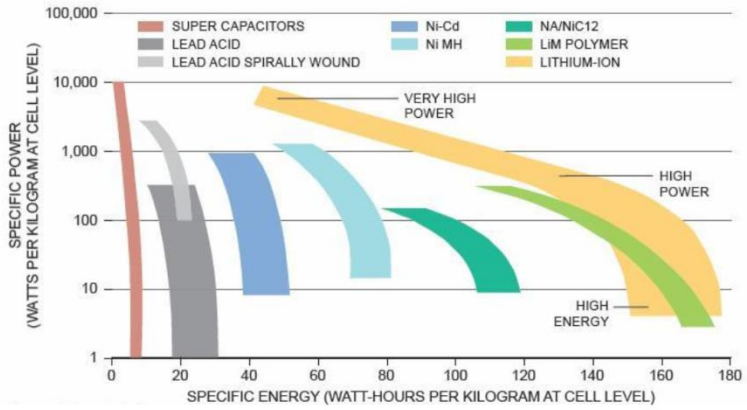

Figure 3.6: Specific power and specific energy of different battery chemistries (source: Johnson Controls)

All the above advantages of Li-ion batteries make them the most compelling choice for hybrid marine applications. Their overall performance, life span and safety are determined by a number of parameters, including the electrodes chemistry and coating thickness, the electrolyte and the manufacturing process. The anode is usually made from carbon or graphite-based material, while the chemistry of the cathode is probably the most important parameter of all, giving its name to the battery technology. It defines to a great extent energy and power characteristics, voltage output and cost. The most commonly used cathode chemistries are presented below, while their features are illustrated in Figure 3.7:

- **Lithium nickel manganese cobalt oxide, $LiNiMnCoO_2$ (NCM or NMC):** It is one of the latest developments in lithium-ion battery technology and the industry-standard in large applications [29]. It offers higher energy density (150-220 Wh/kg) than other lithium-ion technologies, high current power and good overall performance. The various combinations of the three active materials of nickel, manganese and cobalt provide the opportunity for tailor-made energy storage systems that fulfill applications with frequent cycling needs [30]. Also, NMC cells can be customized to serve as high energy cells or high power cells. Its great advantages derive from blending the high specific energy – but poor stability – of nickel with the good stability of manganese. Estimations suggest

that NCM Li-ion cells cost will drop to $100/kWh at the cell level and their energy density will likely reach 300 Wh/kg before 2030 [31].

- **Lithium iron phosphate, $LiFePO_4$ (LFP):** Unlike most of the cathode chemistries, which are layered with a metal oxide, this one has phosphorous-olivine. In terms of specific energy, power and voltage, $LiFePO_4$ falls short compared with other Li-ion technologies (90–120 Wh/kg). Additionally, it has a higher self-discharge rate. Although, its relatively long cycle life, resilience to temperature fluctuations, low cell resistance and excellent safety compensate for the above drawbacks.

- **Lithium manganese oxide spinel, $LiMn_2O_4$ (LMO):** The spinel structure allows higher power capabilities, as well as enhanced safety, due to its high thermal stability. Also, low internal cell resistance enables fast charging and discharging in high C-rates. Its main disadvantages are the relatively lower energy capacity (100–150 Wh/kg) and more limited cycle and calendar life characteristics, especially under higher temperatures. Though, via material modifications, like its combination with nickel, cobalt and/or aluminum, the extension of the cycle life and the enhancement of the specific energy and power are possible.

- **Lithium cobalt oxide, $LiCoO_2$ (LCO):** Even though it offers relatively high energy density (150-220 Wh/kg), the high cost of cobalt and the following drawbacks, result in the gradual displacement of this chemistry by the LMO. Firstly, typically it provides limited specific power, shorter cycle life and low thermal stability. Furthermore, the cell's internal resistance rises gradually and the exothermic release of oxygen at elevated temperatures results in safety concerns. Particular attention should be paid at the charging/discharging currents, as currents higher than the cell's C-rating have as an outcome overheating and excessive stress.

- **Lithium Nickel Cobalt Aluminum Oxide, $LiNiCoAlO_2$ (NCA):** Similar to NMC, it is quite energy dense (200-260 Wh/kg), offers good specific power and a long life cycle. As for its disadvantages, this cathode chemistry is fairly expensive and accompanied by safety concerns.

- **Lithium Titanate, Li_2TiO_3 (LTO):** In the LTO technology the anode of the cell is made of Li-titanate, not graphite. The cathode can be lithium manganese oxide or NMC. Li-titanate offers the advantage of fast charging is able of providing high C-rates during discharge, which can reach up to 10C [30]. Moreover, LTO is safe, has very good low-temperature discharge characteristics and its thermal stability under high temperatures is superior compared with other Li-ion systems. However, the specific energy is very low (65 Wh/kg) and it's a relatively expensive technology.

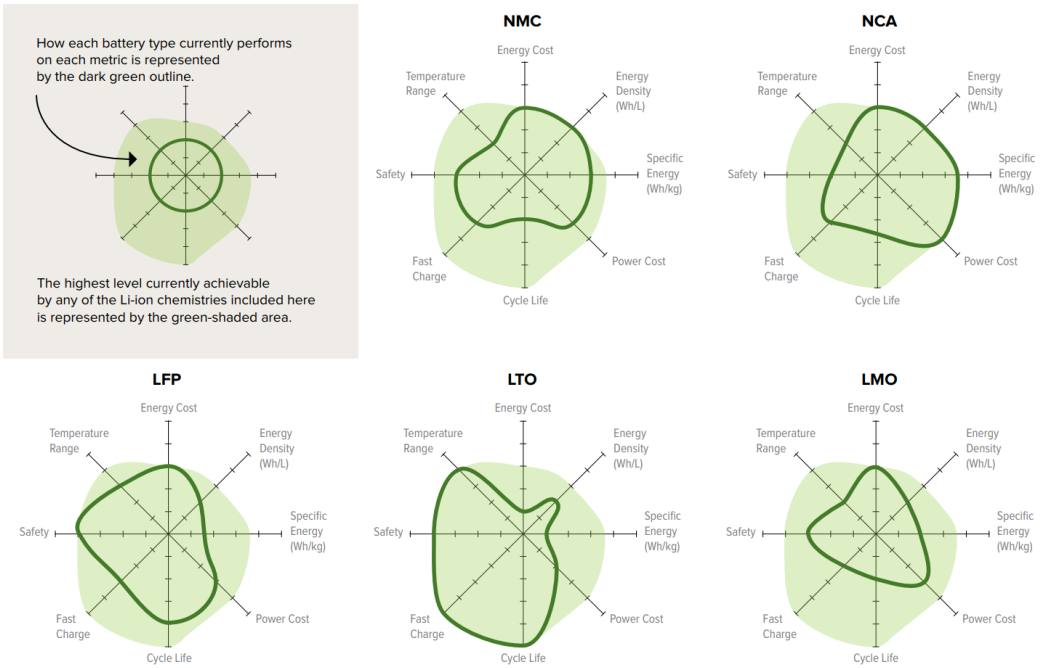

Figure 3.7: The features of various Li-ion battery technologies [20]

3.2.4 Battery characteristics

The main parameters of each battery cell are usually summarized in a datasheet, which is provided by the manufacturer. It includes the nominal capacity, the cell's energy, the maximum discharge current, the temperature range under which the cell can operate, the nominal output voltage and many other data.

As mentioned earlier, both the terminal and the open-circuit voltage are functions of the state of charge. As the battery discharges the output voltage is dropping, a phenomenon depicted in the so-called "discharge curves" of the battery, which some manufacturers provide as well. The x-axis in these figures is either SOC (or DOD), time of discharge or capacity. The discharge curves are dependent on the C-rate and the ambient temperature. Typical discharge curves of a lithium-ion battery are shown in Figure 3.8.

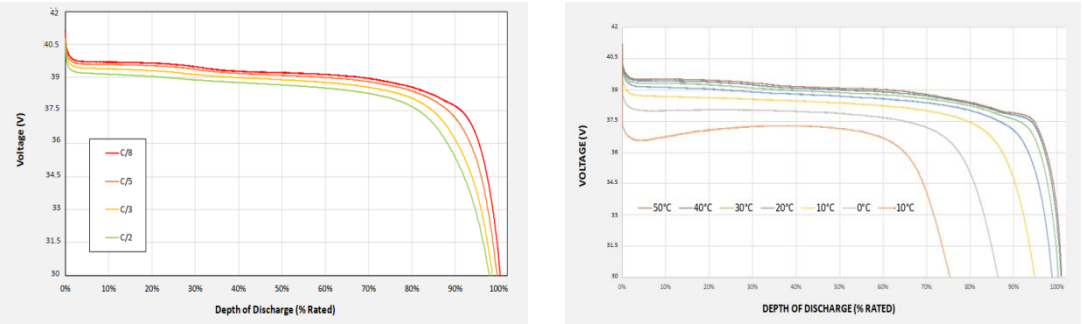

Figure 3.8: Discharge curves of a Li-ion battery, as a function of DOD, discharge rate and temperature (source: LithiumWerks)

Most discharge curves have three sections; i) the exponential area, which appears when the battery is almost fully charged, ii) the nominal area, in which the curve is relatively flat and it ends when the voltage drops below the nominal voltage and iii) the last part,

which represents the end of the discharge when the voltage decreases fast [32]. The above sections are shown in Figure 3.9. The discharge curves play a vital role in the modeling of battery modules, as model parameters are usually extracted from them. This matter will be discussed extensively in a later chapter.

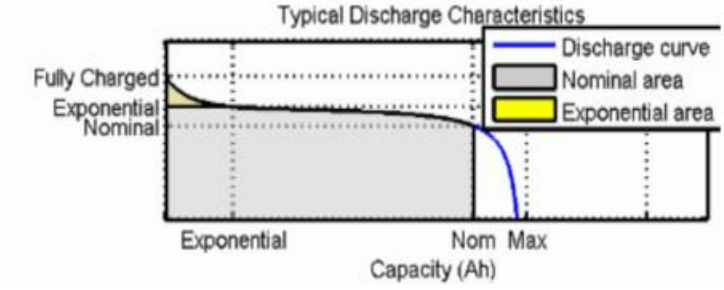

Figure 3.9: Typical sections of a discharge curve (source: Mathworks)

3.2.5 Battery Management System (BMS)

The battery management system is the electronic control system of the battery pack, aiming at safe operation, optimal performance and cycle life [33]. It is responsible for monitoring cell voltage, temperature and current, as well as limiting charging and discharging, for thermal and overcharge protection. Most importantly, BMS accomplishes the complex task of calculating the state of charge and the state of health, parameters that can't be measured with sensors. That is why the BMS is crucial to be tailor-made to the particular cell.

BMS employs voltage and temperature sensors, which allow the detection of undesired temperatures, in order to act and remove heat from the cells. Furthermore, ensures the balanced operation of cells, trying to avoid large SOC deviations from cell to cell and provides the option of isolating the battery from the charger and the load when necessary.

3.2.6 Rules and regulations

The utilization of batteries in vessels is regulated by class rules, to ensure the maximum possible level of safety and efficiency. DNV GL rules for classification address the matter of battery systems in "Part 6: Additional class notations, Chapter 2: Propulsion, power generation and auxiliary systems", in Section 1.

Firstly, a basic division concerning the intended use of batteries on board is made. The additional class notation *Battery (Power)* applies in cases like when the vessel is battery powered or when the battery system is a backup for dynamic positioning [34]. The *Battery (Safety)* notation applies to vessels that use batteries as part of a hybrid system, providing additional power or improving the dynamic performance. Since in this work we study hybrid power systems we will only touch upon the latter class notation.

The rules cite the required certificates, concerning the battery system and charger, as well as the necessary documentation, like arrangement plan of the battery space, risk analysis and fire integrity & detection arrangement. Also, as regards the battery system itself, drawing and manuals for the battery are required. These include an electrical

schematic drawing of the battery pack, exhibiting the configuration of the modules, along with an operation & maintenance manual.

Some key points from the rules are listed below;

- None of the main functions of the ship, like power generation, steering, ballasting and anchoring [35], shall become unavailable for more than the maximum restoration time according to [36], due to any failure of the battery system.

- The battery pack shall be placed aft of the collision bulkhead, in a portion of the vessel's structure or in a space with equivalent structural integrity. This space shouldn't accommodate any heat sources or objects with a high risk of fire. Additionally, the doors of this space shall be alarm protected.

- The designated battery space shall provide ventilation and control of the ambient temperature. Alarms both for high temperature and ventilation malfunction shall be installed.

- The battery space shall be enclosed by A-0 fire integrity and in the case of muster & evacuation stations, additional A60 integrity must be placed.

- A smoke detection system and a water-based fixed fire extinguishing system shall be in place.

- An independent emergency shutdown for disconnecting the battery system shall be installed.

- A flame-retardant material shall be used in the manufacturing of cells, modules and battery casing.

- The battery's ingress protection shall be at minimum IP 44.

- Several tests, like thermal abuse and overcharging, shall be performed to the battery cells, at a recognized laboratory.

3.2.7 Emerging battery technologies

The automotive industry, universities, research labs and others invest enormous amounts of money in battery optimization. As a matter of fact, energy storage companies received over $1.4 billion by venture capital funds in the first half of 2019 alone. The last decade the battery cost has seen a 21% annual decrease in average and it's expected to fall further due to a number of factors; planned Li-ion battery factories that are about to come online in the next five years [37], price competition and economies of scale are the major ones.

Despite the performance improvements and the tremendous cost reductions made the past years, analysts agree on the fact that this technology isn't the best option for longer-duration or longer-range applications. Moreover, lithium-ion batteries require complex and expensive thermal management systems, in order to minimize the fire risks that come with the technology. Their production uses large quantities of cobalt, whose reserves are limited and the mining of which is connected with environmental and

sustainability concerns [31]. The mining of lithium is problematic too, due to its rising price and implications to the health of mining workers [38].

The development of new battery technologies that would at some point replace the lithium-ion is already occurring. They will suit better the various storage goals, like electrifying heavier mobility applications and providing grid balancing. These technologies are expected to be commercialized at a significant degree no later than 2030. The most promising of them are described below.

3.2.7.1 Next-generation lithium-ion

In the prevailing Li-ion technology there is still room for improvement, mostly in terms of energy density and cost. The specific density could reach up to 450 Wh/kg and even a three times reduction in cost is possible [20]. Though, the cycle life is expected to drop. The future developments relevant to this battery type include lower or zero cobalt NMC cathodes, which will address the issues regarding the sensitive supply chain and mining of cobalt referred above. Additionally, both the performance and the cost of other chemistries, like LFP and LMO, are anticipated to be improved.

A recently developed and soon to be commercially implemented advancement in the Li-ion battery field is the replacement of the typical graphite anodes with silicon ones. This aims at raising the energy density of the cells, reportedly even up to 20% [37]. Sila Nanotechnologies is developing a silicon-based powder that can be formed into an anode. Silicon outweighs the carbon found in graphite in holding more lithium, which results in storing more energy. Nonetheless, the batteries employing this approach are characterized by low electrical conductivity and a slow diffusion rate [39].

3.2.7.2 Solid-state

As described earlier, during the operation of a typical battery cell, charged ions are traveling from the anode to the cathode, through a liquid electrolyte. In solid-state batteries, a solid compound characterized by very high ionic conductivity takes the place of the liquid electrolyte. Usually, it is a polymer or ceramic material. Among the many that have been tested are amide-borohydride, sulphide-based solids and glass [40].

The development of this battery technology is surrounded by high expectations, as it is considered by many as one of the most promising things for future energy storage, even referred to as a game-changer [41]. Its major benefit is that it's more fire-resistant, as the solid electrolyte employed is inflammable or at least resistant to self-ignition. That diminishes the risk of thermal runaway and allows tighter cell packaging. Additionally, it offers higher energy density, resulting in smaller batteries and lower cost per kWh [42]. The batteries with solid electrolytes are expected to charge faster, have longer cycle life and provide better shelf-life due to their lower self-discharge [43].

Once again the automobile industry leads the way in the battery technology advancements, as major manufacturers like Ford, Volkswagen and Toyota are investing in solid-state battery research. More specifically, Toyota has far more solid-state related patents than any other company, having invested almost $14 billion in its battery operations in total [37].

The high capacity potential and stability of lithium metal batteries, combined with the enablement of recharging via the solid-state technology advancements, would probably make lithium metal the prime material for solid-state batteries. Rechargeability challenges will be tackled in technologies using sulfur, zinc and aluminum, too. The employment of these less expensive materials will drop further the cost of energy storage.

Even though the solid-state technology is considered by many as lithium ion's likely successor, many start-ups are currently working on upgrading lithium-ion batteries instead of replacing them. Due to the enormous investments in lithium-ion battery factories, solid-state related manufacturers like Ionic, focus on designing polymer electrolytes that can work inside lithium-ion batteries. That eliminates the existing factories' need for expensive new equipment and allows the commercialization of solid-state technology. This can enable very cost-effective rechargeable alkaline batteries in the future.

Nevertheless, as the solid-state batteries employ a solid electrolyte and its conductivity is dependent on the temperature, some question its performance in low temperatures where the conductivity is reduced. The fully developed technology is expected to emerge in the late 2020s [44], firstly using graphite-based anodes and later with metallic lithium.

3.2.7.3 Lithium-metal (Li-metal)

The main difference between lithium-ion and lithium-metal batteries is that the first are rechargeable, while the second are not easily and safely recharged. Actually, this particular drawback of lithium-metal batteries led to the invention of lithium-ion technology [45]. The two battery technologies differ also on the material used on the anode, as lithium batteries employ lithium metal instead of graphite.

Solid-state technology, as mentioned, has the potential to make Li-metal rechargeable and consequently, broaden its range of applications, including electric vehicles (EV). Benefits will also emerge regarding the already high energy density of Li-metal batteries, as it is expected to reach up to 600 Wh/kg in the future.

The enabling of until today not safe chemistries, like Li-metal, will reduce system costs as safety, cooling and controls equipment will not be necessary anymore, or at least at the degree it is currently. This can result in up to three times lower battery cell costs. Safer lithium-metal batteries can also be attained through advanced liquid electrolytes that confine the growth of dendrites. These needle-like structures are the cause of the limited use of these batteries so far, as they sometimes lead to failure or even to fire [46].

3.2.7.4 Lithium-Sulphur (Li-S)

Apart from the troubled and costly supply of lithium, Li-ion batteries usually employ minerals like cobalt, nickel and rare earths. That results in an expensive product and also, environmental concerns arise, regarding the mining of those materials. By using sulphur instead as the cathode, Li-S batteries will likely be competitive in terms of cost with future Li-ion batteries. Sulphur is the 16th most abundant element on nature and its annual mining production is about 70 million tonnes [47]. That makes it's relatively

cheap compared to the minerals described above and results in low cost of battery materials, Figure 3.10.

Due to the employment of very light active materials, sulfur in the positive electrode and metallic lithium as the negative electrode, its theoretical energy density can be almost as four times higher than that of Li-ion [43]. That benefit makes it a good fit for heavy and weight-sensitive mobility applications, like aviation. Using a solid-state electrolyte is necessary for the commercialization of Li-S technology, as the liquid-based Li-S has short cycle life and high self-discharge. Consequently, Li-S is expected to reach the market right after solid-state Li-ion technology.

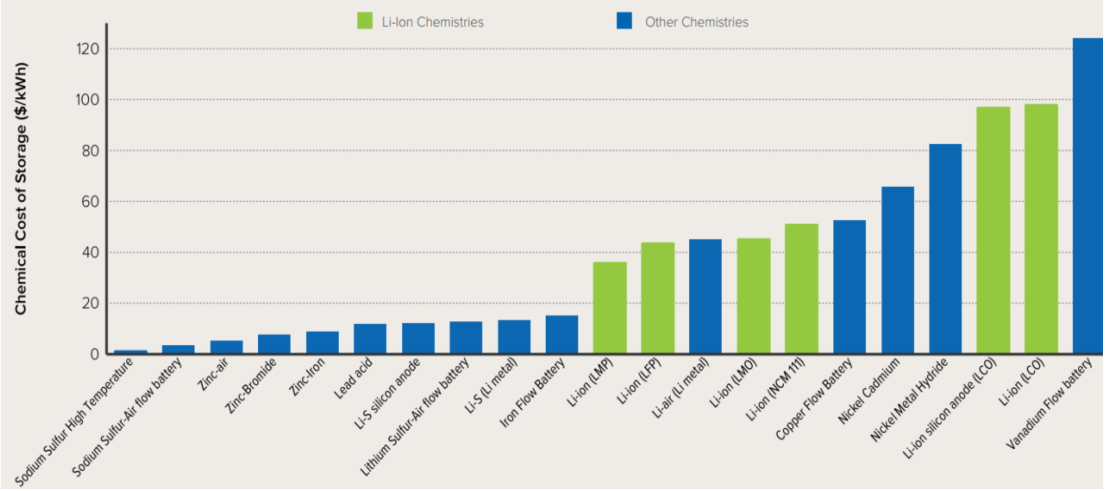

Figure 3.10: An estimation of the cost of raw materials employed in different battery technologies [20]

3.2.7.5 Flow

Lithium-ion batteries are already being used in grid-scale applications, like backup power for hospitals but, they aren't the best fit for larger size utilization, like for example, providing backup power for cities [48]. A more appropriate solution for such use is flow batteries, which although can't compete with Li-ion batteries in terms of energy density, offer reliable long-duration storage solutions. For instance, the world's largest flow battery is expected to come online in 2020, in Dalian, China, with the ability to store 800 MWh. Additionally, flow batteries have a cycle life greater than 20,000 cycles at 100% DOD and can operate under very high-temperature environments [49].

Flow technology differs from one found in a typical battery, as it employs large tanks of liquid electrolytes to store electrical charge, Figure 3.11. The electrolyte flows through the battery system with the help of circulation pumps. Inside the battery stack, a membrane separates the two electrolytes but allows ion exchange. When electric current is created the spent electrolyte returns to the tank.

The number of battery stacks determines the maximum power while scaling up the tanks results in storing and providing higher amounts of energy. This peculiarity allows flow batteries to have their power and energy decoupled. When provided with external current the battery recharges by restoring the charge of the spent electrolytes. Since the electrolytes flow through all the cells and stacks simultaneously, there is one common SOC for all the stacks, rather than each cell having an individual one. This renders SOC balancing not necessary, as it is in Li-ion batteries.

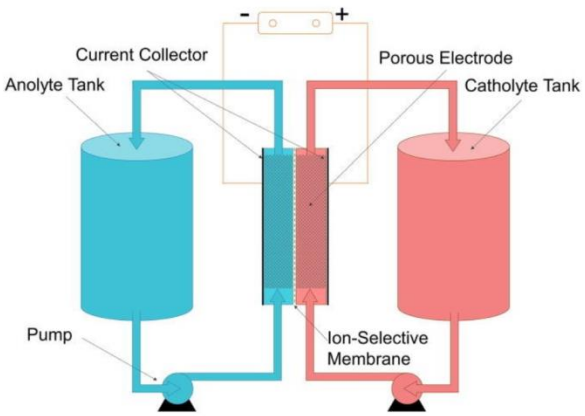

Figure 3.11: The typical configuration of a flow battery [50]

There are three categories of flow batteries: redox flow, which is the most commonly encountered, hybrid flow and membrane-less flow batteries [50]. The first one employs a liquid phase reduction-oxidation reaction, while hybrid flow batteries have a liquid-solid transition. The latest development in the sector, membrane-less flow batteries, doesn't require the separation of the electrolytes.

Between the different chemistries and electrolyte components used in flow batteries vanadium is the most frequently employed, due to its ability to charge and discharge for thousands of cycles. Zinc-bromine, polysulfide-bromine, iron-chromium, and iron-iron are also used. Right now many of those chemistries are widespread and are under a cost optimization process. Vanadium price has risen the last years and it's expected to rise higher because the demand is growing. The benefits and prospects of flow batteries have attracted considerable investments in the last few years, with support from investors like Bill Gates, Jeff Bezos and Jack Ma [51].

3.2.7.6 Zinc

Zinc batteries, especially those that employ inexpensive cathodes like air, can provide high energy density up to 350 Wh/kg while keeping the cost low. They are already cheaper than lithium-ion batteries and their cost will drop further. More specifically, zinc metal systems destined for long-duration grid-scale storage claim to be up to 80% less expensive than similar lithium-ion systems and can operate in the wide -45°C to 70°C temperature range [52]. Some zinc products are less power-dense and with lower cycle life than Li-ion batteries, but their life is expected to be improved in the following years.

For this to happen, the dendrite formation shall be resolved, which will also assist in the matter of rechargeability. This can be achieved via both solid-state and liquid electrolyte advancements for zinc-air batteries. These batteries function by getting oxygen from the air. Tiny holes in the top of the cell allow the introduction of oxygen molecules, which then contact the porous carbon cathode [53]. After several chemical reactions, electrons are released. By not including one of the reactants inside the cell, space is saved and consequently, the size and weight are diminished.

Zinc-air batteries are relatively safe as they don't contain toxic compounds, they aren't flammable and can be recycled. Even though zinc is a common element, its large-scale

production raises environmental concerns, due to the sulfur dioxide and cadmium-vapor release [38].

3.2.7.7 Sodium-ion (Na-ion)

The current circumstances around the cost of lithium, the projections of its price skyrocketing the following years and fire-related concerns, have led to studies of alternative battery materials. One of these is sodium, which is cheaper due to its abundance in nature and has similar intercalation chemistry to lithium [54].

Among the various cathode materials tested, phosphates and fluorophosphates are the most promising, mostly because of the great stability they offer. Carbonaceous materials and other compounds like titanates have been researched for use in the negative electrodes. Regarding electrolytes, solid-state solutions have been studied and some ceramic materials are known for their safe operation, as well as their satisfactory conductivity at room temperature. Gel polymer electrolytes fillers are also an option.

A significant problem of Na-ion batteries is their relatively low durability. Provided that this matter is addressed in the following years, the technology could serve many applications that don't require high voltages, like wearable devices [55]. For high-voltage operations, though, the difference in electric potential between the anode and the cathode needs to be improved. That is not expected to be achieved soon, but researchers are optimistic that Na-ion batteries will have a considerable market share in the future. More specifically, the current state of technology's development is as it was for the Li-ion batteries a decade ago [56].

3.2.8 Marine battery hybrid system arrangements

The benefits of energy storage can be implemented in various ways in a marine power system, resulting in different system arrangements. Batteries can be used as assistance to the generator sets in the supply of auxiliary loads, for participation in the propulsion of the vessel or both of these purposes. In the first case, the vessel has mechanical propulsion with battery hybrid power plant. The battery is integrated into the electrical grid of the vessel, while the propulsion is handled conventionally by the main engine, Figure 3.12 (a). The battery hybrid propulsion & power plant arrangement is illustrated in Figure 3.12 (b). This configuration employs electrical propulsion, as the diesel generator sets and the battery packs feed large propulsion motors. Additionally, both of these power sources contribute to the supply of the hotel load. The operator of the vessel has the option of using one of the above-mentioned power sources or running them in parallel. That offers the significant advantage of zero-emission operation during port stays, through the exclusive operation of batteries, resulting in lower port fees and noise levels.

Batteries can also be utilized in assisting the main engine in propulsion. In a battery hybrid electrical/mechanical propulsion topology a Power Take-In/Power Take-Out (PTI/PTO) shaft generator is employed. During periods when the main engine would usually operate in the inefficient low-power region, this machinery enables the operation of the main engine closer to its optimal loading condition, using its excess torque to produce electric current (PTO mode).

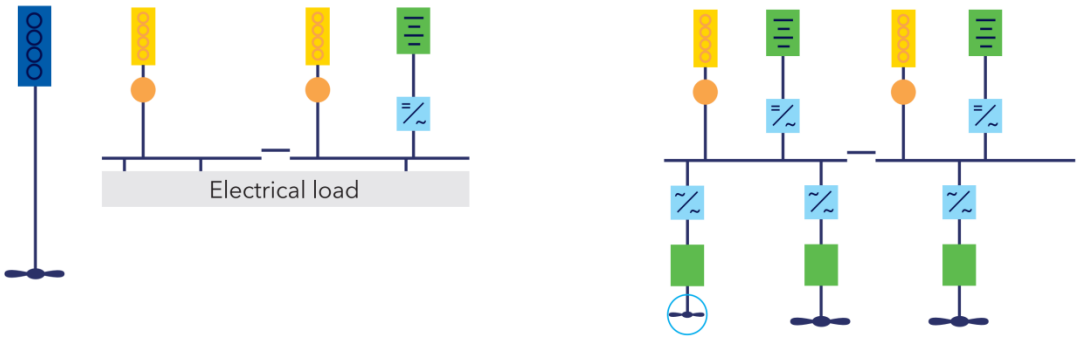

Figure 3.12: Mechanical propulsion with battery hybrid power plant (a) and battery hybrid propulsion & power plant (b) [28]

This current can be used for the supply of auxiliary loads or be stored in the battery packs. On the other hand, when in need, the propulsion load can be supplied by either just the gensets/battery pack or through a combination of the main engine with these two power sources (PTI mode). During such an instance the shaft generator is used as a motor. In Figure 3.13 a hybrid arrangement employing a PTI/PTO machine, thrusters, as well as DC and shore supply is shown. All the above arrangements require power converters that convert AC to DC and the opposite.

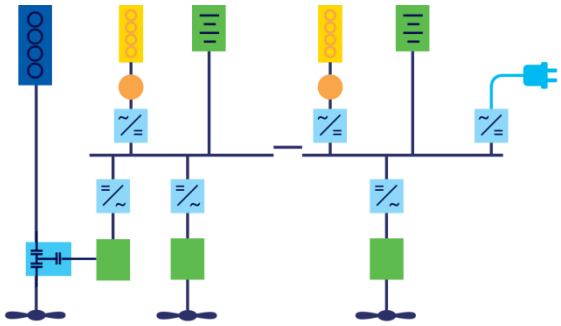

Figure 3.13: Battery hybrid electrical/mechanical propulsion with PTI/PTO machine and shore connection [28]

3.2.9 Vessels utilizing battery technology

Motivated by environmental and cost-related reasons and enabled by the significant technological advancements achieved in the past years, owners have employed battery systems in various ways in their vessels. According to DNV GL, the number of operating vessels with batteries has grown 12 times since 2011 [57]. More specifically, in 2020 192 ships incorporate batteries in their power systems and 159 more are under construction, Figure 3.14. The next years the number of operating vessels will remain the same and the under-construction vessels will be increased, reaching 196 in 2026. More than half of the existing vessels employ a hybrid power system, while the plug-in hybrid and the pure electric vessels take each about 20% of the total number of ships with battery pack installments, Figure 3.15. Furthermore, Norway is the country with the most vessels that utilize ESS and the most popular battery technology is NMC, with $LiFePO_4$ coming second. Finally, the ship type

that has taken the most advantage of batteries is by far roll-on/roll-off passenger (RoPax) ferries and the second in line is offshore supply vessels (OSV).

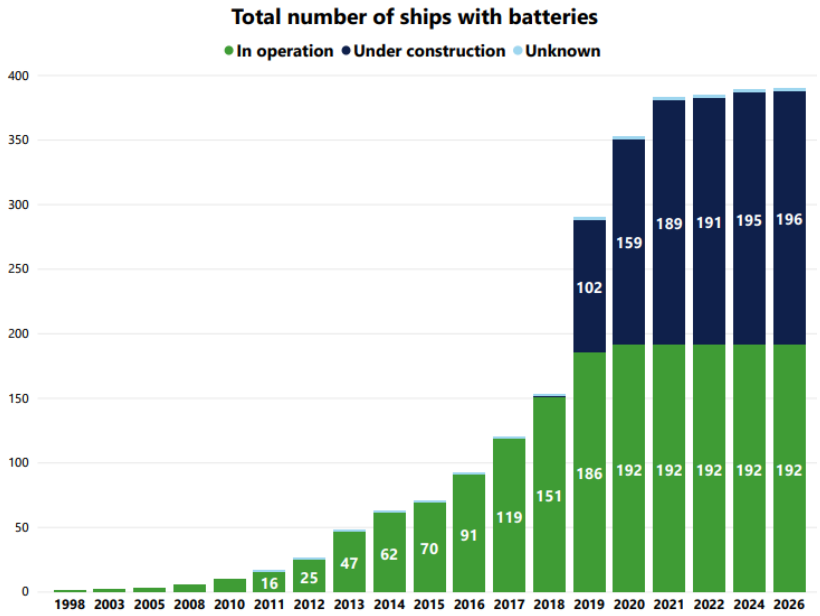

Figure 3.14: The number of vessels in operation and under construction that employ battery technology [57]

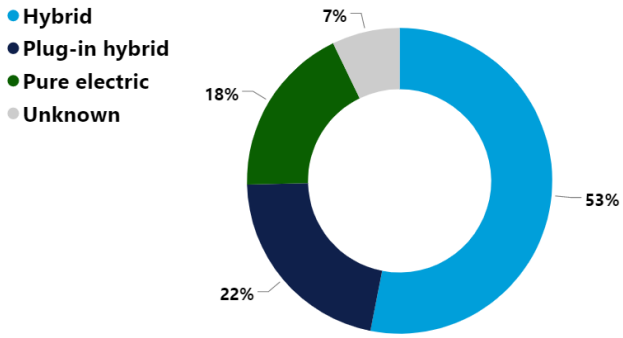

Figure 3.15: Hybrid, plug-in hybrid and pure electric vessels as a percentage of the total number of ships with batteries [57]

Two of the above mentioned RoPax ferries are Tycho Brahe and its sister ship Aurora. They are two 238 m long fully electric passenger ferries, which are operated by ForSea, between Helsingborg, Sweden and Helsingör, Denmark. This 4 km ferry route takes about 20 minutes to be completed and transfers over 7.4 million passengers and almost 2 million vehicles annually, with zero-emissions. Specifically, about 28,000 tonnes of carbon dioxide emissions are prevented every year, improving the air quality in both cities [58]. The vessels were constructed back in 1991 as conventional diesel engine-driven ferries and at the end of 2018, they were converted to fully electric vessels, employing a 4160 kWh SPBES lithium-ion battery pack each [59]. The battery modules are placed inside four containers installed on top of the ships. The charging process employs an industrial robot installed onshore, which reaches out and pulls the shore cable from the ship, Figure 3.16. This is achieved by 3D laser scanning and wireless communication between the vessel and the shore. Furthermore, renewable energy sources like wind and solar energy provide the required energy to the charging station.

Figure 3.16: The robot used for charging Tycho Brahe and Aurora (source: SPBES)

Almost 400 km farther north, the world's largest plug-in hybrid ship, Color Hybrid, operates since early 2019 on the 2.5 h route Sandefjord – Strømstad, between Norway and Sweden. With a capacity of 2,000 passengers and up to 500 cars, the 160 m RoPax ferry features a 5000 kWh battery pack, weighting 65 tonnes [60]. That empowers it to travel almost one hour at a speed of less than 12 knots. This is enough to exit the berth in Sandefjord silently, without producing any emissions. At this port, the vessel's battery is recharged overnight via a shore power connection. During sailing, the battery and the four diesel engines installed are contributing to the supply of the total power demand, lowering fuel consumption and emissions. Color Hybrid was named Ship of the Year at the 2019 Nor-Shipping exhibition.

Figure 3.17: Color Hybrid, the world's largest plug-in hybrid ship (source: electrek)

Viking Lady, an offshore supply vessel owned by Eidesvik Offshore, was the first vessel to install a high-temperature fuel cell back in 2009 [61]. As part of the FellowSHIP (Fuel Cells for Low Emission Ships) project, which was a fifteen-year R&D project undertaken jointly by DNV GL, Wärtsilä and the ship's owners, the vessel implemented a 300 kW fuel cell. The benefits of the hybrid configuration led to an additional retrofit of the ship's power system in 2012, this time employing a 450 kWh lithium-ion battery pack manufactured by Corvus Energy [62]. The combination of the four dual-fuel engines installed with the fuel cell and the battery pack resulted in a 15% reduction in fuel

consumption in sea trials. The battery's ability to cover the load variations during dynamic positioning and the battery/fuel cell operation during port stay have offered significant reductions in maintenance costs, noise and vibrations.

Eidesvik Offshore also owns Viking Princess, another OSV converted to hybrid back in 2017. One of the four LNG dual-fuel engines originally installed on board was replaced by Wärtsilä's containerized hybrid energy storage solution, which employs a 533kWh Corvus Energy Orca Energy battery pack installed on deck. That supplies the load peaks while cruising, providing the additional energy needed when for example the vessel climbs a wave. Moreover, when approaching a rig the battery assists the engines in dynamic positioning and during port stay the maximum utilization of batteries is targeted, reducing emissions and noise pollution. Despite the retrofit and the replacement of the genset, the vessel preserved its DP2 classification [63].

Sten Tor and Sten Odin, delivered in 2018, were the first chemical tankers to incorporate batteries in their power systems [64]. Owned by Stenersen, the two 17,500 DWT sister ships, have a length of 155 m and their operation exclusively inside the Baltic and North Sea ECA was a major reason for their hybrid system configuration. The Orca Energy battery pack assists both on the hotel load and propulsion [65].

In 2019 the Aurora Spirit, a 125,000 DWT shuttle tanker owned by Teekay Offshore, was launched, equipped with a 610 kWh Li-ion battery by Corvus Energy and conventional LNG engines. The flexible power distribution system supplied by Wärtsilä utilizes peak shaving while engines operate at constant load and as a result, significant decreases in the annual energy consumption are achieved.

Norled's Ampere was the world's first all-electric car and passenger ferry and it was launched in 2015, Figure 3.18. Covering a route of 6 km between Lavik and Oppedal in about 20 minutes, the aluminum catamaran vessel is powered by a 1090 kWh Corvus Energy battery pack that weighs 11 tonnes [66]. The ferry has a capacity of 350 passengers and 120 vehicles and its length is 76 m. During the 10 minute boarding of the passengers and cars, the vessel's battery pack is being recharged by electricity produced by hydropower and stored in a 260 kWh battery at each dock [67]. The all-electric ferry saves about 1 million liters of diesel and emits 37 tonnes of NO_x less per year.

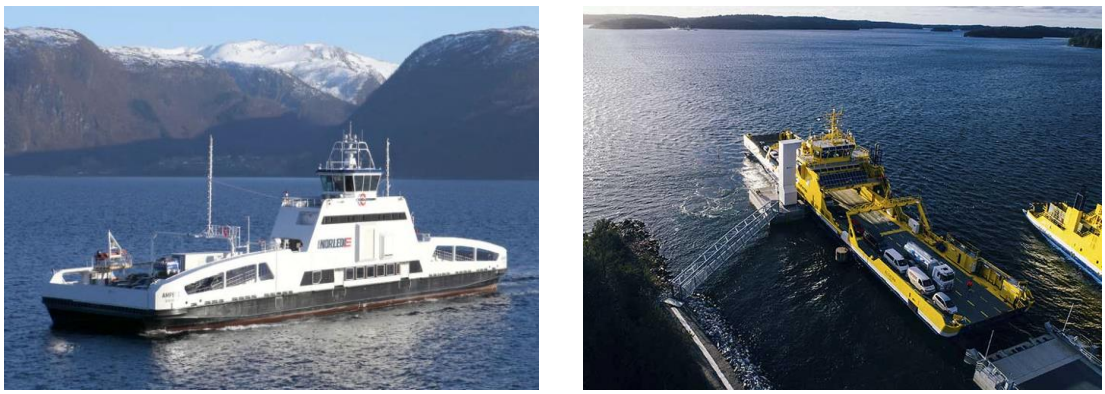

Figure 3.18: The Ampere (left) and the Electra (right) ferries (sources: CruiseShip Portal & SPBES)

Since 2017, Electra travels between Nauvo and Parainen in the Turku archipelago, Finland. Operated by FinFerries, it was the first hybrid/electric Ro-Ro to recharge its battery directly from the domestic power grid [68]. The ferry is equipped with two

SPBES 530 kWh battery packs, each one powering a 900 kW azimuth thruster, placed at each end of the ship. Three diesel generators are also installed and contribute to the loads. During each voyage, about 15% of the batteries' capacity is consumed, while the total lifetime of the packs is 10 years. The ferry docks with a vacuum auto-mooring system and the batteries charge for about 5 minutes during the embarkation. As part of the hybrid system, the vessel employs additionally photovoltaic cells, resulting in 60% fewer emissions compared with the other ship that operates on the route.

4 Case Study

In this chapter, the conceptual hybridization of a bulk carrier's electric grid is under study. One of the diesel generators installed on board was replaced by a lithium-ion battery pack, whose dynamic behavior was modeled utilizing a high fidelity battery model.

4.1 The vessel under study

The examined ship is a 171,000 DWT bulk carrier, which has a total length of 279 m, a breadth of 45 m, a depth of 24.1 m and a design draught of 16.50 m. It was built in 2012 and it is equipped with an HYUNDAI-B&W 6S70MC main engine, with 22,920 BHP maximum continuous rating, at 91 RPM. The ship's electricity generation plant comprises three HYUNDAI-HiMSEN 8H17/28 diesel generators, Figure 4.1, whose specifications are presented in Table 4.1.

Table 4.1: The specifications of the three diesel generators installed on board

Engine	
Type	8H17/28
MCR	920 kW
Speed	900 RPM
Generator	
Model	HFC7 506-84K
Output	1081.3 kVA, 865 kW
Voltage	450 V
Current	1387.2 A
Frequency	60 Hz
Poles & PF	8 P, 3 PHA, 0.8 PF

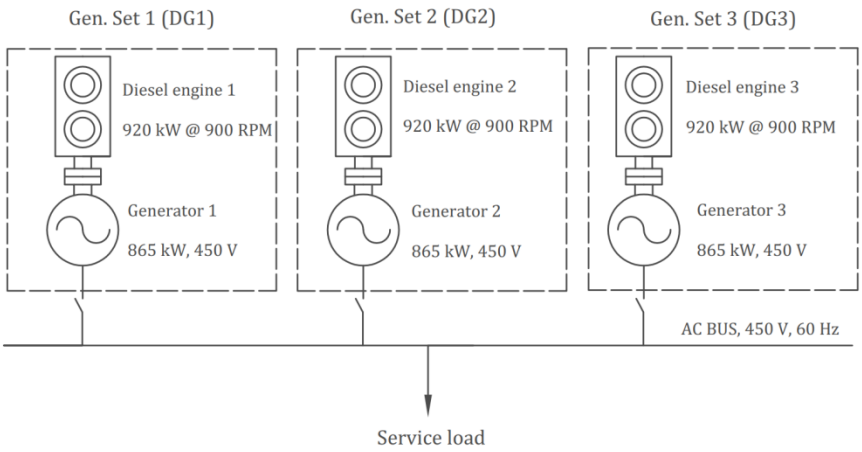

Figure 4.1: The existing electricity generation plant of the ship

Actual measurements of the three generator sets' power output and fuel oil consumption were utilized in this study. The sum of the outputs was considered as the

load the proposed hybrid power system had to cover, Figure 4.2. The comparison between the efficiency of the two power systems was carried out for three trips, each lasting approximately twenty days. Each trip consists of the sailing period and the two port stays, in Port A and Port B, respectively. It can be noticed that during the port stays there are load fluctuations, for which maneuvering, ballasting or deballasting, crane or/and hatch cover operation, and mooring are typically responsible.

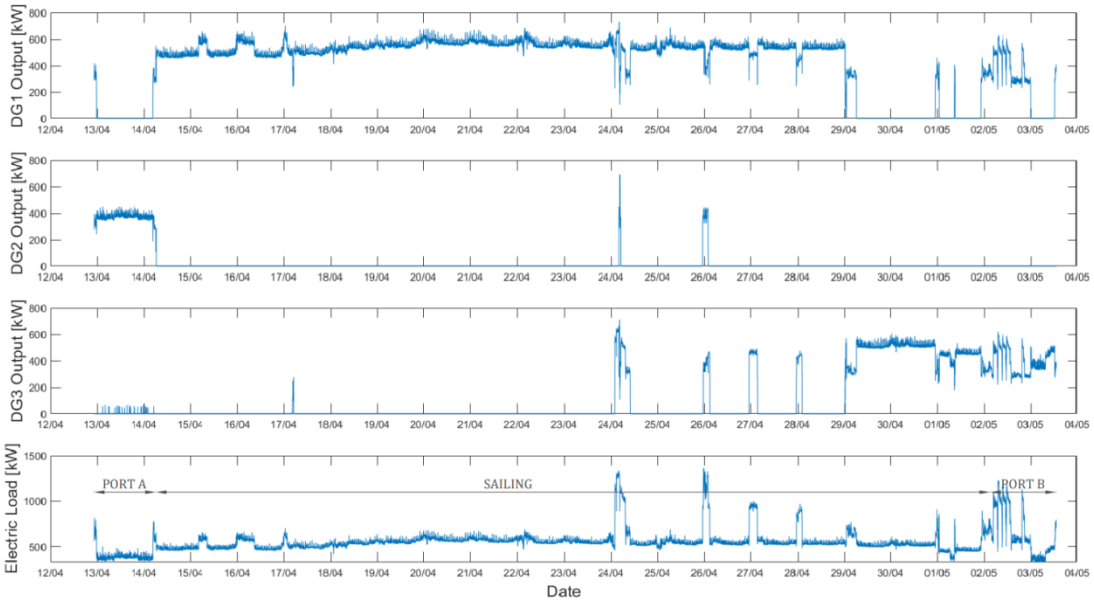

Figure 4.2: The generator sets' output measurements and their total for the first voyage

4.2 The proposed hybrid power system

The proposed HPS in charge of the electricity generation on board deploys a lithium-ion battery pack, which replaces one of the installed diesel generators, Figure 4.3. Given the fact that the battery operates with direct current and the rest of the power system with AC, a power converter is necessary. The general concept of this configuration is the operation of the two engines in their optimal loading condition and the charging or discharging of the battery pack, depending on whether there is energy excess or deficit. Of course, like any other major changes made on a vessel, this hybridization concept needs to be approved by the class. This study is a first-order analysis that complies with the basic rules described in paragraph 3.2.6.

4.2.1 Generator sets

In paragraph 3.1.1 was displayed that the SFOC curve has a minimum value, which typically corresponds to a load somewhere in the range of 60% - 100% of the MCR. In this case, since the SFOC curve of the engines wasn't available, in order to determine their optimum loading condition, as well as to decide which generator set was going to be replaced by the battery, the fuel consumption measurements of the three generators were compared for four loads; 70%, 75%, 80% and 85% of the MCR. It was found that from these loading conditions the more fuel-efficient was at 80% of the MCR, Table 4.2. An approximation of the SFOC curve is presented in Figure 4.4. In 80% of the MCR, the

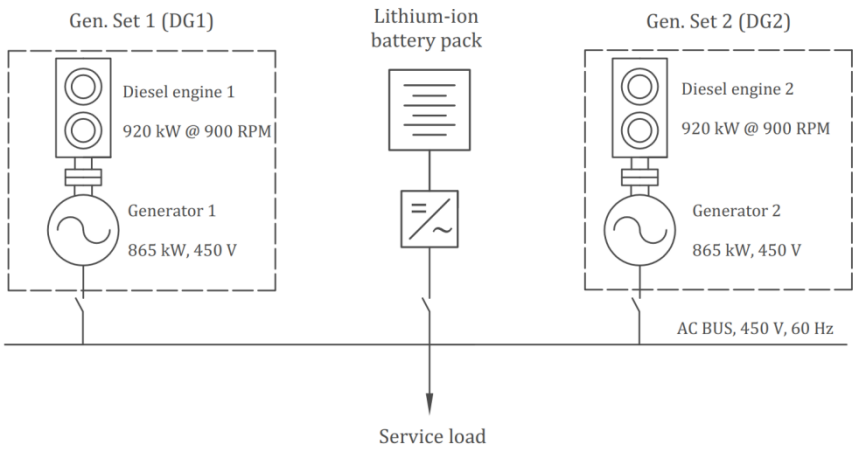

Figure 4.3: The proposed hybrid system for the generation of electricity on board

No. 2 diesel generator (DG2) displayed much higher instant fuel consumption than the two other gensets and for that reason, it was the diesel generator that gave its place to the battery pack, Table 4.3. Therefore, the second diesel generator of Figure 4.3 is actually the No. 3 diesel generator (DG3) of the original power system. Dismissing the value of the instant consumption of DG2, the average consumption of the two remaining engines was calculated and the SFOC was found equal to 208.89 g/kWh.

Table 4.2: The SFOC for the four studied loading conditions

Load (%MCR)	**70%**	**75%**	**80%**	**85%**
Average SFOC (g/kWh)	245.59	229.23	220.06	237.17

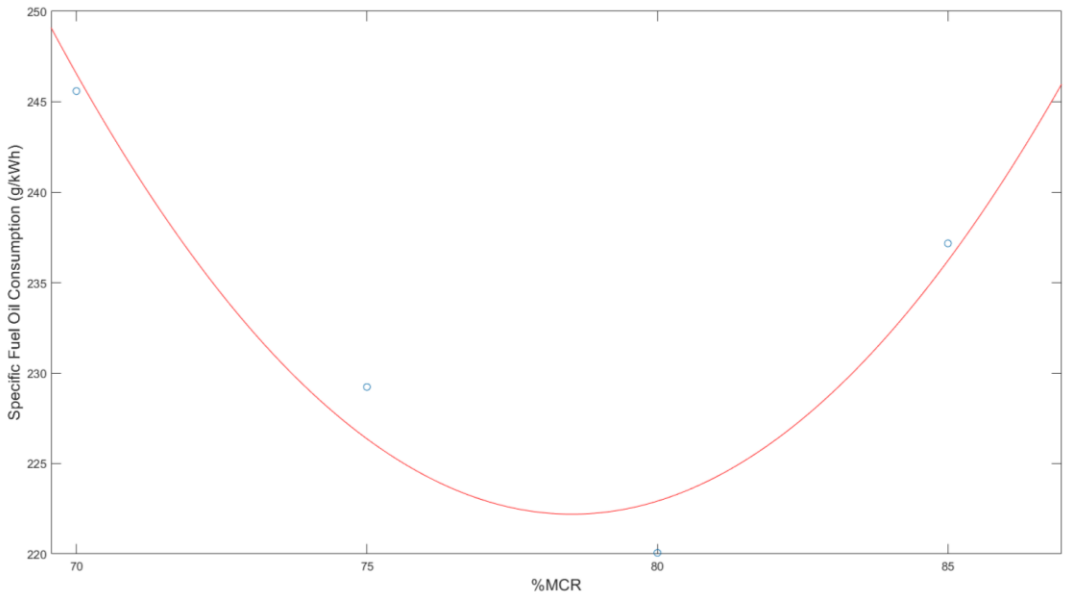

Figure 4.4: The estimated SFOC curve of the three engines

Table 4.3: The instant fuel oil consumption of the three engines at 80% of MCR

	DG1	DG2	DG3
Average instant FOC (t/24h)	3.6895	4.2815	3.6903

This value is higher than the one measured in the shop tests, at the 100% of MCR load, and definitely higher from the one given in the manufacturer's specification sheet. That's due to the engine's aging and differences in the ambient conditions under which the measurements were made.

4.2.2 Battery

4.2.2.1 Modeling

To examine the performance and efficiency of the proposed hybrid system, the battery installment needs to be properly modeled. Realistic battery modeling is a complex task, as the discharging is characterized by non-linear phenomena, like the decline of the output voltage. Furthermore, the effective capacity of the battery pack drops as the discharge current increases. These parameters, as well as temperature effects and aging, are represented in different battery models.

High fidelity battery models fall into three main categories; experimental, electrochemical and electric circuit-based. As the first two types are not appropriate for state of charge estimation, which is vital for this investigation, a simple equivalent circuit model by Tremblay & Dessaint is employed in this study [69]. This model represents the dynamic behavior of many battery technologies – including lithium-ion, using a controlled voltage source in series with a resistance, Figure 4.5.

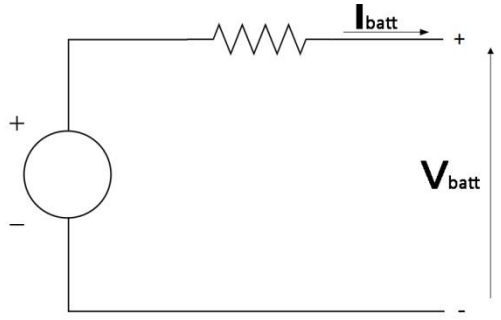

Figure 4.5: The equivalent circuit model of a battery

In this model, the only state variable is SOC and the internal resistance is considered constant during charging and discharging. Also, the amplitude of the current doesn't affect the resistance, just like it's not affecting the capacity of the battery, meaning there is no Peurkert effect. Finally, the temperature influence is neglected in the model, as well as the self-discharge of the battery.

The battery voltage can be calculated with the below equation, Figure 4.5:

$$V_{batt} = E - R\, I_{batt} \tag{4.1}$$

where

R is the internal resistance (Ω)
I_{batt} is the battery current (A)
E is the no-load voltage (V), which is calculated in this model via the following formula:

$$E = E_0 - K\frac{Q}{Q - \int I_{batt}\, dt} + Aexp(-B\int I_{batt}\, dt) \tag{4.2}$$

where

Q is the battery capacity (Ah)
E_0, K, A and B are the model parameters

As stated in Chapter 3, the module discharge curves are essential for its modeling, as model parameters are derived from them. These curves alongside other important specifications of the module are sometimes provided by the manufacturer. For this particular model, five values are of interest and they are extracted from the curves; the fully charged voltage (E_{Full}), the end of the exponential zone voltage (E_{Exp}) and charge (Q_{Exp}), and lastly, the end of the nominal zone voltage (E_{Nom}) and charge (Q_{Nom}). These points can be seen in Figure 4.6. The precision in which they are obtained has an impact on the overall performance of the model. Despite the fact that the model's parameters are extracted from the discharge characteristics of the module, their values are supposed to be the same for charging, too.

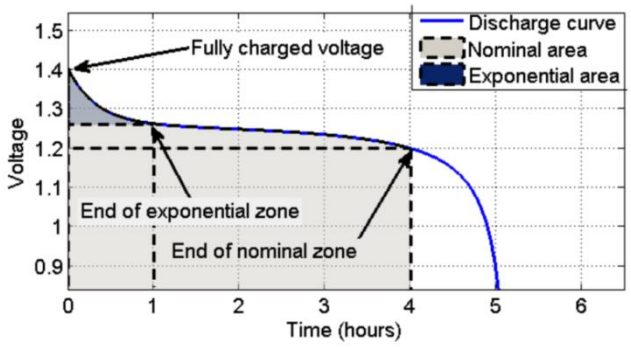

Figure 4.6: A typical discharge curve and the five points of interest for the battery model [69]

Having the above points, the model parameters can be calculated. The voltage drop during the exponential zone (A) is estimated as follows:

$$A = E_{Full} - E_{Exp} \tag{4.3}$$

The charge at the end of the exponential zone (3/B):

$$B = \frac{3}{Q_{Exp}} \tag{4.4}$$

The polarization voltage (K):

$$K = \frac{(E_{Full} - E_{Nom} + A(e^{-B\,Q_{Nom}} - 1))(Q - Q_{Nom})}{Q_{Nom}} \tag{4.5}$$

Finally, the voltage constant (E_0):

$$E_0 = E_{Full} + K + R\, I_{batt} - A \tag{4.6}$$

Regarding the internal resistance R of the cell, even though its value is generally given in the manufacturer's datasheet, the model's authors claim that this value may not allow the accurate modeling of the battery cell. For that reason, they propose the following formula through which a starting point for the estimation of the resistance can be obtained:

$$R = V_{Nom} \frac{1 - \eta}{0.2\, Q_{Nom}} \tag{4.7}$$

where

η is the average efficiency of the module

The state of charge at the i-th moment of the simulation is estimated using the Ampere-hour counting method:

$$SOC(i) = SOC(i-1) - \frac{1}{Q} \int I_{batt}(i)\, dt \tag{4.8}$$

where

SOC(i-1) is the state of charge at the previous moment

The above equations are employed in the modeling of the behavior of a single battery module. As the bulk carrier's electric grid has significant power demands, many modules are connected both in series and in parallel, forming the battery pack. This makes possible to achieve the desired battery pack capacity, as well as the required voltage and current levels.

In order to model the charging and discharging process of the battery pack, the DC battery system is studied. Its power is given by the following formula:

$$P_{batt} = V_{batt}\, I_{batt} \tag{4.9}$$

Using the Equation (4.1) we get:

$$P_{batt} = (E - R\, I_{batt})\, I_{batt} \tag{4.10}$$

and by replacing the no-load voltage from Equation (3.1):

$$P_{batt} = \left(E_0 - K \frac{Q}{Q - \int I_{batt}\, dt} + Aexp(-B \int I_{batt}\, dt) - R\, I_{batt} \right) I_{batt} \tag{4.11}$$

where the constants are given by the Equations (4.3), (4.4), (4.5) and (4.6).

The above equation is being solved numerically every moment of the simulation, to determine the current I_{batt} that is coming in or out of the battery. This is illustrated in

Figure 4.7, where the load was 650 kW, the power the battery had to provide was 691.49 kW and the current was found equal to 2173.9 A. This value corresponds to a specific battery pack configuration, with 8 modules connected in-series and 30 in-parallel. Generally, during discharging the battery current, and as a result, the battery power is positive, while during charging these magnitudes are negative. Having estimated the battery current, the SOC of the battery is calculated using Equation (4.8).

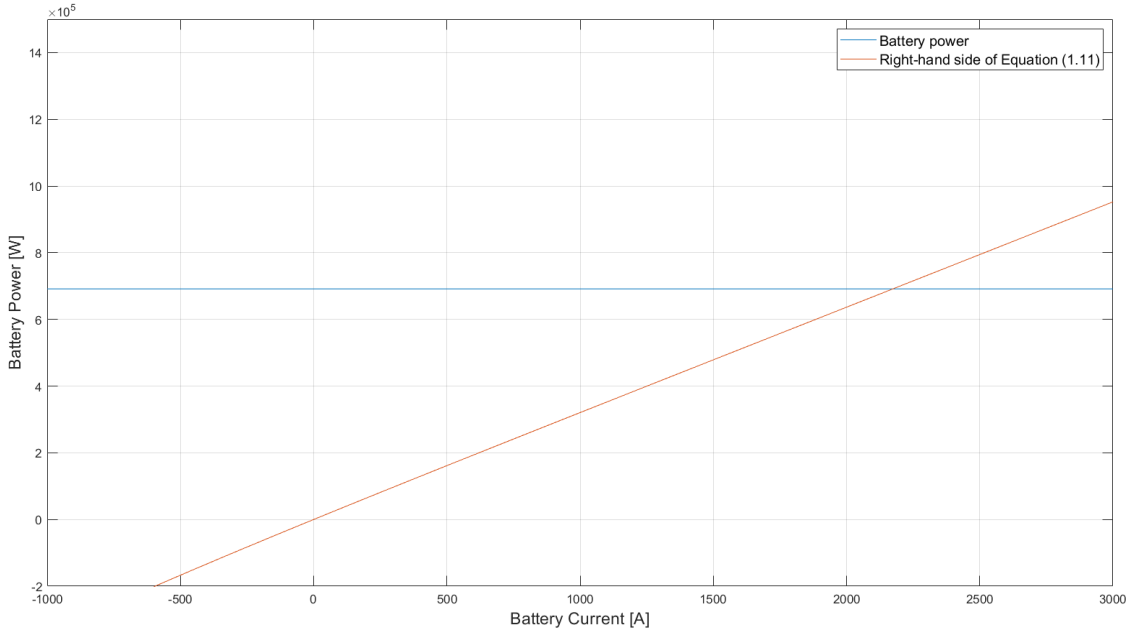

Figure 4.7: The numerical estimation of the battery current for a certain load

Concerning the determination of the charging/discharging power of the battery pack, three important parameters shall be taken into account; the generator shaft efficiency (η_s), the efficiency of the converter (η_{conv}) and the charging/discharging efficiency of the battery (η_{ch}, η_{disch}).

The actual electric power demand of the ship is not exactly equal to the sum of the engines' output measurements, but in fact, the demand is the sum multiplied by the shaft efficiency. The power losses on the shaft of the generator lead to heavier operation of the coupled diesel engine, in order to be able to supply the entire load, Figure 4.8. To this effect, when the battery charges the actual charging power is lower than the system's excess power, as the charging efficiency and the losses on the converter tend to reduce it. The same applies to the discharging process, even though in this study the discharging efficiency was taken equal to one. The energy flow in the original power system (OPS) and the hybrid one are illustrated in the form of Sankey diagrams in Figure 4.9. Despite the fact that charging and discharging the battery has as a result lower system efficiency, the more efficient operation of the gensets in the HPS is expected to reduce the total fuel burnt.

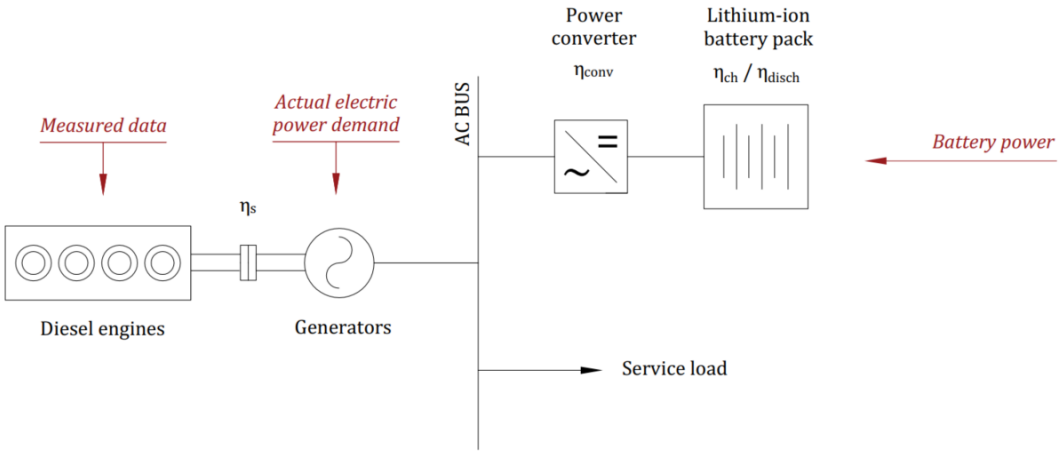

Figure 4.8: The several efficiencies of the hybrid power system's parts

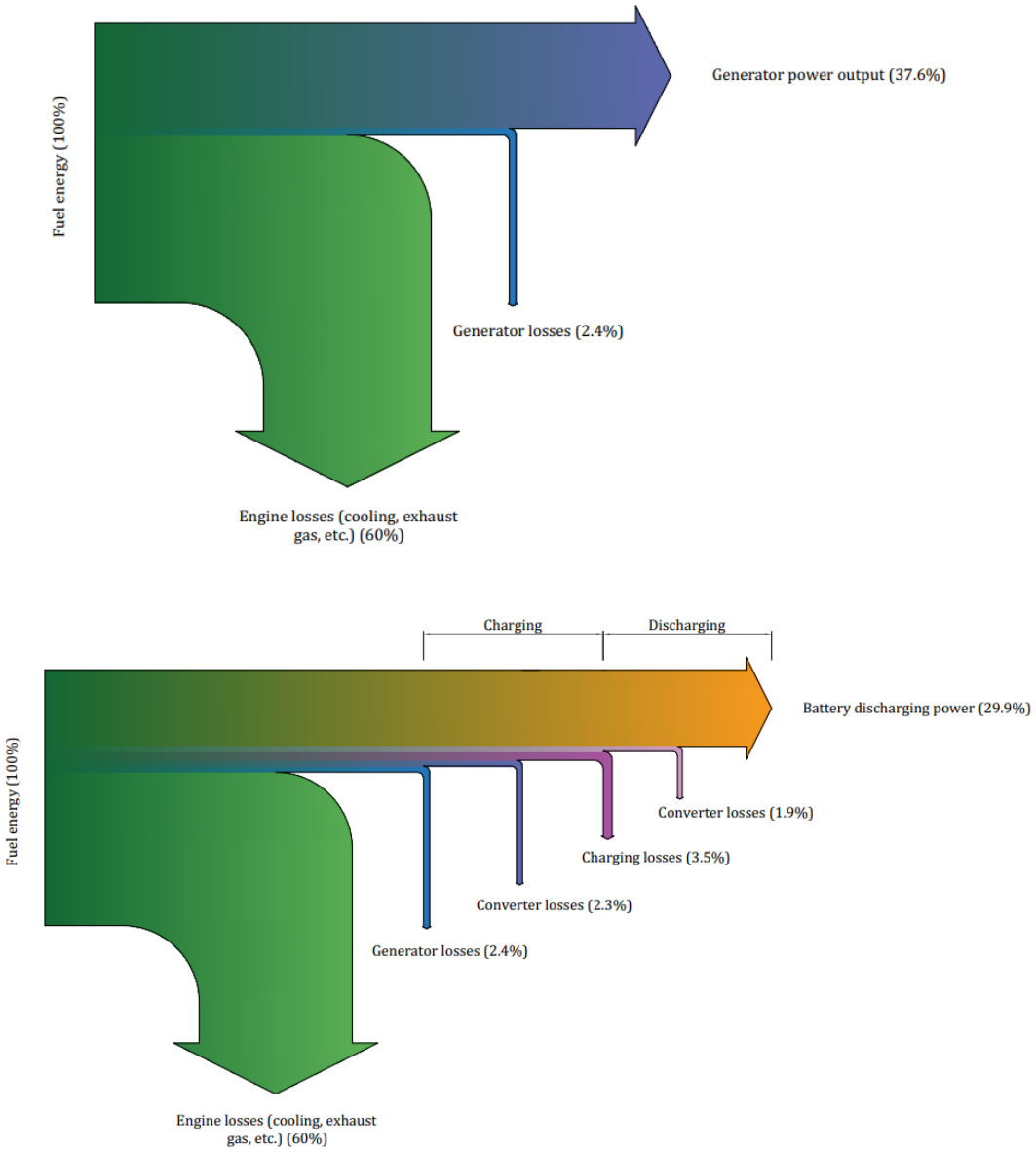

Figure 4.9: The Sankey diagrams for the original (top) and the hybrid (bottom) power system

Taking into consideration the above factors, the charging and discharging process of the battery can be modeled. The magnitude of the charging/discharging power is determined depending on the way the hybrid power system covers the load. For instance, when the diesel generators are off and the entire load is supplied by the battery pack, the power it has to deliver is equal to:

$$P_{disch} = \frac{P_{load,meas}\,\eta_s}{\eta_{conv}\,\eta_{disch}} \tag{4.12}$$

where

$P_{load,meas}$ is the sum of the measurements of the engines' instant power outputs at this moment (kW)

Similarly, when the battery is charging with the excess energy from the operation of a diesel engine the charging power is equal to:

$$P_{ch} = (P_{DG} - P_{load,meas})\,\eta_s\,\eta_{conv}\,\eta_{ch} \tag{4.13}$$

where

P_{DG} is the power output of the operating diesel generator at this moment (kW)

4.2.2.2 Module selection and battery model validation

The battery module selection process for the ship's hybrid system is limited by the availability of the discharge curves of each module, as the implementation of a battery model that provides an accurate representation of the battery dynamics requires these curves. Many manufacturers don't provide them and as a result, the use of their batteries is not possible, as the curves are essential for the model above and generally for most models.

After research on several battery manufacturers' websites, the Valence U-Charge® U27-36XP module was selected, Figure 4.10. Its cells' chemistry is lithium iron phosphate ($LiFePO_4$), which is known for long cycle life and excellent safety. This module is DNV GL and ABS approved, and its specifications are presented in

Table 4.4. The discharge curves for four different C-rates, at 23°C ambient temperature are shown in Figure 4.11.

Figure 4.10: The Valence U-Charge® U27-36XP module (source: LithiumWerks)

Having the module's discharge curves, it's possible to validate the battery model, i.e. its ability to represent the module's dynamic behavior. To achieve this, the five necessary values for each C-rate were extracted from the manufacturer's discharge curves. They are presented in Table 4.5. Then, the model parameters were calculated, in the manner described in the previous paragraph. Their values can be seen in Table 4.6.

Table 4.4: Valence U-Charge® U27-36XP module specifications (source: LithiumWerks)

Electrical Specifications	
Voltage (nominal)	38.4 V
Capacity @ C/5, 25 °C (typical)	50 Ah
Energy	1.92 kWh
Discharge Cont./Peak (30 sec)	100 A / 150 A
Discharge Cutoff Voltage	30 V
Recommended Charge Voltage	43.8 V
Discharge Temperature	-10 °C to 50 °C
Charge Temperature	0 °C to 45 °C
Self Discharge @ 25 °C	< 2% per month
Specific Energy	102 Wh/kg
Energy Density	162 Wh/l
Charge Efficiency	> 90%
Cycle Life (@80% DOD)	> 4000 cycles
Cycle Life (@70% DOD)	> 10000 cycles
Mechanical Specifications	
Height (excluding bolts)	225 mm
Width	172 mm
Length	306 mm
Weight	18.7 ± 0.1 kg
IP Rating	IP56

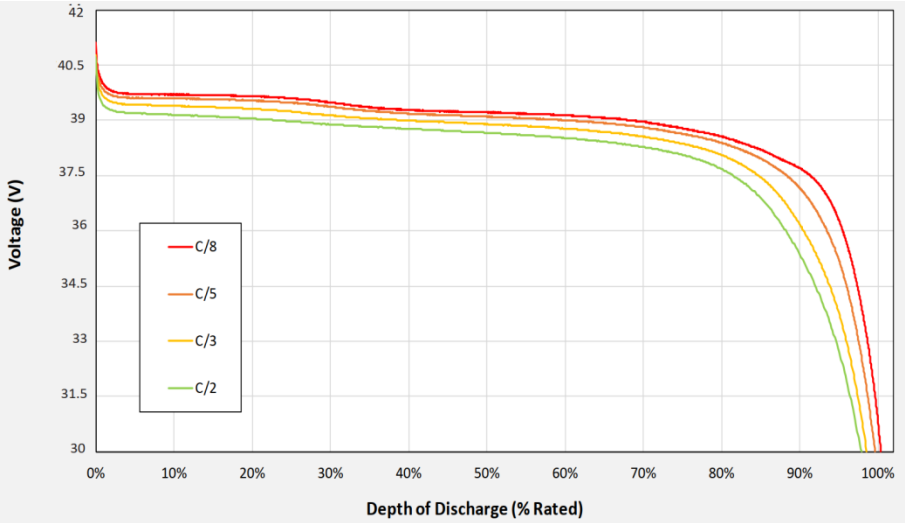

Figure 4.11: The discharge curves of Valence U-Charge® U27-36XP module, at 23°C ambient temperature (source: LithiumWerks)

The battery model was implemented in MATLAB® and its validation was accomplished by comparing by superposition the manufacturer's discharge curves with those obtained with the model, Figure 4.12. In this figure, it can be observed that the battery model achieves a quite accurate representation of the dynamic behavior of the U27-36XP module.

Table 4.5: The values extracted from the manufacturer's discharge curves

C-Rate	Discharge curve values				
	E_{Full}	E_{Exp}	Q_{Exp}	E_{Nom}	Q_{Nom}
C/8	41.1633	39.7449	1.9807	38.4000	41.4010
C/5	40.8878	39.6429	1.4493	38.4000	40.0000
C/3	40.7653	39.4286	1.8116	38.4000	37.6087
C/2	40.7143	39.2041	1.8357	38.4000	33.5024

Table 4.6: The model parameters for each C-rate

C-Rate	Model parameters				
	A	B	K	E_0	R
C/8	1.4184	1.5146	0.2793	40.1055	0.013
C/5	1.2449	2.0700	0.3107	40.0836	0.013
C/3	1.3367	1.6560	0.3389	39.9841	0.013
C/2	1.5102	1.6342	0.3960	39.9250	0.013

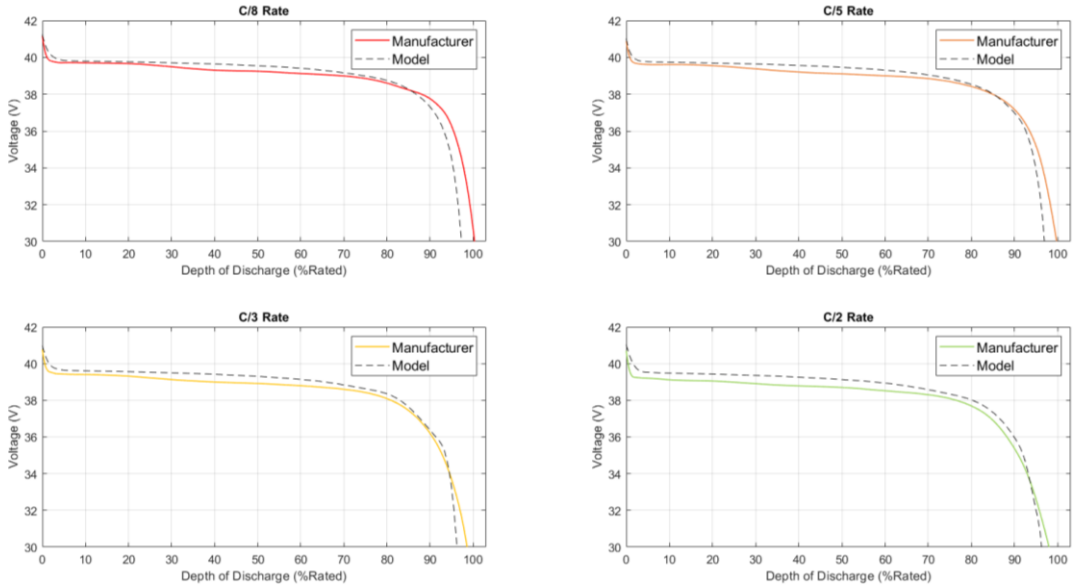

Figure 4.12: The validation of the battery model for each C-rate discharge curve

Regarding the resistance value that was used in the above simulations, since the manufacturer's datasheet doesn't include this parameter, four different values were examined to achieve the best accuracy; the one derived from the model's proposed formula (0.48 Ω), two values from similar battery modules made by another manufacturer (0.017 Ω, 0.013 Ω) and one slightly higher than those two (0.024 Ω). That was investigated for the C/5 rate and it was found that the model's fidelity was

improving with the decrease of the resistance, Figure 4.13. Therefore, the resistance was taken equal to 0.013 Ω.

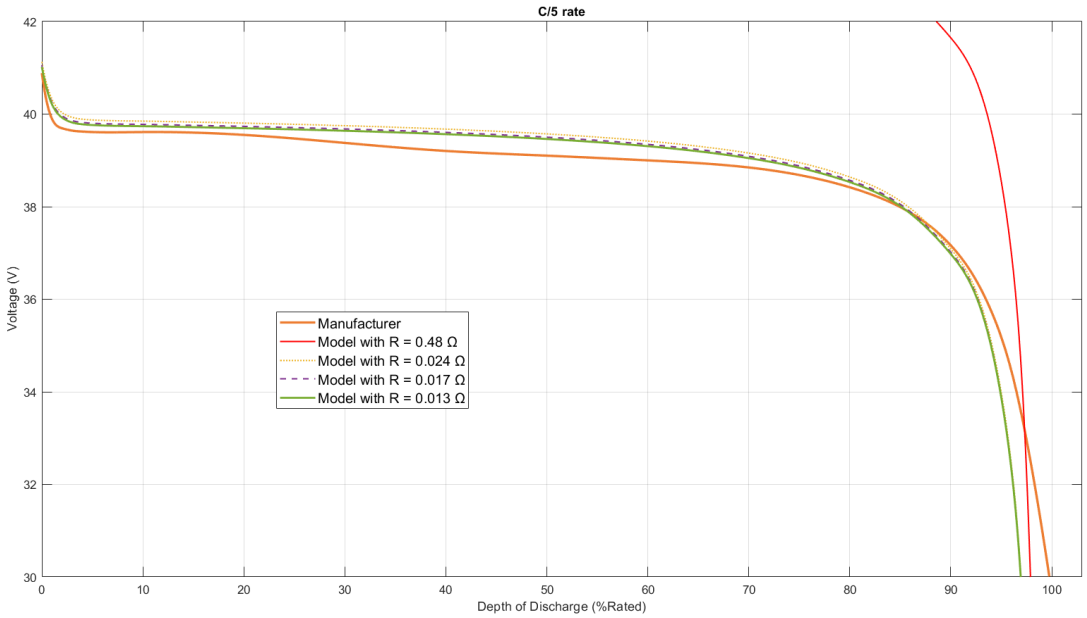

Figure 4.13: The examination of which resistance value results in the highest model accuracy

4.2.2.3 Modules configuration

Since the battery model described earlier represents accurately the dynamic behavior of the selected module, it was used in the modeling of the whole battery pack that was installed on board.

The battery pack consists of a number of modules connected in parallel, $n_{parallel}$, and some modules connected in series, n_{series}. With the series connection, the required voltage output is met, while with the parallel connection the desired capacity and the necessary current output are achieved, Figure 4.14. During battery operation, all the modules are assumed that they are charging and discharging with the same rate, meaning that their individual SOC is the same as the SOC of the entire battery pack. Generally, the balancing of the state of charge of the individual modules is a task for which responsible is the battery management system.

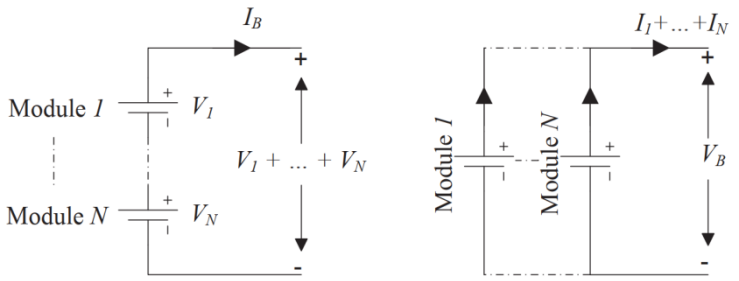

Figure 4.14: The series (left) and the parallel (right) configuration of battery modules [25]

For the proposed hybrid system eight U27-36XP modules were connected in series and different values of $n_{parallel}$ were tested, in order to determine the most fuel and cost-

efficient solution. Generally, the minimum number of modules connected in parallel is defined by the maximum C-rate the battery module can provide. As can be seen in

Table 4.4 the maximum output current of a U27-36XP module is 150 A and its nominal capacity at the C/5 rate is equal to 50 Ah. Due to the lack of additional capacity values, the capacity was assumed constant and independent of the rate in which the battery module is discharging. Dividing the maximum module current with its capacity, the maximum C-rate of the module was found equal to 3C. On the battery pack level, by increasing the number of modules connected in parallel both the capacity and the maximum output current of the pack are scaled up. The quotient of these magnitudes shall not exceed the maximum C-rate mentioned above.

The maximum current the battery has to provide during a simulation alters with the different configuration of modules, i.e. the size of the pack. That is because as the capacity of the pack varies the battery operates on different periods. That has as a result to sometimes supply power in periods with high loads, and thus high current demands and other times under lower current requirements.

The upsizing of the number of parallel-connected modules results in the diminishing of the number of battery cycles during a voyage. That has as an outcome the extension of its lifetime and the minimization of the times the battery pack has to be replaced throughout the life of the vessel. Additionally, the higher the capacity of the battery pack, the lower the discharging currents, which also affect the longevity of the battery.

The model parameters defined in paragraph 4.2.2.1 are calculated for the whole battery pack in correlation with the model parameters of a single module [32]:

$$Q_{pack} = \mathrm{n}_{\mathrm{parallel}}\, Q \tag{4.14}$$

$$R_{pack} = \frac{\mathrm{n}_{\mathrm{series}}}{\mathrm{n}_{\mathrm{parallel}}}\, R \tag{4.15}$$

$$E_{Full,pack} = \mathrm{n}_{\mathrm{series}}\, E_{Full} \tag{4.16}$$

$$E_{Exp,pack} = \mathrm{n}_{\mathrm{series}}\, E_{Exp} \tag{4.17}$$

$$Q_{Exp,pack} = \mathrm{n}_{\mathrm{parallel}}\, Q_{Exp} \tag{4.18}$$

$$E_{Nom,pack} = \mathrm{n}_{\mathrm{series}}\, E_{Nom} \tag{4.19}$$

$$Q_{Nom,pack} = \mathrm{n}_{\mathrm{parallel}}\, Q_{Nom} \tag{4.20}$$

where

Q, R, E_{Full}, E_{Exp}, Q_{Exp}, E_{Nom}, Q_{Nom} are the model parameters for a module and the left-hand side of the above equations are the model parameters for the battery pack

The energy of each configuration of the battery pack is calculated by integrating equation (4.9):

$$\int P_{pack}\, dt = \int V_{pack}\, I_{pack}\, dt \tag{4.21}$$

By considering V_{pack} as the nominal value of the voltage and by substituting the integral of the battery current with the total battery capacity, the pack's energy is derived:

$$E_{pack} = V_{pack,nom}\, Q_{pack} \tag{4.22}$$

Using equation (4.14):

$$E_{pack} = V_{pack,nom}\, \mathrm{n}_{\mathrm{parallel}}\, Q \tag{4.23}$$

where

$V_{pack,nom}$ = 8·38.4 V = 307.2 V
Q = 50 Ah

4.2.3 Power converter

Since the ship's distribution system operates with alternating current and the lithium-ion battery pack uses DC, power conversion is required. Generally, since during the charging process the power flows from the AC bus to the battery, a rectifier is employed, which converts AC to DC. Similarly, during discharging an inverter converts the DC into AC, to be supplied to the ship's loads. Recently bi-directional converters have become available, combining the two above functions. Furthermore, complete conversion systems, which embody the required transformers, circuit breakers, etc. have emerged.

Table 4.7: The EssPro c1000 power converter module specifications

Power	500 - 1250 kW
Connection frequency	50 or 60 Hz
DC voltage range	250 - 1120 V
AC voltage range	200 - 480 V
System efficiency (including transformer)	>94%
Converter efficiency	>97%
Ambient temperature range	-30°C to +50°C
Cooling	Forced air, HVAC and chillers
Overload	120% for 10 min 150% for 30 sec 200% for 2 sec

A solution of that kind was selected for this case study, namely the ABB EssPro™ Power Conversion System. It comes in scalable pre-packaged modules or as a fully

containerized solution [14], Figure 4.15. Two EssPro c1000 modules connected in parallel were integrated into the vessel's grid, in order to meet the required power level. In this way the output power capability is increased, the thermal stress is distributed over a broader area and there is redundancy in the case of failure [70]. The module's specifications are presented in Table 4.7.

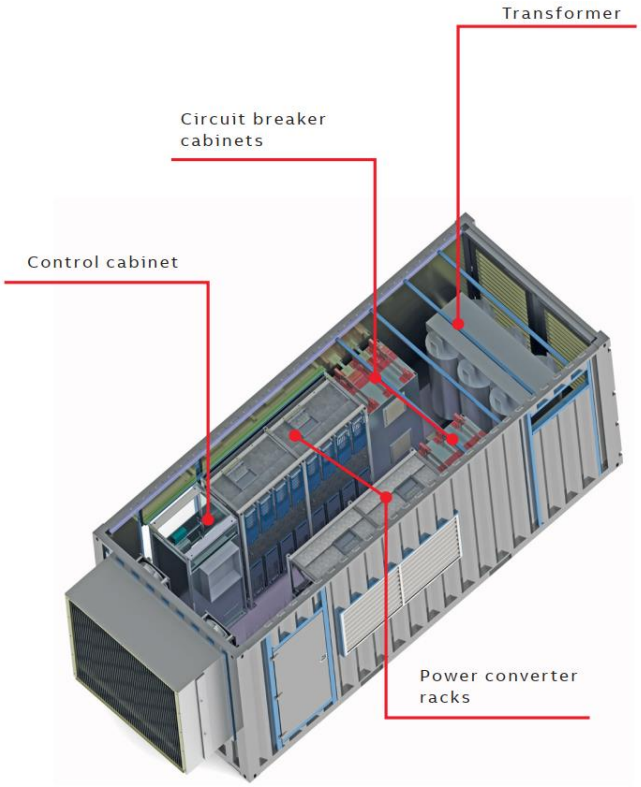

Figure 4.15: The containerized version of the EssPro™ PCS (source: ABB)

5 Energy Management System

Hybrid power systems, due to the employment of multiple power sources, require a control strategy that dictates the division of power between the components of the hybrid system. This is usually referred to as Energy Management System (EMS) and at every moment it determines which parts will contribute and to what degree, in order to fulfill the power demand. Here a rule-based strategy was developed in MATLAB®, which via a set of rules and depending on some key parameters, decides how the load is going to be covered.

5.1 Philosophy

The first parameter that influences the EMS's decision regarding the split of power between the diesel generators and the battery pack is the magnitude of the load. The power demand is divided into four regions; region A, B, C and D, Figure 5.1. Region A is the low load zone and it's confined by an upper limit, P_{min}, which was taken equal to 600 kW. That corresponds to 65% of the engines' MCR. Region B is limited by the predetermined operation point of a single engine, while region C by the combined power output of the two diesel engines. Lastly, in region D the power demand is higher than the combined output of the two diesel engines.

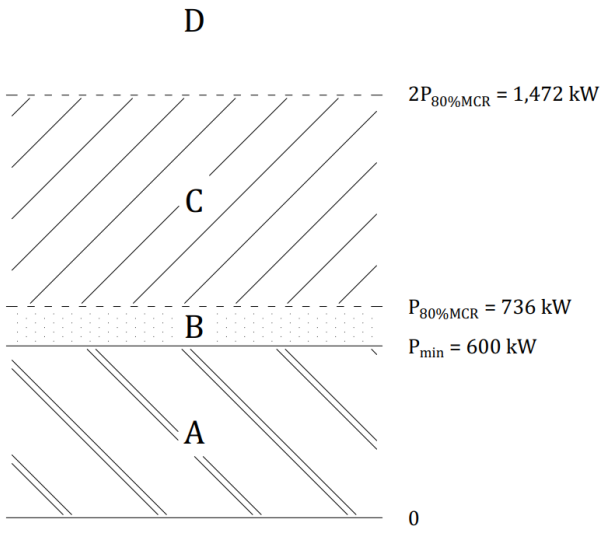

Figure 5.1: The division of the instantaneous power demand into four regions

The fundamental principle of the particular EMS is the fact that the two diesel generators run exclusively at a predetermined operation point, which is their optimum loading condition. The logic of this decision is based on the fact at this point the fuel consumption is minimized. In the previous chapter, it was displayed that this occurs at 80% of the MCR, namely 736 kW. Through this restriction, low-load engine operation, which results in increased fuel consumption and maintenance, is avoided. The utilization of the battery pack offers the advantage of peak-shaving operation; when the engine's power falls short of the demand the battery contributes by discharging, while in the opposite situation the battery charges, utilizing the diesel engine's excess energy.

Another crucial parameter for the management strategy is the SOC of the battery pack. Fully charging or discharging the battery has a negative effect on its longevity [13]; therefore the developed EMS attempts to confine the SOC between a minimum and a maximum value, SOC_{min} and SOC_{max}. Generally, the deeper the battery discharges, i.e. the higher the value of the depth of discharge, the shorter its lifetime, Figure 5.2. On the other hand, as the SOC_{min} value decreases the operational range of the battery is augmented and thus, longer discharging is possible.

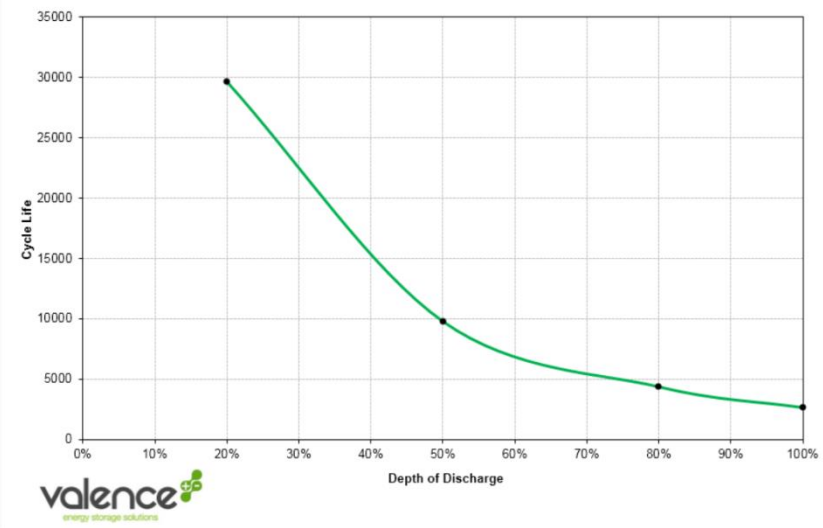

Figure 5.2: The influence of the DOD to the lifetime of a module (source: LithiumWerks)

In this study two SOC_{min} values were examined, 20% and 30%, as for these values the cycle life was provided by the manufacturer. Regarding the SOC_{max}, its value was taken equal to 90%, as that is a value commonly used in relevant publications [25], [71], [21]. Nevertheless, at the beginning of each simulation, the SOC was set to 100%. Based on the instantaneous SOC, the generator sets are turned off or on and similarly, the battery discharges or charges.

Regarding the operation of the generator sets, a minimum uninterrupted operation time of about 40 minutes is aimed, since it is neither practical nor economical to constantly starting and shutting them off. In that regard, an indicator for the state of each genset was used, n_1 and n_2. Every moment the engine is running the indicator is increased by one and under some circumstances, its value is zeroed. Whether a diesel generator is already running at a specific moment or not affects the EMS output, in a way that will be illustrated later.

Apart from counting the duration of each operating session of an engine, the total genset's runtime in the course of a voyage, N_i, is measured. That enables the balanced operation of the two installed engines, which is always endeavored at a vessel, for reasons related to engine wearing and maintenance. Moreover, since the engines work at a specific loading condition, their runtime is used in the calculation of the total fuel consumption of the trip:

$$FOC_{trip} = SFOC_{80\%MCR}\, P_{80\%MCR}\, (N_1 + N_2)\, 10^{-6} \quad [tonnes] \tag{5.1}$$

where

$SFOC_{80\%MCR}$ = 208.89 g/kWh, the SFOC at 80% of the MCR

$P_{80\%MCR}$ = 736 kW, the predetermined operation point of the diesel generators
N_1, N_2 the total runtimes of the two diesel engines in the course of a voyage (h)

Taking into consideration the values of the above-mentioned parameters during the (i-1)-th moment of the simulation, the energy management system determines whether the i-th moment a diesel generator will be running or not and if the battery will be in charging, discharging or standby mode.

The EMS decision is based on a set of rules, which are applied regardless of the magnitude of the load. These are the following:

i. When one of the diesel generators is already running, i.e. the n_i indicator is different than zero, this engine usually continues to run, unless the EMS decides to shut them off. That might happen because the SOC_{max} value has been reached and the gensets have operated for the minimum required time. Also, if the load decreases significantly while two generators are in operation, the EMS shuts down the genset with the higher total runtime, as it's no longer needed. Similarly, in the case where the load diminishes and falls into the low-load region, and the level of the SOC is sufficient while one genset is running, this generator is being shut down and the battery takes over.

ii. When there is excess energy from the operation of an engine and the battery isn't fully charged, the battery charges until it reaches the SOC_{max} value. If by that time the minimum runtime of the engines has been reached, the engine is being turned off.

In addition to the above, there are some customized rules that are associated with the region of Figure 5.1 the instantaneous load appertains to. The exact EMS logic for each load demand region is presented below.

Region A: In the low load zone, if one diesel generator is already in operation, it continues to run and the excess energy is used to charge the battery. In the case where both engines are running the one with the highest total runtime is turned off, while the other continues to operate. Finally, when neither of the genets is running and the SOC is above the lower limit, the battery discharges and supplies the load. When the SOC is lower than SOC_{min}, the engine with the less runtime is turn on and the battery charges. The EMS strategy for region A is presented in the form of a flowchart in Figure 5.3.

Region B: For this region, there are two possibilities; the load being lower than the operation point of a genset and a far more infrequent condition, where the load coincides with the engine's predetermined output. In the first scenario, the EMS strategy is identical with the logic of region A. In the second case the only distinction is that there is no excess energy and as a result, no battery charging when an engine is running. The flowchart for region B is shown in Figure 5.4.

Region C: In this region, the load can't be supplied by the operation of just one generator. For this reason, when a genset is already running and there is adequate charge in the battery, the battery contributes by discharging. If the SOC is lower than SOC_{min} the second diesel engine is started and the battery charges with its excess energy. Furthermore, in the case where both engines are running their operation is continued and charging takes place. Lastly, in the case where both of the gensets are off, the battery discharges and supplies the load, if the SOC is adequate. When the SOC is low both engines are started and the battery charges. The flowchart for region C is presented in Figure 5.5.

Region D: In the last region a slightly different logic is employed. Since the load is higher than the combined output of the two diesel generators, both engines will be running at all times. When the SOC isn't enough the engine with the higher total runtime runs at the optimum operation point, like all the other cases, while the other operates in a load-following mode. That is the only instance where a generator is operated in this way. Nevertheless, it was noticed that this case never occurred during the simulations of the three voyages. Finally, when the charge of the battery is adequate, both engines run at the predetermined point of operation and the battery supplies the rest of the power needed. The EMS strategy for region D is illustrated in Figure 5.6.

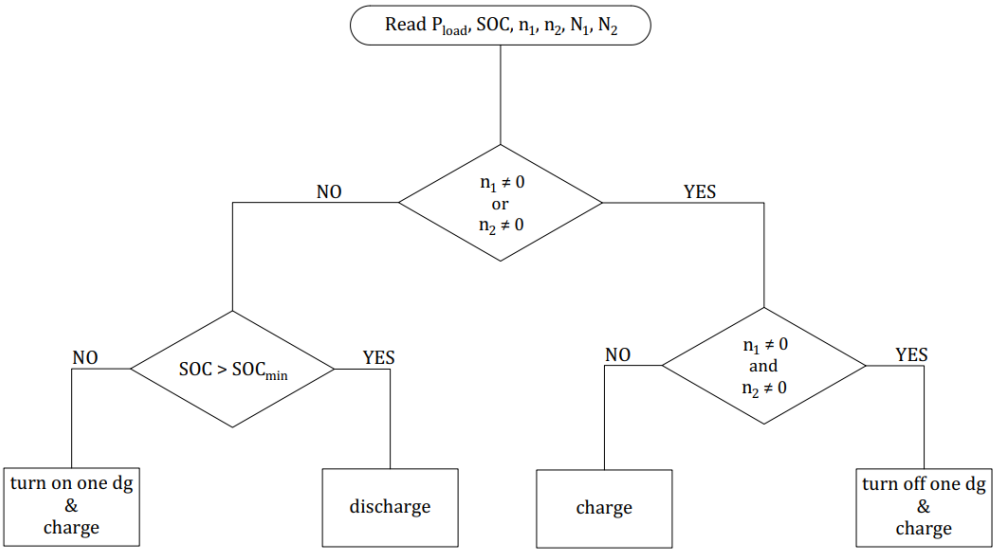

Figure 5.3: The EMS flowchart for region A

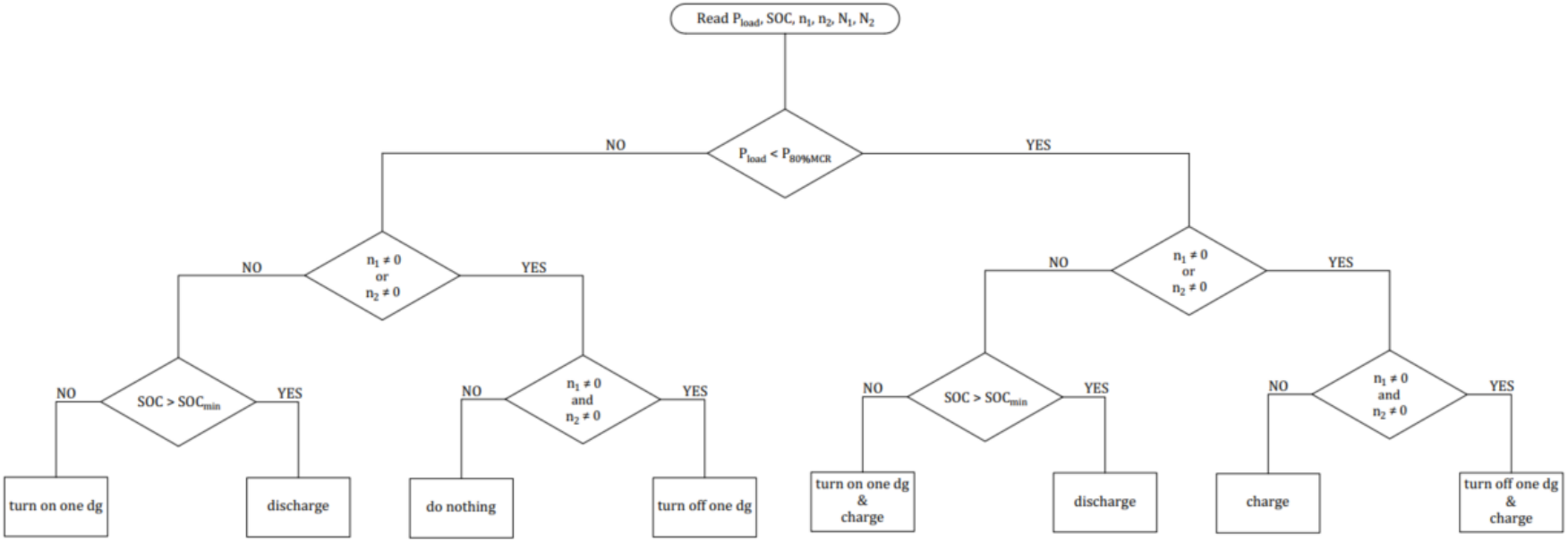

Figure 5.4: The EMS flowchart for region B

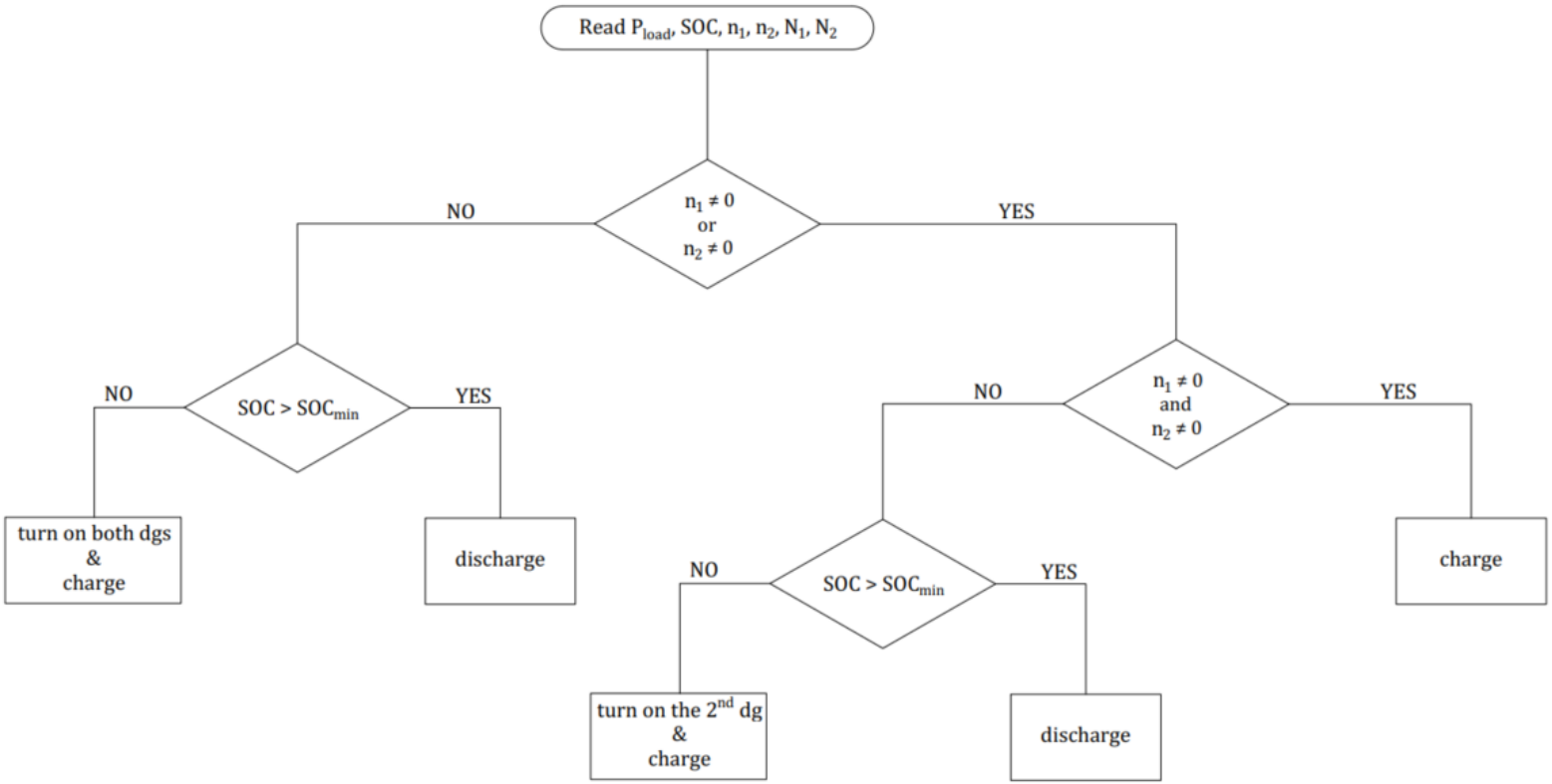

Figure 5.5: The EMS flowchart for region C

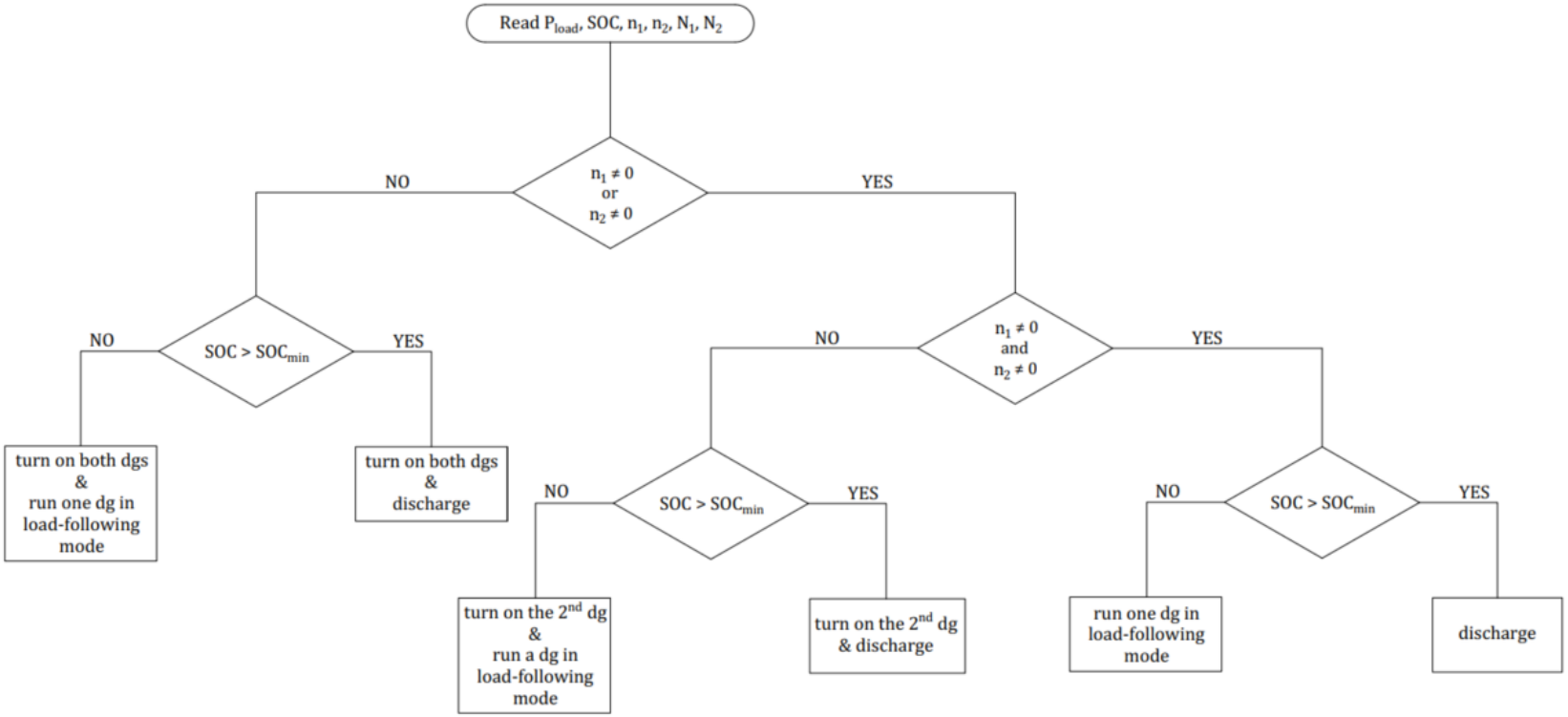

Figure 5.6: The EMS flowchart for region D

6 Results & Discussion

The performance of the proposed hybrid power system was examined via simulations of three voyages, namely Voyage A, B and C, for which power output measurements of the three diesel generators of the original power system were available. This provides a more comprehensive overview of the system's behavior and enables the estimation of results' average values. The hybrid system's efficiency was compared with the original system in terms of fuel consumption, emissions and operating hours of the generator sets.

The impact of the lower limit of the battery pack's state of charge was investigated, by testing two SOC_{min} values. Furthermore, several values of parallel-connected modules were simulated, to assess the performance of various-sized batteries. A feasibility study was conducted, investigating the costs and savings of the hybrid system, in the case when the selected module is utilized and when another one is used. Finally, the case of shutting both diesel generators off and using exclusively the battery during a port stay was examined, because such a prospect would result in significant noise pollution decrease and additional cost reduction.

6.1 The performance of the original power system

As mentioned in Chapter 4 the bulk carrier's original power system consists of three identical generator sets, from which only one is usually running and a second one assists when high loads occur. The sum of the engines' output multiplied with the generator shaft efficiency was considered the load the proposed hybrid system had to cover. The load and the operation of the generators during Voyage A, B and C are presented in Figure 6.1, Figure 6.2 and Figure 6.3, respectively.

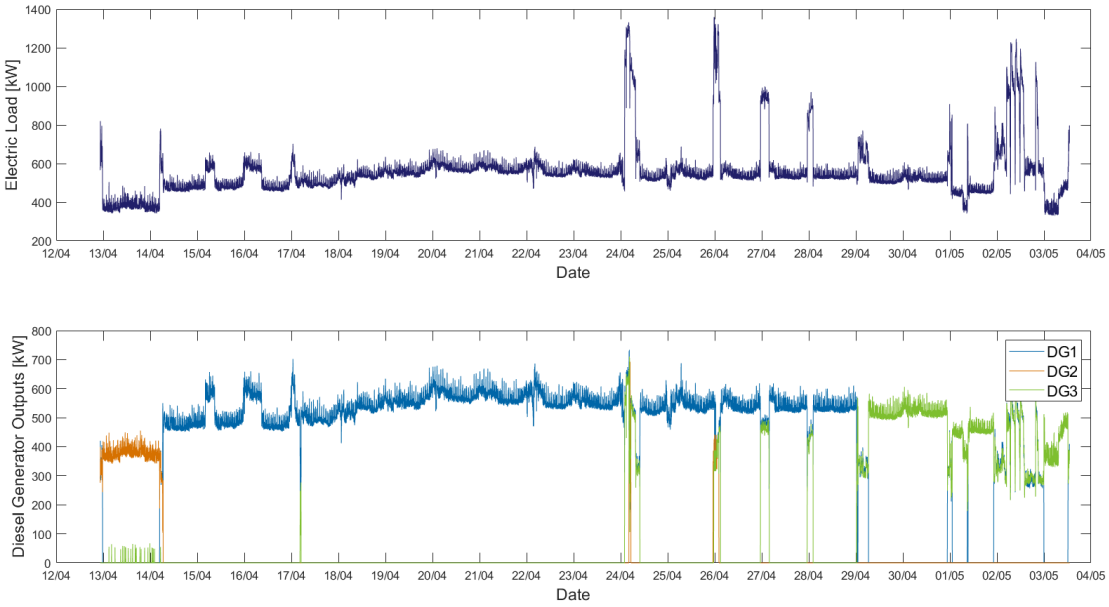

Figure 6.1: The load and the output of the three generator sets of the OPS during Voyage A

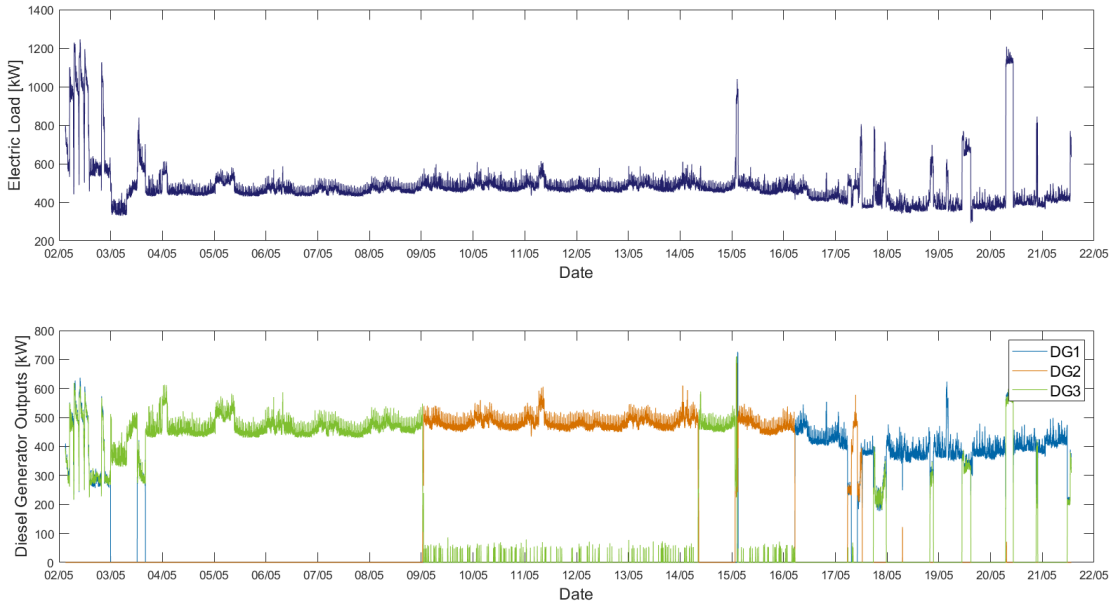

Figure 6.2: The load and the output of the three generator sets of the OPS during Voyage B

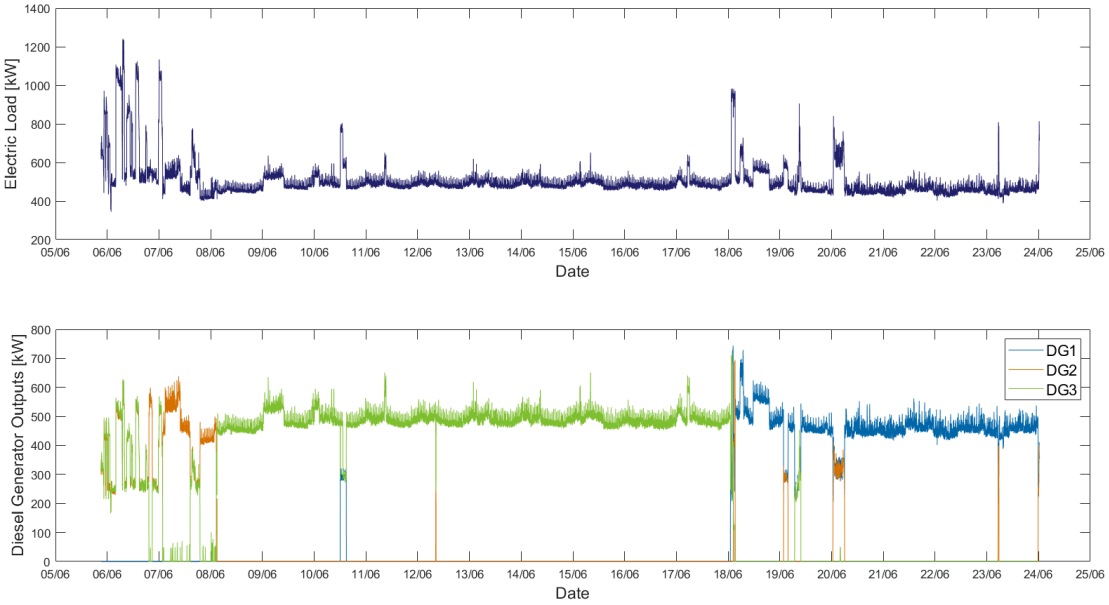

Figure 6.3: The load and the output of the three generator sets of the OPS during Voyage C

Voyage related details, like fuel consumption and the operating hours of the gensets, are shown in Table 6.1. The pollutants emitted during each voyage are illustrated in Table 6.2. Their estimation was carried out using the emissions factors presented in Table 2.3. In Table 6.3 the operating hours of the generator sets, the fuel consumption and the emissions for the port stays and the actual cruising periods of the voyages A, B and C are presented.

Table 6.1: The three voyages' details

Voyage particulars	Voyage A	Voyage B	Voyage C
Duration (days)	20.6	19.4	18.1
DG1 runtime (h)	391.7	150.6	146.2
DG2 runtime (h)	36.1	162.6	63.4
DG3 runtime (h)	128.4	204.9	275.2
DGs total runtime (h)	556.2	518.1	484.8
Average daily fuel consumption (t/24h)	3.33	2.99	3.05
Total fuel consumption (t)	66.19	55.95	53.26
Mean electric load (kW)	553.9	482.2	504.5
Max. electric load (kW)	1359.9	1245.8	1241.2

Table 6.2: The emission during each voyage

Emissions	Voyage A	Voyage B	Voyage C
CO_2 (t)	212.22	179.37	170.75
CH_4 (kg)	4.0	3.4	3.2
N_20 (kg)	9.9	8.4	8.0
NO_x (t)	5.78	4.88	4.65
CO (kg)	183.4	155.0	147.5
NMVOC (kg)	203.9	172.3	164.0
SO_x (kg)	174.8	147.7	140.6
PM (kg)	67.5	57.1	54.3

Table 6.3: Comprehensive details for the port stays and the cruising periods of the three voyages

Voyage particulars	Voyage A			Voyage B			Voyage C		
	Port A1	Cruising	Port A2	Port B1	Cruising	Port B2	Port C1	Cruising	Port C2
DGs total runtime (h)	33.0	467.4	55.7	55.7	362.7	99.7	70.8	295.9	118.0
Total fuel oil consumption (t)	3.20	57.30	5.70	5.70	40.58	9.67	6.75	34.22	12.28
Emissions									
CO_2 (t)	10.25	183.69	18.27	18.27	130.09	31.01	21.65	109.72	39.38
CH_4 (kg)	0.2	3.4	0.3	0.3	2.4	0.6	0.4	2.1	0.7
N_20 (kg)	0.5	8.6	0.9	0.9	6.1	1.5	1.0	5.1	1.8
NO_x (t)	0.28	5.00	0.50	0.50	3.54	0.84	0.59	2.99	1.07
CO (kg)	8.9	158.7	15.8	15.8	112.4	26.8	18.7	94.8	34.0
NMVOC (kg)	9.8	176.5	17.6	17.6	125.0	29.8	20.8	105.4	37.8
SO_x (kg)	8.4	151.3	15.0	15.0	107.1	25.5	17.8	90.3	32.4
PM (kg)	3.3	58.4	5.8	5.8	41.4	9.9	6.9	34.9	12.5

6.2 The performance of the hybrid power system

To assess the performance of the HPS a set of values for the parallel-connected modules of the battery were examined, resulting in different battery capacities and system performances. More specifically, battery pack configurations with 30, 50, 100, 150, 200,

300 and 400 parallel-connected modules were investigated. The energy of these battery configurations corresponds to values from 461 kWh to 6144 kWh. For each $n_{parallel}$ value tested it was verified that the maximum C-rate of the battery pack during the simulations was lower than the battery module's maximum allowable, i.e. 3C. Additionally, two values of the lower allowable state of charge SOC_{min} were investigated, namely 20% and 30%. The lower this magnitude is the biggest the available discharging range is, thus the number of cycles per voyage is reduced. On the other hand, as demonstrated in Chapter 5, the lifetime of the battery decreases as the DOD is increased, meaning that more battery pack replacements are required throughout the lifetime of the vessel. For that reason, the two SOC_{min} values were compared in terms of fuel savings and cost. The simulation parameters that remain constant throughout the several cases that were studied are illustrated in Table 6.4.

Table 6.4: The simulation parameters that remain constant throughout the several cases that were studied

Parameters	Symbol	Value
No. of modules connected in-series	n_{series}	8
Nominal voltage of the battery pack (V)	V_{nom}	307.2
Max. state of charge	SOC_{max}	90%
Initial state of charge	SOC_{in}	100%
Min. runtime of the gensets (min)		40
Operation point of the diesel engines (%MCR)		80%
Operation point of the diesel engines (kW)		736
Specific fuel oil consumption @ 80%MCR (g/kWh)		208.89
Charging efficiency	η_{ch}	0.90
Discharging efficiency	η_{disch}	1
Generator shaft efficiency	η_s	0.94
Converter efficiency	η_{conv}	0.94

Since each simulation is characterized by the number of battery modules connected in-parallel, the voyage under study and the lower limit of SOC set, a specific code name was appointed to every simulation, in order to be easier distinguished. The above-mentioned parameters, in that order, comprise the name of each simulation. For example, in the case of 100 parallel-connected modules, for the Voyage B and with a lower allowable SOC value of 30% the name of the simulation is 100B30.

The battery pack parameters that derive from the Equations (4.3) – (4.5), (4.7) and (4.14) – (4.20) are presented in Table 6.5, as a function of the number of parallel-connected modules.

In Table 6.6 an estimation of the weight and volume of the battery pack is shown, for various numbers of parallel-connected modules. These values don't take into consideration the weight and volume of the racks, the cooling installation and the surrounding of the enclosed space the battery pack is placed into. Since the operation of the No.2 diesel generator set of the OPS is substituted by the battery pack in the HPS, its designated space can be utilized for the battery installation. The dimensions of the genset are L5.95 m x B1.50 m x H2.31 m, resulting in a total volume of 20.62 m^3, and its weight is 16.7 tonnes [72], meaning that for all the module configurations examined the installation of the battery pack at this very location is possible. Of course, an appropriate space for the battery shall be constructed, as its operation is temperature sensitive and a designated enclosed space for the battery is a class rule requirement.

Table 6.5: The battery pack parameters for each of the 7 values of $n_{parallel}$ examined

$n_{parallel}$	**30**	**50**	**100**	**150**	**200**	**300**	**400**
Q_{pack} (Ah)	1750	2500	5000	7500	10000	15000	20000
R_{pack} (Ω)	0.0055	0.0038	0.0019	0.0013	0.00096	0.00064	0.00048
$E_{full,\ pack}$ (V)	327.1	327.1	327.1	327.1	327.1	327.1	327.1
$E_{exp,\ pack}$ (V)	317.1	317.1	317.1	317.1	317.1	317.1	317.1
$Q_{exp,\ pack}$ (Ah)	50.7	72.5	144.9	217.4	289.9	434.8	579.7
$E_{nom,\ pack}$ (V)	307.2	307.2	307.2	307.2	307.2	307.2	307.2
$Q_{nom,\ pack}$ (Ah)	1400	2000	4000	6000	8000	12000	16000
A_{pack} (V)	9.96	9.96	9.96	9.96	9.96	9.96	9.96
B_{pack} (1/Ah)	0.0591	0.0414	0.0207	0.0138	0.0103	0.0069	0.0052
K_{pack} (V)	2.4856	2.4856	2.4856	2.4856	2.4856	2.4856	2.4856

Table 6.6: The weight and volume of the battery pack as a function of $n_{parallel}$

$n_{parallel}$	**30**	**50**	**100**	**150**	**200**	**300**	**400**
Weight (t)	0.71	1.08	2.02	2.95	3.89	5.76	7.63
Volume (m^3)	0.5	0.7	1.3	1.9	2.5	3.6	4.8

6.2.1 SOC_{min} = 30%

6.2.1.1 Voyage A

The hybrid power system's performance during Voyage A and when the $n_{parallel}$ is equal to 30 is illustrated in Figure 6.4. It can be observed that the limited capacity of the battery, which is due to the low number of modules connected in-parallel, results in frequent charging and discharging. Though, the confinement of the SOC between 30% and 90% is achieved as intended. The cycles per day are numerous, even up to 15 a day. The operation of the diesel generators looks almost continuous and that's because the battery discharges in a short time and can no longer cover the load.

In Figure 6.5 the simulation where 200 modules were connected in-parallel is presented. The battery takes longer to discharge and the diesel generators operate for significant amounts of time without interruption – even up to 24 h, to restore the original charge of the bigger battery pack. Moreover, the intended split of total gensets runtime to the two diesel generators is achieved to a satisfactory degree.

In the same graph, the battery current and voltage are illustrated and it can be noticed that during the charging process the current is negative, while during discharging it is positive. Furthermore, during charging the voltage of the battery takes higher values than when discharging and that the charging process takes more time. The latter observation can be explained by the fact that the battery charges with the excess energy of one or two generator sets, which isn't a large amount of energy. On the contrary, during discharging the battery has to supply much more energy in order to cover the load, which leads to a shorter discharging period. Additionally, the charging efficiency of the selected module is 90%, while the discharging is equal to 100%.

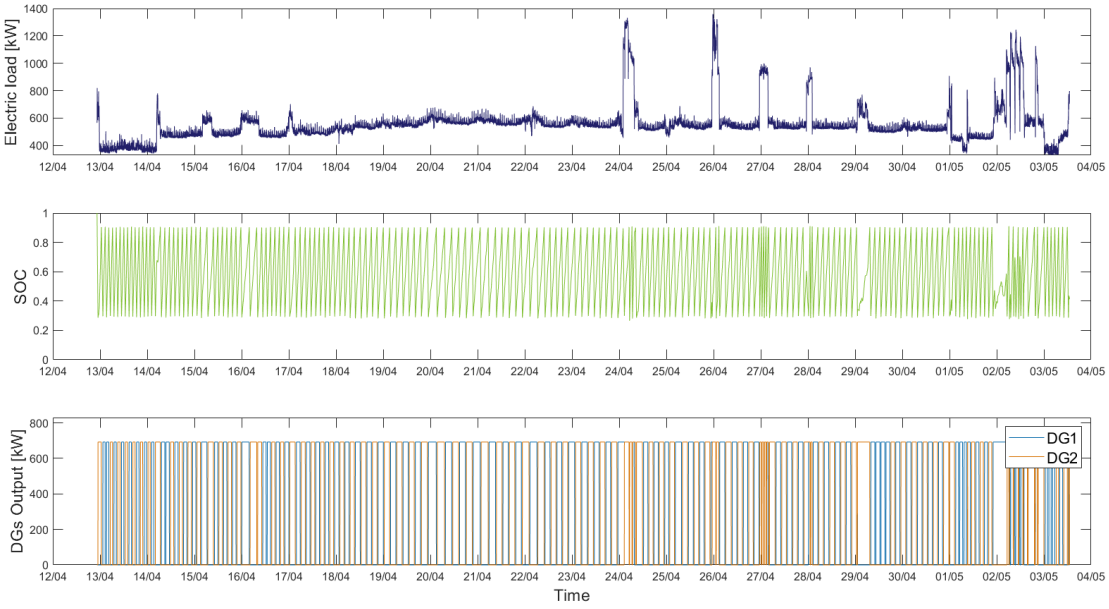

Figure 6.4: The operation of the gensets and the SOC of the battery during the 30A30 simulation

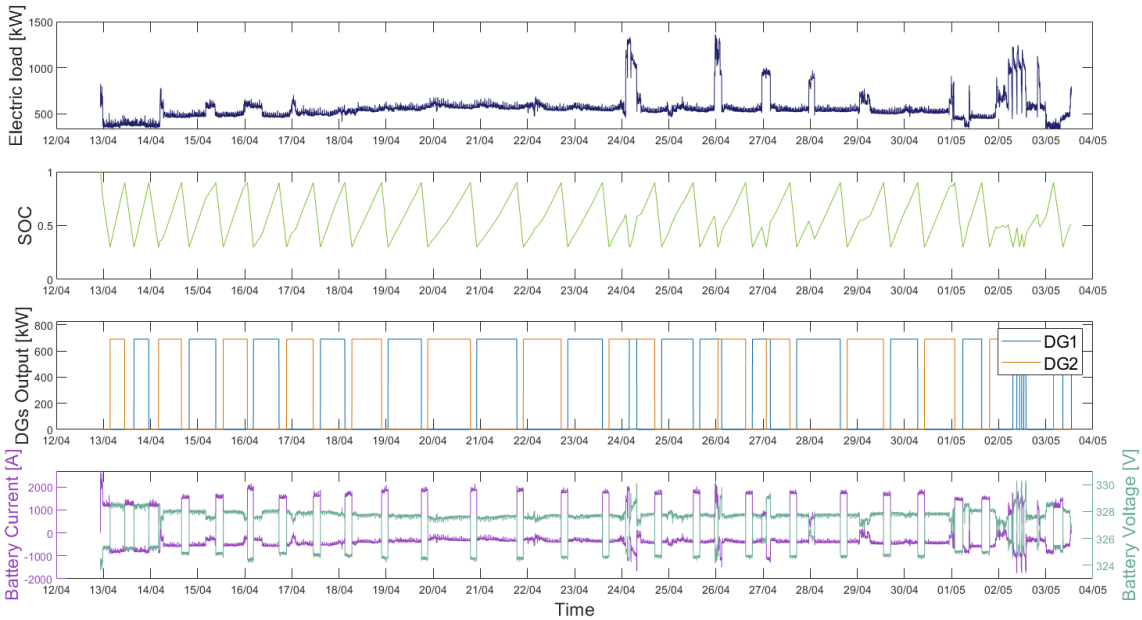

Figure 6.5: The battery behavior and the operation of the gensets during the 200A30 simulation

In Table 6.7 various parameters for all the Voyage A simulations are presented, like the battery current and voltage range, the cycles and energy of the battery pack and the runtime of the battery pack and the diesel generators. The latter, as well as the total fuel consumption of the voyage, are decreasing with the increase of parallel-connected modules, as the battery is able to provide the necessary power for longer and substitutes the operation of the gensets more often. The cycles are also being reduced with higher $n_{parallel}$ values, but as this value increases the rate of decrease of the cycles is diminished.

In Table 6.8 the achieved decrease of fuel consumption, runtime of the gensets and emissions in comparison with the original power system are illustrated. An average of 3.71% and 25.46% decrease in fuel consumption and diesel generators runtime,

respectively, were achieved via the employment of the hybrid power system during Voyage A. The maximum fuel consumption decrease, 4.73%, was displayed when the number of parallel-connected modules was equal to 300.

Table 6.7: The Voyage A simulations results for different $n_{parallel}$ values and when SOC_{min} = 30%

Battery pack							
No. of modules connected in-parallel	**30**	**50**	**100**	**150**	**200**	**300**	**400**
Capacity (Ah)	1500	2500	5000	7500	10000	15000	20000
Min. current (A)	-1570	-1676	-1734	-1765	-1755	-1755	-1674
Max. current (A)	3920	3999	3743	2703	2696	2687	3176
Max. C-rate (1/h)	2.6	1.6	0.7	0.4	0.3	0.2	0.2
Voltage range (V)	317.1 - 369.7	317.7 - 346.0	320.1 - 334.4	322.6 - 331.6	323.6 - 330.3	324.5 - 329.1	324.8 - 328.5
Average voltage (V)	330.3	328.4	327.4	327.2	327.2	327.1	327.1
Energy (kWh)	461	768	1536	2304	3072	4608	6144
Runtime (discharge) (h)	103.6	105.5	107.3	110.4	113.7	114.8	110.9
Cycles/voyage	241	169	114	84	91	68	64
Diesel generators							
DG1 runtime (h)	209.0	207.9	201.7	206.6	195.9	189.2	183.8
DG2 runtime (h)	209.9	209.4	214.2	208.4	216.9	220.9	228.0
DGs total runtime (h)	418.9	417.3	415.9	414.9	412.9	410.2	411.8
Fuel oil consumption (t)	64.40	64.16	63.94	63.79	63.48	63.06	63.31
Emissions							
CO_2 (t)	206.48	205.69	204.99	204.52	203.51	202.18	202.97
CH_4 (kg)	3.9	3.8	3.8	3.8	3.8	3.8	3.8
N_20 (kg)	9.7	9.6	9.6	9.6	9.5	9.5	9.5
NO_x (t)	5.62	5.60	5.58	5.57	5.54	5.50	5.52
CO (kg)	178.4	177.7	177.1	176.7	175.8	174.7	175.4
NMVOC (kg)	198.4	197.6	196.9	196.5	195.5	194.2	195.0
SO_x (kg)	170.0	169.4	168.8	168.4	167.6	166.5	167.1
PM (kg)	65.7	65.4	65.2	65.1	64.7	64.3	64.6

Generally, the higher the number of parallel-connected modules is the higher the decrease in fuel consumption and the operating hours of the diesel generators. There is only one instance where this isn't the case; the decrease percentages of fuel consumption and gensets runtime during the 400B30 simulation are lower than those of the 300B30 simulation. A possible explanation for this phenomenon is that the performance of the HPS also relates to the cycling of the battery.

Table 6.8: The decrease of gensets operating hours, fuel consumption and emissions during the Voyage A simulations, when SOC_{min} = 30%

% Decrease	**No. of modules connected in-parallel**							**Average**
	30	**50**	**100**	**150**	**200**	**300**	**400**	
DGs total runtime	24.68%	24.97%	25.22%	25.39%	25.76%	26.25%	25.96%	25.46%
Fuel oil consumption	2.70%	3.08%	3.41%	3.63%	4.10%	4.73%	4.36%	3.71%
Emissions	2.70%	3.08%	3.41%	3.63%	4.10%	4.73%	4.36%	3.71%

In Figure 6.6 the cycles and the percentage drop in fuel consumption are presented for Voyage A, as a function of $n_{parallel}$ and the energy of the pack. Additionally, the fitted curves for these magnitudes are illustrated, to demonstrate that the decrease percentage is increasing linearly with increasing $n_{parallel}$, while the number of cycles per voyage is inversely proportional with $n_{parallel}$.

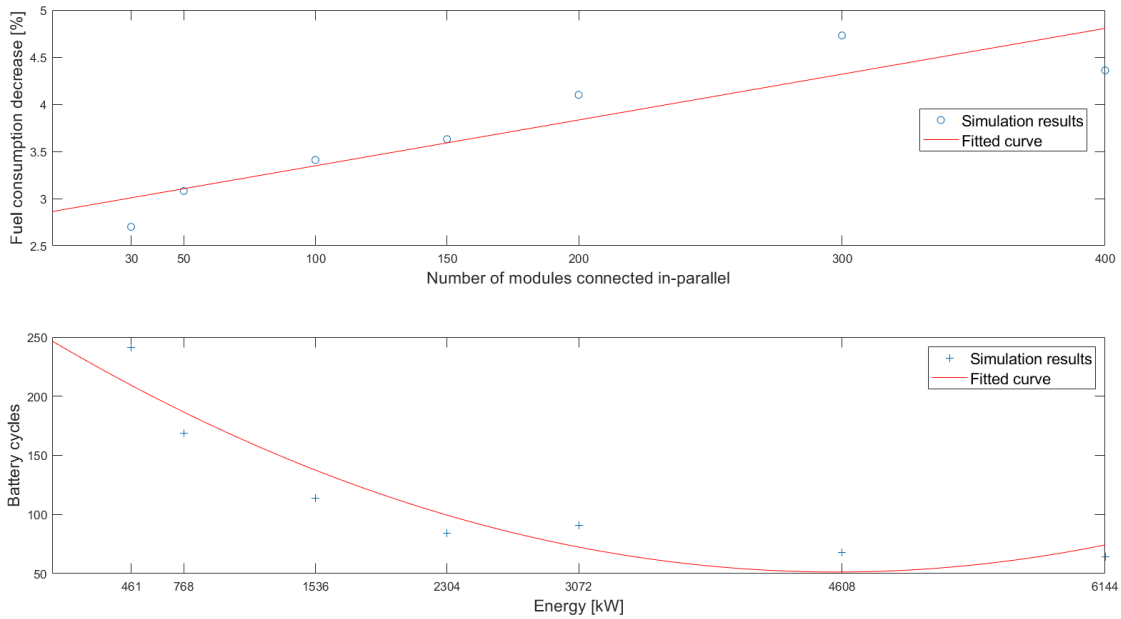

Figure 6.6: The fuel consumption decrease percentage, the cycles and their fitted curves for Voyage A

6.2.1.2 Voyage B

The same seven values of parallel-connected modules were tested for the Voyage B. In Figure 6.7 the load, the state of charge, the power of the diesel generators and the battery pack during Voyage B are presented. This simulation represents the performance of the HPS with 300 parallel-connected modules and as it can be noticed, a charging/discharging cycle is taking almost a day.

In Figure 6.8 a detail of the same simulation is shown. More specifically, the period from 05/05 to 14/05 is illustrated, where it can be observed that the battery and the diesel generator operations are alternated, as well as that the battery charges when the gensets are running, as expected. Regarding the charging process, it can also be added that the battery power at these periods is considered negative and that it is quite lower the power output of the battery during discharging. As explained earlier, most of the times the battery discharges to cover the entire load, while when charging it charges utilizing the excess energy of the gensets. Furthermore, the battery's discharging power at any moment it is not equal with the load at this moment, but higher, preserving though the same aspect. That is due to the losses at the power converter; during discharging the battery must provide more power than it's required since a portion of that power will be lost in the conversion process. Similarly, the power that eventually comes into the battery during charging is less than the excess power of the system, due to the efficiencies of the converter and the battery.

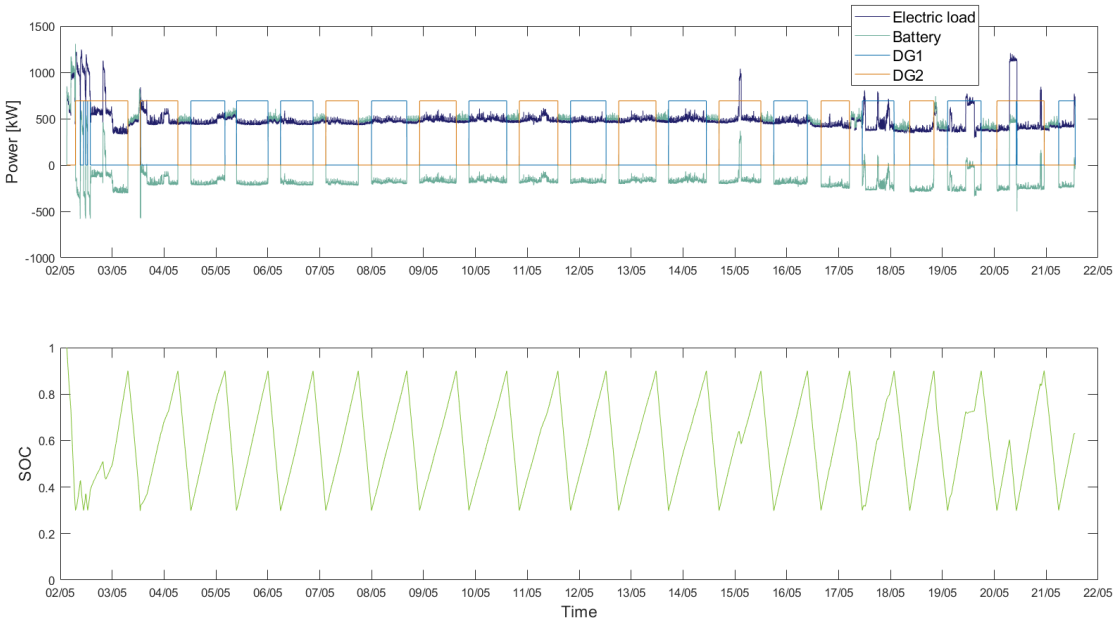

Figure 6.7: The load, the power of the battery and the gensets and the SOC during the 300B30 simulation

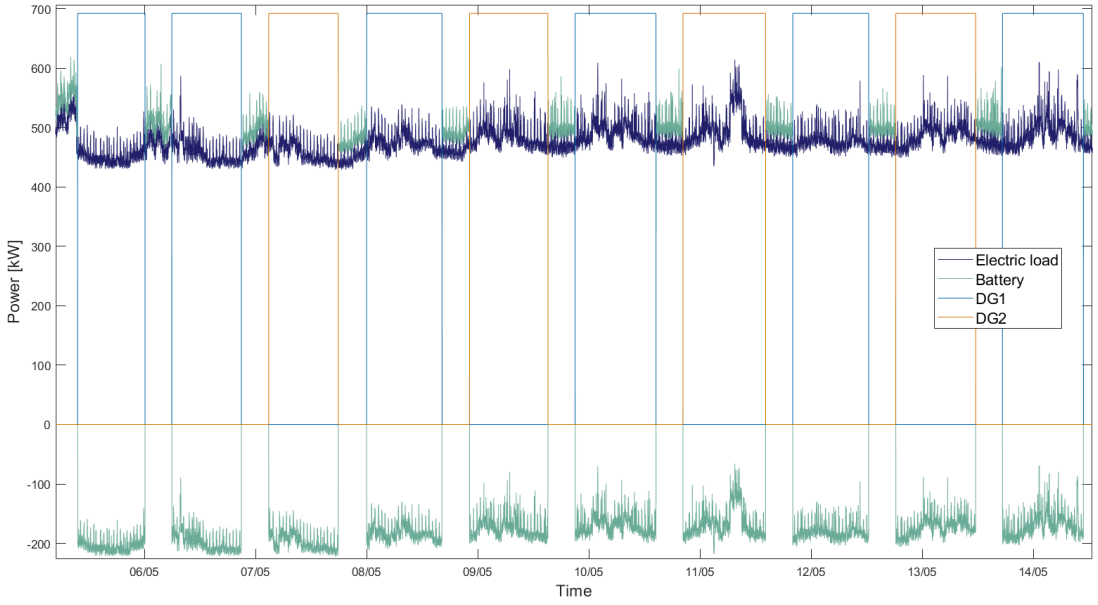

Figure 6.8: The load, the power of the battery and the gensets for the period of nine days during the 300B30 simulation

The various simulation results for Voyage B are shown in Table 6.9 and the achieved via the HPS decreases in diesel generator operating hours, fuel consumption and emissions are illustrated in Table 6.10. The average fuel consumption decrease percentage was 4.61%, while the maximum achieved decrease was 5.91% when the battery consisted of 400 parallel-connected modules. The diesel generators were running on average 33% less compared with the OPS. In Figure 6.9 the cycles, the percentage drop in fuel consumption and their fitted curves are illustrated as a function of the parallel-connected modules.

Table 6.9: The Voyage B simulations results for different $n_{parallel}$ values and when SOC_{min} = 30%

Battery pack							
No. of modules connected in-parallel	**30**	**50**	**100**	**150**	**200**	**300**	**400**
Capacity (Ah)	1500	2500	5000	7500	10000	15000	20000
Min. current (A)	-1578	-1667	-1734	-1749	-1755	-1761	-1764
Max. current (A)	3893	4113	2642	3706	3631	4040	4031
Max. C-rate (1/h)	2.6	1.6	0.5	0.5	0.4	0.3	0.2
Voltage range (V)	317.2 - 371.5	317.6 - 346.4	321.4 - 334.4	321.4 - 331.6	322.4 - 330.3	323.3 - 329.1	324.1 - 328.6
Average voltage (V)	331.2	328.7	327.5	327.3	327.2	327.1	327.1
Energy (kWh)	461	768	1536	2304	3072	4608	6144
Runtime (discharge) (h)	130.3	131.9	135.9	137.8	135.9	136.3	134.8
Cycles/voyage	251	161	102	78	65	55	42
Diesel generators							
DG1 runtime (h)	176.1	175.3	174.7	172.7	171.9	171.2	171.6
DG2 runtime (h)	175.9	174.6	173.5	173.2	174.2	174.2	170.8
DGs total runtime (h)	352.1	349.9	348.2	345.9	346.1	345.4	342.4
Fuel oil consumption (t)	54.13	53.79	53.54	53.18	53.22	53.11	52.64
Emissions							
CO_2 (t)	173.53	172.46	171.64	170.48	170.61	170.26	168.77
CH_4 (kg)	3.2	3.2	3.2	3.2	3.2	3.2	3.2
N_20 (kg)	8.1	8.1	8.0	8.0	8.0	8.0	7.9
NO_x (t)	4.72	4.69	4.67	4.64	4.64	4.63	4.59
CO (kg)	149.9	149.0	148.3	147.3	147.4	147.1	145.8
NMVOC (kg)	166.7	165.7	164.9	163.8	163.9	163.6	162.1
SO_x (kg)	142.9	142.0	141.3	140.4	140.5	140.2	139.0
PM (kg)	55.2	54.9	54.6	54.2	54.3	54.2	53.7

Table 6.10: The decrease of gensets operating hours, fuel consumption and emissions during the Voyage B simulations, when SOC_{min} = 30%

% Decrease	**No. of modules connected in-parallel**							**Average**
	30	**50**	**100**	**150**	**200**	**300**	**400**	
DGs total runtime	32.05%	32.47%	32.79%	33.24%	33.19%	33.33%	33.91%	33.00%
Fuel oil consumption	3.26%	3.85%	4.31%	4.96%	4.88%	5.08%	5.91%	4.61%
Emissions	3.26%	3.85%	4.31%	4.96%	4.88%	5.08%	5.91%	4.61%

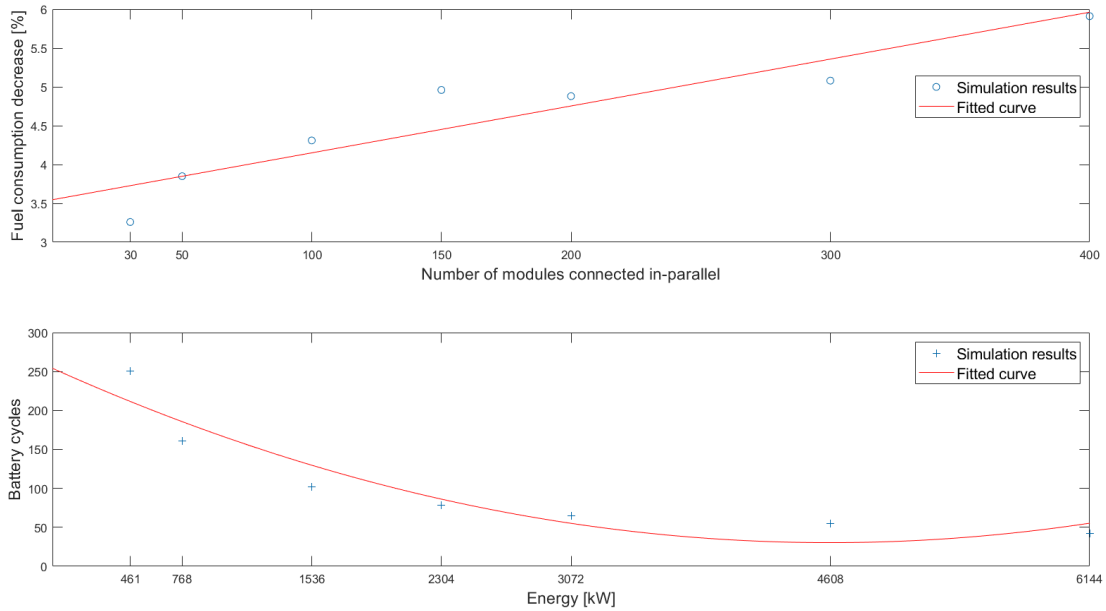

Figure 6.9: The fuel consumption decrease percentage, the cycles and their fitted curves for Voyage B

6.2.1.3 Voyage C

This particular voyage is the shortest of the three and consequently exhibits the lowest OPS fuel consumption and diesel generators runtime. The electric load during the 400C30 simulation as well as the power output of the diesel generators and the input/output power of the battery are presented in Figure 6.10.

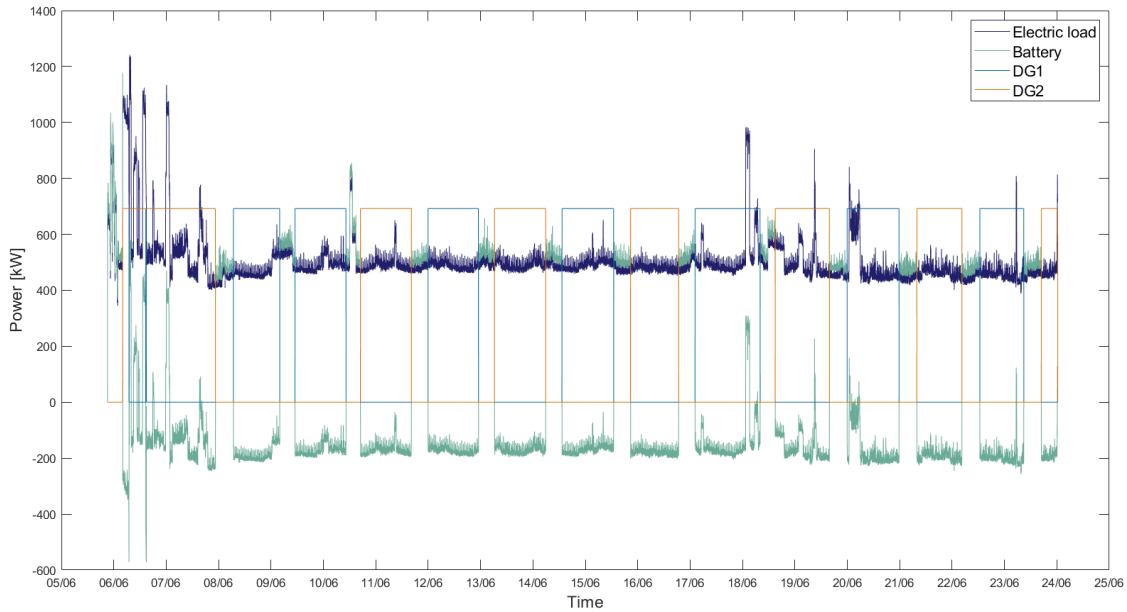

Figure 6.10: The load and the power of the battery and the gensets during the 400C30 simulation

In Figure 6.11 the first two days of the same simulation are illustrated. This period of time is one of the rare occasions where the battery doesn't complete full charging/discharging cycles. The battery is charging and discharging for short periods and the SOC is oscillating between values that are between SOC_{min} and SOC_{max}. This

behavior is not the optimum, as the more frequent the cycling of the battery is the shorter its lifetime. The battery is designed for a number of operation cycles and some of them are "spent" providing only small amounts of energy.

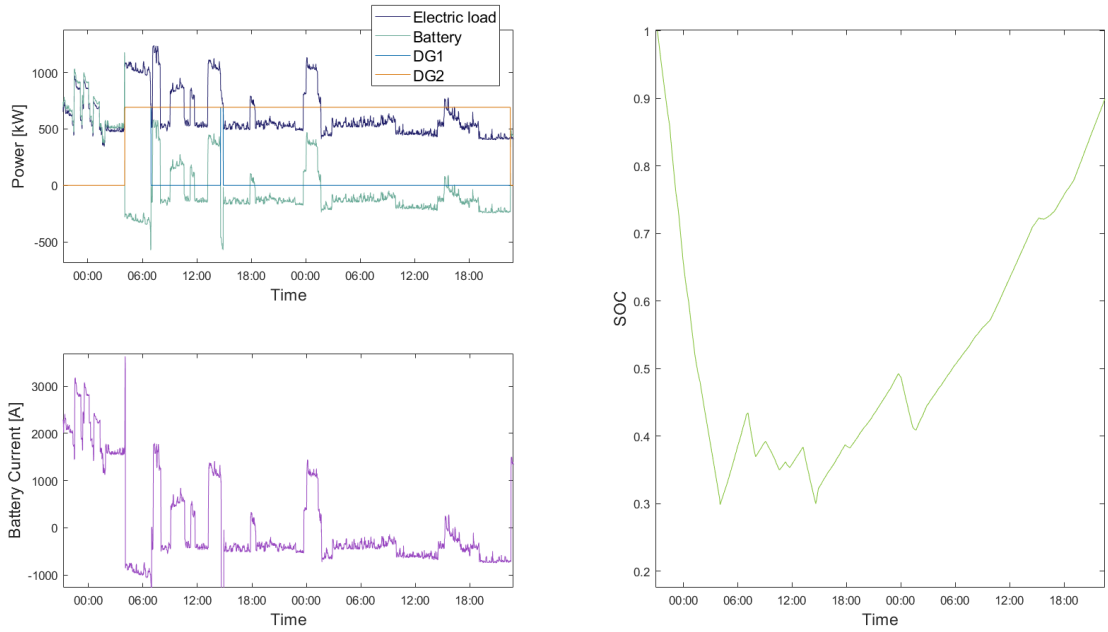

Figure 6.11: The load, the power, the current and the SOC of the battery and the output of the gensets during the first two days of the 400C30 simulation

The root cause of this behavior is the aspect of the load; at times it is higher than the operation point of the diesel generators and shortly after it is lower. During the first case the EMS's decision depends on the SOC of the battery; when the SOC is enough the battery assists the generator by discharging and when it's not the second generator is started. During the second case, the load is covered by a genset that is already running. The low-SOC instance can be noticed some hours earlier than 6:00 and about 15:00 of the first day, where the DG1 is started. The adequate-SOC case occurs around 00:00, between 6:00 and 14:00 and 18:00 of the first day and around 00:00 of the second day. Actually, around 00:00 of the first day, since no diesel generator is already running and the SOC is high the load is supplied exclusively by the battery. That's when the vessel is in port, thus the noise reduction achieved is a significant advantage of the proposed hybrid solution.

The results for Voyage C are presented in Table 6.11 and the decreases in diesel generator operating hours, fuel consumption and emissions are shown in Table 6.12. The achieved via the HPS average fuel consumption decrease percentage was 2.80% and the diesel generators were running on average 30.54% less compared with the OPS. The decrease of fuel consumption and the runtime of the diesel generators during Voyage C were proportional to the number of parallel-connected modules. In Figure 6.12 the cycles, the percentage drop in fuel consumption and their fitted curves are illustrated, as a function of the parallel-connected modules and the energy of the battery pack.

Table 6.11: The Voyage C simulations results for different $n_{parallel}$ values and when SOC_{min} = 30%

Battery pack							
No. of modules connected in-parallel	**30**	**50**	**100**	**150**	**200**	**300**	**400**
Capacity (Ah)	1500	2500	5000	7500	10000	15000	20000
Min. current (A)	-1561	-1689	-1710	-1763	-1770	-1737	-1740
Max. current (A)	4136	3676	3221	3225	3197	3228	3631
Max. C-rate (1/h)	2.8	1.5	0.6	0.4	0.3	0.2	0.2
Voltage range (V)	317.1 - 371.4	318.0 - 346.5	320.6 - 334.3	322.1 - 331.6	323.1 - 330.3	324.0 - 329.1	324.5 - 328.5
Average voltage (V)	330.7	328.5	327.5	327.3	327.2	327.1	327.1
Energy (kWh)	461	768	1536	2304	3072	4608	6144
Runtime (discharge) (h)	110.4	112.5	113.8	114.0	114.0	112.0	116.6
Cycles/voyage	213	142	88	67	57	44	44
Diesel generators							
DG1 runtime (h)	170.4	169.2	168.2	168.7	167.6	168.8	168.2
DG2 runtime (h)	170.0	169.6	169.1	167.9	168.8	166.1	164.3
DGs total runtime (h)	340.4	338.8	337.3	336.6	336.4	334.9	332.5
Fuel oil consumption (t)	52.34	52.09	51.86	51.75	51.72	51.49	51.12
Emissions							
CO_2 (t)	167.80	167.00	166.28	165.91	165.82	165.08	163.90
CH_4 (kg)	3.1	3.1	3.1	3.1	3.1	3.1	3.1
N_20 (kg)	7.9	7.8	7.8	7.8	7.8	7.7	7.7
NOx (t)	4.57	4.54	4.53	4.52	4.51	4.49	4.46
CO (kg)	145.0	144.3	143.7	143.3	143.3	142.6	141.6
NMVOC (kg)	161.2	160.4	159.7	159.4	159.3	158.6	157.5
SO_x (kg)	138.2	137.5	136.9	136.6	136.5	135.9	135.0
PM (kg)	53.4	53.1	52.9	52.8	52.8	52.5	52.1

Table 6.12: The decrease of gensets operating hours, fuel consumption and emissions during the Voyage C simulations, when SOC_{min} = 30%

% Decrease	**No. of modules connected in-parallel**							**Average**
	30	**50**	**100**	**150**	**200**	**300**	**400**	
DGs total runtime	29.78%	30.11%	30.42%	30.57%	30.61%	30.92%	31.41%	30.54%
Fuel oil consumption	1.72%	2.19%	2.62%	2.83%	2.89%	3.32%	4.01%	2.80%
Emissions	1.72%	2.19%	2.62%	2.83%	2.89%	3.32%	4.01%	2.80%

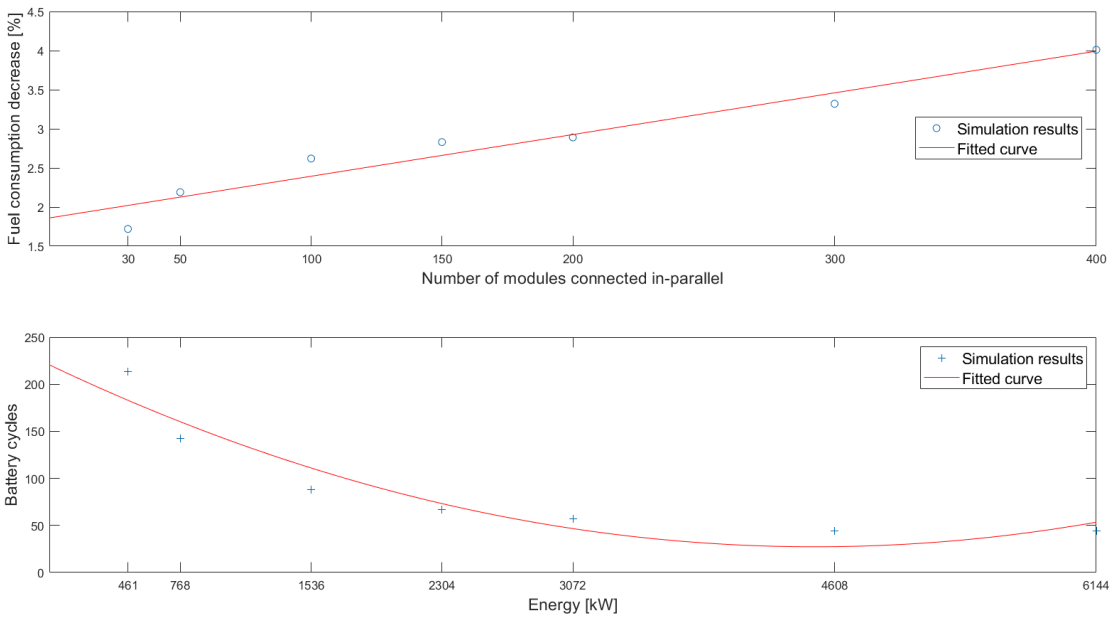

Figure 6.12: The fuel consumption decrease percentage, the cycles and their fitted curves for Voyage C

6.2.2 SOC_{min} = 20%

The same scenarios examined in the previous paragraph were simulated again, this time considering a lower state of charge limit equal to 20%. The comparison between the outcomes of the simulations performed with SOC_{min} = 30% and those with SOC_{min} = 20% are illustrated in Table 6.13, Table 6.14 and Table 6.15 for the Voyage A, Voyage B and Voyage C, respectively.

Table 6.13: The comparison between the simulations performed with SOCmin = 30% and those with SOCmin = 20% for the Voyage A

No. of modules connected in-parallel	**30**	**50**	**100**	**150**	**200**	**300**	**400**
Capacity (Ah)	1750	2500	5000	7500	10000	15000	20000
Energy (kWh)	538	768	1536	2304	3072	4608	6144
SOCmin = 30%							
Runtime (discharge) (h)	103.6	105.5	107.3	110.4	113.7	114.8	110.9
Cycles	241	169	114	84	91	68	64
Average voltage (V)	330.3	328.4	327.4	327.2	327.2	327.1	327.1
DGs total runtime decrease	24.68%	24.97%	25.22%	25.39%	25.76%	26.25%	25.96%
Fuel oil consumption decrease	2.70%	3.08%	3.41%	3.63%	4.10%	4.73%	4.36%
SOCmin = 20%							
Runtime (discharge) (h)	103.5	107.0	111.5	112.3	114.3	110.6	112.7
Cycles	218	152	106	92	83	65	70
Average voltage (V)	330.33	328.35	327.42	327.24	327.17	327.13	327.12
DGs total runtime decrease	24.70%	25.05%	25.41%	25.55%	25.92%	25.76%	25.74%
Fuel oil consumption decrease	2.72%	3.17%	3.64%	3.82%	4.30%	4.08%	4.06%

Table 6.14: The comparison between the simulations performed with SOCmin = 30% and those with SOCmin = 20% for the Voyage B

No. of modules connected in-parallel	**30**	**50**	**100**	**150**	**200**	**300**	**400**
Capacity (Ah)	1750	2500	5000	7500	10000	15000	20000
Energy (kWh)	538	768	1536	2304	3072	4608	6144
SOCmin = 30%							
Runtime (discharge) (h)	130.3	131.9	135.9	137.8	135.9	136.3	134.8
Cycles	251	161	102	78	65	55	42
Average voltage (V)	331.2	328.7	327.5	327.3	327.2	327.1	327.1
DGs total runtime decrease	32.05%	32.47%	32.79%	33.24%	33.19%	33.33%	33.91%
Fuel oil consumption decrease	3.26%	3.85%	4.31%	4.96%	4.88%	5.08%	5.91%
SOCmin = 20%							
Runtime (discharge) (h)	129.8	133.0	135.4	135.1	135.1	133.3	135.7
Cycles	216	143	84	71	58	37	39
Average voltage (V)	331.2	328.7	327.5	327.3	327.2	327.1	327.1
DGs total runtime decrease	32.00%	32.50%	32.89%	32.88%	33.41%	33.50%	33.75%
Fuel oil consumption decrease	3.19%	3.90%	4.46%	4.45%	5.20%	5.33%	5.68%

Table 6.15: The comparison between the simulations performed with SOCmin = 30% and those with SOCmin = 20% for the Voyage C

No. of modules connected in-parallel	**35**	**50**	**100**	**150**	**200**	**300**	**400**
Capacity (Ah)	1750	2500	5000	7500	10000	15000	20000
Energy (kWh)	538	768	1536	2304	3072	4608	6144
SOCmin = 30%							
Runtime (h)	110.4	112.5	113.8	114.0	114.0	112.0	116.6
Cycles	213	142	88	67	57	44	44
Average voltage (V)	330.7	328.5	327.5	327.3	327.2	327.1	327.1
DGs total runtime decrease	29.78%	30.11%	30.42%	30.57%	30.61%	30.92%	31.41%
Fuel oil consumption decrease	1.72%	2.19%	2.62%	2.83%	2.89%	3.32%	4.01%
SOCmin = 20%							
Runtime (h)	109.2	112.3	113.3	115.6	114.7	114.4	118.0
Cycles	187	128	75	61	53	44	43
Average voltage (V)	330.80	328.52	327.47	327.25	327.18	327.13	327.11
DGs total runtime decrease	29.71%	30.15%	30.52%	30.86%	31.03%	31.15%	31.57%
Fuel oil consumption decrease	1.63%	2.24%	2.76%	3.25%	3.48%	3.65%	4.23%

As expected, the extended operating range of the battery due to the lower SOC_{min} had as a result the decrease of the cycles during the course of a voyage. This decrease is up to 32.73% for the 300A20 simulation, while the average value for the 18 of the 21 simulations is a 10.96% decrease, Table 6.16. Two of the three remaining simulations, namely 150A20 and 400A20, exhibited an increased number of cycles per voyage, compared with the simulations carried out with SOC_{min} = 30%. Lastly, the 300C20 simulation exhibited the same number of cycles when SOC_{min} was set to 20% and 30%. Overall, an 8.49% reduction in cycles was achieved when the SOC_{min} value was decreased from 30% to 20%.

Concerning the rest of the simulations results, the total discharging time of the battery, the average voltage, the decrease percentage of the gensets' runtime and of the fuel consumption are very close in the simulations performed with SOC_{min} = 20% and in those performed with SOC_{min} = 30%. Generally, in 15 out of 21 simulations the decrease percentage was higher during simulations considering a lower SOC limit of 20%.

Table 6.16: The percentage change of the cycles per voyage during simulations where SOC_{min} = 20% and simulations where SOC_{min} = 30%

No. of modules connected in-parallel	**30**	**50**	**100**	**150**	**200**	**300**	**400**
Voyage A	-9.54%	-10.06%	-7.02%	9.52%	-8.79%	-4.41%	9.38%
Voyage B	-13.94%	-11.18%	-17.65%	-8.97%	-10.77%	-32.73%	-7.14%
Voyage C	-12.21%	-9.86%	-14.77%	-8.96%	-7.02%	0.00%	-2.27%

In Figure 6.13 the performance of the HPS during the Voyage B, when the parallel-connected modules are 300 and when SOC_{min} = 20% is presented. The attempted confinement of the SOC between 20% and 90% is achieved and, with few exceptions, the battery has full charging/discharging cycles between these two values. Comparing this graph with Figure 6.7, which depicts the same simulation only with SOC_{min} equal to 30%, it can be noticed that the battery is discharging for longer periods due to its extended SOC range. To this effect, the diesel generators are running for longer, to restore the original charge of the battery over a longer SOC range.

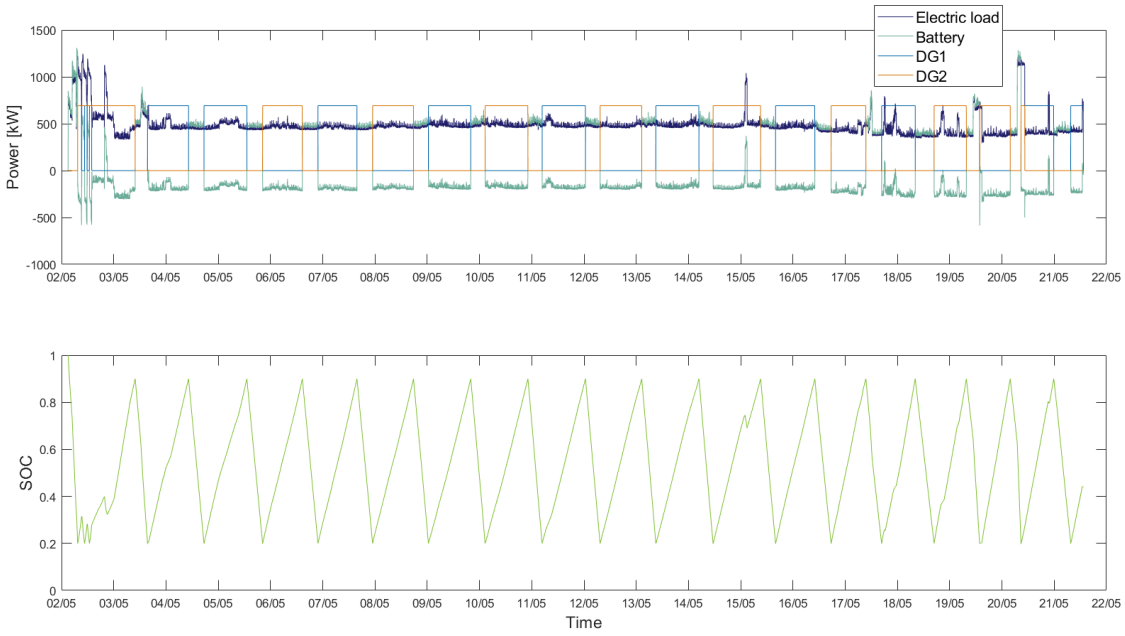

Figure 6.13: The load, the power of the battery and the gensets and the SOC during the 300B20 simulation

In conclusion, the implementation of the Li-ion battery pack in the vessel's power plant resulted in reductions both in the operating hours of the diesel generators and in the fuel consumption and emissions. By upsizing the battery pack the decrease percentages of the above parameters are increased, while the minimum allowable SOC has an effect mostly on the battery cycles per voyage and secondarily, on the fuel consumption reduction. In the 42 simulations that were conducted the fuel consumption decrease compared with the OPS was between 1.63% and 5.91%, while on average 3.74% less

fuel was burnt via the utilization of the battery pack. The same numbers apply for the emissions of the HPS. Regarding the operating hours of the gensets, a reduction from 24.68% to 33.91% was exhibited and the gensets were operated on average 29.69% less compared with the OPS.

In a recent study conducted jointly by MAN, DNV GL and Corvus Energy a similar hybridization project was investigated [73]. One of the four diesel generators installed on board a 1,700 TEU container feeder was replaced by a 500 kWh battery pack, which was utilized for peak shaving and spinning reserve for the gensets. Four cases where examined, with the number of active reefers ranging from zero to 250. The study reported fuel savings between 0.7% and 2.2% and a reduction in the gensets run time between 17.3% and 29.5%, depending on how many reefers were active.

These results are quite close with the current research's findings, as for a similar battery size, that of 461 kWh, the proposed hybrid system exhibited a fuel reduction between 1.63% and 3.26% and the decrease in the operating hours of the gensets was in the range between 24.68% and 33.75%.

6.3 Feasibility study

The reductions in the running hours of the diesel generators and the fuel consumption result in savings throughout the lifetime of the vessel. In this paragraph, a feasibility study was performed, to determine the exact amount of the cost reduction achieved and also, to investigate whether these savings can justify the battery pack investment. Additionally, the optimum battery pack configuration was specified, as well as the optimal minimum allowable SOC value from an economic perspective.

The MGO price at the time this study was written was \$680/t [74]. That was the average price in 20 major global bunkering ports, including Fujairah, Hong Kong, Piraeus, Rotterdam and Singapore. The price of MGO is constantly increasing and in order to estimate the future savings, it was supposed that in 2030 the price will be \$1000/t, a value used in the aforementioned DNV GL study [73]. Through linear interpolation, the MGO price was estimated for each year of operation. Regarding the cost of genset' maintenance, it was taken equal to \$10 per hour of operation, as MAN suggests [13], while the battery pack doesn't need any maintenance works. Finally, the cost of a lithium-ion battery pack in 2020 was considered equal to \$500/kWh and in 2030 equal to \$400/kWh.

Using the above-mentioned costs, the savings achieved via the employment of the hybrid power system were calculated. Firstly, the average values of the fuel consumption decrease and the gensets' operating hours, as well as the cycles recorded on the simulations of the three voyages were estimated. That was performed for both SOC_{min} = 30% and SOC_{min} = 20%, Table 6.17, Table 6.18. Additionally, the average duration of the three voyages was found equal to 19.39 days.

Since the vessel was built in 2012 and a typical lifetime of a merchant ship is 25 years, the vessel has about 17 years of service left. This value was used to specify the savings the HPS will yield until the vessel is decommissioned. Furthermore, using this value the total battery cycles were determined, thus the times the pack will be replaced.

Table 6.17: The average values of the three voyages' simulations results, when SOC_{min} = 30%

No. of modules connected in-parallel	**30**	**50**	**100**	**150**	**200**	**300**	**400**
DGs total runtime decrease	28.84%	29.18%	29.48%	29.73%	29.85%	30.17%	30.43%
Fuel consumption decrease	2.56%	3.04%	3.45%	3.81%	3.96%	4.38%	4.76%
Cycles	235	157	101	76	71	56	50

Table 6.18: The average values of the three voyages' simulations results, when SOC_{min} = 20%

No. of modules connected in-parallel	**30**	**50**	**100**	**150**	**200**	**300**	**400**
DGs total runtime decrease	28.80%	29.21%	29.54%	29.71%	30.07%	30.30%	30.43%
Fuel consumption decrease	2.51%	3.07%	3.54%	3.78%	4.26%	4.57%	4.76%
Cycles	207	141	88	75	65	49	51

Merchant vessels are operating all year round, except possibly for some days that they are under repair works, due to an unexpected malfunction. Moreover, at least two examinations of the ship's bottom are required in a five-year period [75]. One of them must be performed during the special survey and the other can be executed via an in-water survey (IWS), provided that the ship's age isn't greater than 15 years.

In order to specify the exact duration of the above-mentioned works, the opinion of two experienced technical superintendents was asked. They stated that the duration of both the repair works' and the dry-docks depend on the owning company's maintenance strategy, as well as the age of the vessel. When the maintenance is done meticulously repairs take on average 3-5 days per year. The 5th year dry-dock takes about 10 days, the 10th year 14 days, the 15th about 17 and the 20th a little longer than 20 days. The downtime throughout the lifetime of the vessel is presented in Table 6.19. In the first 15 years between the dry-docks there is an IWS, which lasts 1 day. After the first 15 years, the IWS are replaced with dry-docks. Based on the annual operating days of the vessel the number of voyages per year was calculated, considering that the average duration of a voyage is 19.39 days.

For the remaining years of service, i.e. from 2020 to 2036, the average number of the voyages per year was estimated, using the values of Table 6.19 and found equal to 18.30 voyages/year. This value was used in a preliminary economic analysis, which was performed for the seven sizes of the battery pack and the two SOC_{min} values. In this analysis, the price of the fuel and the battery pack were considered constant throughout the lifetime of the vessel. The savings on a voyage, annual and lifetime basis were calculated, as well as the required replacements of the battery pack, Table 6.20 and Table 6.21.

The comparison between the average simulation results when SOC_{min} = 30% and when SOC_{min} = 20% are presented in Table 6.22. In four out of seven battery sizes the lower SOC_{min} value results in greater savings and in six out of seven sizes in fewer cycles. Nevertheless, the limited cycle life that comes with the lower minimum allowable SOC value leads to the double battery pack replacements, which skyrockets the cost. Therefore, applying a SOC_{min} equal to 30% is a better option. Even in this case though, the preliminary analysis shows that the proposed hybrid system is not a feasible investment, as the total cost of the battery is greater than the lifetime savings.

Table 6.19: The annual downtime throughout the lifetime of the vessel

No. of year	Year	Downtime for repairs	Downtime for dry-dock or IWS	Total downtime	Operating days	Voyages/year
1	2012	3		3	362	18.67
2	2013	3		3	362	18.67
3	2014	3	1	4	361	18.61
4	2015	3		3	362	18.67
5	2016	3	10	13	352	18.15
6	2017	3.5		3.5	361.5	18.64
7	2018	3.5		3.5	361.5	18.64
8	2019	3.5	1	4.5	360.5	18.59
9	2020	3.5		3.5	361.5	18.64
10	2021	3.5	14	17.5	347.5	17.92
11	2022	4		4	361	18.61
12	2023	4		4	361	18.61
13	2024	4	1	5	360	18.56
14	2025	4		4	361	18.61
15	2026	4	17	21	344	17.74
16	2027	4.5		4.5	360.5	18.59
17	2028	4.5		4.5	360.5	18.59
18	2029	4.5	20	24.5	340.5	17.56
19	2030	4.5		4.5	360.5	18.59
20	2031	4.5	22	26.5	338.5	17.45
21	2032	5		5	360	18.56
22	2033	5		5	360	18.56
23	2034	5	24	29	336	17.33
24	2035	5		5	360	18.56
25	2036	5		5	360	18.56

Another useful indication derived from the preliminary economic analysis is the fact that the smaller the battery is the more appealing the hybrid solution becomes. For the given battery module all the battery sizes result in not feasible investments, but for a module with longer lifetime and thus, fewer replacements, the hybrid solution would be profitable. This scenario was investigated in detail in the following paragraph. It can be noticed that with rising battery sizes both the savings and the battery cost are increasing, but the latter at a much higher rate.

Taking into consideration the above conclusions, the configuration with 30 modules connected in-parallel and a lower SOC value of 30% was chosen for further investigation. To investigate in depth whether the proposed HPS is viable a detailed feasibility study was conducted, utilizing the Net Present Value (NPV) method. This technique takes into account the time value of money and is calculated using the sum of the differences between the present value of cash inflows and cash outflows that occur during the project's lifetime, Equation (6.1), [76]. If the NPV is a positive number or zero the investment is acceptable and if it's negative it's not. During this analysis, the annual savings due to the fuel consumption decrease and the battery costs were estimated by utilizing the projections of the prices of MGO and batteries mentioned earlier, Table 6.23.

$$NPV = \sum_{t=1}^{n} \frac{R_t}{(1+i)^t} \tag{6.1}$$

where

R_t is the net cash inflow-outflow during the period t ($)
i is the discount rate or return than could be earned in an alternative investment
n is the project's lifetime (years)

The discount rate used was found equal to 3.41% via the following formula and by considering a nominal discount rate of 6% and an inflation rate of 2.5% [77]:

$$i = \frac{i' - f}{1 + f} \tag{6.2}$$

The details of the feasibility study are illustrated in Table 6.24. Average savings of $53,050 are achieved via the HPS implementation, $27,420 due to the less required maintenance and $25,630 due to the lower fuel consumption. Nevertheless, the NPV is negative and thus, the project is not viable.

Table 6.20: The preliminary economic analysis for the simulations with SOC_{min} = 30%

No. of modules connected in-parallel	**30**	**50**	**100**	**150**	**200**	**300**	**400**
Energy (kWh)	461	768	1536	2304	3072	4608	6144
Per voyage							
Cycles	235	157	101	76	71	56	50
DGs total runtime decrease (h)	149.9	151.7	153.2	154.5	155.1	156.8	158.1
Fuel consumption decrease (t)	1.50	1.78	2.01	2.22	2.31	2.56	2.78
Maintenance savings ($)	1,499	1,517	1,532	1,545	1,551	1,568	1,581
Fuel consumption savings ($)	1,018	1,208	1,370	1,513	1,574	1,740	1,892
Total savings ($)	2,517	2,725	2,902	3,058	3,125	3,307	3,473
Per year							
Cycles	4300	2879	1854	1397	1299	1019	915
DGs total runtime decrease (h)	2742	2775	2803	2827	2839	2868	2893
Fuel consumption decrease (t)	27	33	37	41	42	47	51
Maintenance savings ($)	27,421	27,749	28,030	28,274	28,388	28,684	28,932
Fuel consumption savings ($)	18,634	22,105	25,064	27,681	28,794	31,835	34,618
Total savings ($)	46,055	49,854	53,094	55,954	57,182	60,520	63,549
Per lifetime							
Cycles	73099	48940	31521	23744	22085	17316	15553
DGs total runtime decrease (h)	46615	47174	47651	48066	48260	48763	49184
Fuel consumption decrease (t)	466	553	627	692	720	796	865
Maintenance savings ($)	466,149	471,738	476,510	480,657	482,602	487,631	491,842
Fuel consumption savings ($)	316,780	375,778	426,080	470,569	489,492	541,202	588,498
Total savings ($)	782,928	847,516	902,591	951,226	972,094	1,028,833	1,080,340
Battery Pack							
Required replacements	7.3	4.9	3.2	2.4	2.2	1.7	1.6
Required replacements (rounded)	8	5	4	3	3	2	2
Replacements interval (years)	2.1	3.4	4.3	5.7	5.7	8.5	8.5
Initial battery pack cost ($)	230,400	384,000	768,000	1,152,000	1,536,000	2,304,000	3,072,000
Total battery cost ($)	1,843,200	1,920,000	3,072,000	3,456,000	4,608,000	4,608,000	6,144,000
Savings - Cost ($)	-1,060,272	-1,072,484	-2,169,409	-2,504,774	-3,635,906	-3,579,167	-5,063,660

Table 6.21: The preliminary economic analysis for the simulations with SOC_{min} = 20%

No. of modules connected in-parallel	**30**	**50**	**100**	**150**	**200**	**300**	**400**
Energy (kWh)	461	768	1536	2304	3072	4608	6144
Per voyage							
Cycles	207	141	88	75	65	49	51
DGs total runtime decrease (h)	149.6	151.8	153.5	154.4	156.2	157.5	158.1
Fuel consumption decrease (t)	1.47	1.80	2.07	2.21	2.49	2.67	2.78
Maintenance savings ($)	1,496	1,518	1,535	1,544	1,562	1,575	1,581
Fuel consumption savings ($)	997	1,221	1,408	1,501	1,694	1,817	1,891
Total savings ($)	2,494	2,739	2,943	3,045	3,257	3,391	3,472
Per year							
Cycles	3788	2580	1616	1366	1183	890	927
DGs total runtime decrease (h)	2738	2777	2809	2825	2859	2881	2893
Fuel consumption decrease (t)	27	33	38	40	46	49	51
Maintenance savings ($)	27,382	27,772	28,092	28,251	28,590	28,812	28,932
Fuel consumption savings ($)	18,246	22,347	25,767	27,462	31,000	33,242	34,593
Total savings ($)	45,628	50,119	53,859	55,713	59,590	62,054	63,525
Per lifetime							
Cycles	64390	43860	27477	23226	20115	15138	15760
DGs total runtime decrease (h)	46550	47213	47757	48026	48603	48980	49185
Fuel consumption decrease (t)	456	559	644	687	775	831	865
Maintenance savings ($)	465,498	472,126	477,568	480,262	486,027	489,799	491,847
Fuel consumption savings ($)	310,184	379,900	438,035	466,859	527,005	565,111	588,085
Total savings ($)	775,682	852,026	915,603	947,121	1,013,033	1,054,911	1,079,932
Battery Pack							
Required replacements	16.1	11.0	6.9	5.8	5.0	3.8	3.9
Required replacements (rounded)	17	11	7	6	6	4	4
Replacements interval (years)	1.0	1.5	2.4	2.8	2.8	4.3	4.3
Initial battery pack cost ($)	230,400	384,000	768,000	1,152,000	1,536,000	2,304,000	3,072,000
Total battery cost ($)	3,916,800	4,224,000	5,376,000	6,912,000	9,216,000	9,216,000	12,288,000
Savings - Cost ($)	-3,141,118	-3,371,974	-4,460,397	-5,964,879	-8,202,967	-8,161,089	-11,208,068

Table 6.22: The differences between the simulations with SOC_{min} = 30% and those with SOC_{min} = 20%

No. of modules connected in-parallel	**30**	**50**	**100**	**150**	**200**	**300**	**400**
DGs total runtime decrease	0.04%	-0.02%	-0.07%	0.02%	-0.21%	-0.13%	0.00%
Fuel consumption decrease	0.05%	-0.03%	-0.10%	0.03%	-0.30%	-0.19%	0.00%
Cycles	-11.91%	-10.38%	-12.83%	-2.18%	-8.92%	-12.57%	1.33%
Savings per lifetime (30% - 20%)							
Maintenance savings ($)	651	-388	-1,058	395	-3,425	-2,169	-5
Fuel consumption savings ($)	6,596	-4,122	-11,955	3,710	-37,513	-23,910	412
Total savings ($)	7,246	-4,510	-13,012	4,106	-40,939	-26,078	407
Required replacements (30%)	8	5	4	3	3	2	2
Required replacements (20%)	17	11	7	6	6	4	4

Table 6.23: The projections of the MGO and battery prices

Year	**Battery cost ($/kWh)**	**MGO price ($/t)**
2020	500	680
2021	490	712
2022	480	744
2023	470	776
2024	460	808
2025	450	840
2026	440	872
2027	430	904
2028	420	936
2029	410	968
2030	400	1000
2031	390	1032
2032	380	1064
2033	370	1096
2034	360	1128
2035	350	1160
2036	340	1192

Table 6.24: The Net Present Value method for the battery pack with $n_{parallel}$ = 30 and SOC_{min} = 30%

Year	Voyages	Cycles	DGs runtime decrease (h)	Fuel consumption decrease (t)	Maintenance savings ($)	Fuel savings ($)	Total savings ($)	Battery cost ($)	Net cash flow ($)	Present value ($)
2020	18.64	4381	2793.4	27.92	27,934	18,983	46,917	230,400	-183,483	-177,424
2021	17.92	4211	2685.2	26.84	26,852	19,107	45,959		45,959	42,974
2022	18.61	4374	2789.6	27.88	27,896	20,741	48,637	221,184	-172,547	-156,014
2023	18.61	4374	2789.6	27.88	27,896	21,633	49,529		49,529	43,304
2024	18.56	4362	2781.8	27.80	27,818	22,463	50,281	211,968	-161,687	-136,699
2025	18.61	4374	2789.6	27.88	27,896	23,417	51,313		51,313	41,950
2026	17.74	4168	2658.2	26.56	26,582	23,165	49,747	202,752	-153,005	-120,958
2027	18.59	4368	2785.7	27.84	27,857	25,167	53,023		53,023	40,533
2028	18.59	4368	2785.7	27.84	27,857	26,057	53,914		53,914	39,853
2029	17.56	4126	2631.1	26.29	26,311	25,453	51,765	188,928	-137,163	-98,043
2030	18.59	4368	2785.7	27.84	27,857	27,839	55,696		55,696	38,497
2031	17.45	4102	2615.7	26.14	26,157	26,977	53,134	179,712	-126,578	-84,601
2032	18.56	4362	2781.8	27.80	27,818	29,580	57,398		57,398	37,096
2033	18.56	4362	2781.8	27.80	27,818	30,469	58,288	170,496	-112,208	-70,126
2034	17.33	4072	2596.4	25.95	25,964	29,268	55,232		55,232	33,378
2035	18.56	4362	2781.8	27.80	27,818	32,249	60,067		60,067	35,101
2036	18.56	4362	2781.8	27.80	27,818	33,138	60,957	156,672	-95,715	-54,086
									NPV	-545,263

6.4 Utilizing another battery module

The reason why the proposed hybrid solution turned out to be economically unviable is that the installed battery pack needs frequent replacement, due to its limited cycle life. As mentioned in Chapter 4, the battery module selection process was limited by the availability of the modules' discharge curves. These curves are essential for the modeling of the battery pack and the realistic representation of the dynamic behavior of the battery was one of the main objectives of this study. The most popular manufactures of batteries destined for marine applications, like Corvus Energy and SPBES, don't provide these curves and as a consequence, their modules couldn't be utilized.

Without the above-mentioned limitation, the SPBES Titanate 35 module could have been the one implemented in the HPS. This module is quite similar to the Valence U-Charge® U27-36XP module that was selected but offers a much longer cycle life. More specifically, the Titanate 35 module has a 22.5 times longer cycle life than the one selected. A comparison between the two modules is presented in Table 6.25.

Table 6.25: A comparison between the Valence U-Charge® U27-36XP and the SPBES Titanate 35 module

	Valence U-Charge® U27-36XP	**SPBES Titanate 35**
Voltage (nominal)	38.4 V	54 V
Capacity (typical)	50 Ah	70 Ah
Energy	1.92 kWh	3.5 kWh
Max. C-rate (Continuous)	2C	4C
Voltage range	30 - 41 V	44 - 64 V
Specific Energy	102 Wh/kg	39 Wh/kg
Energy Density	162 Wh/l	50 Wh/l
Charge Efficiency	> 90%	> 99%
Cycle Life (@80% DOD)	> 4000 cycles	90000 cycles
Self Discharge	< 2% per month	< 2% per month
Height	225 mm	380 mm
Width	172 mm	320 mm
Length	306 mm	580 mm
Weight	18.7 kg	90 kg
IP Rating	IP56	IP67

It can be noticed that, apart from the longer cycle life, the Titanate 35 module provides the double maximum C-rate, much higher charge efficiency and better protection against the intrusion of solid objects and water. On the other hand, its energy density is 3.3 times lower and its specific energy is 2.6 times lower than the U27-36XP module. That results in a larger and heavier battery pack.

Due to the differences in the specifications of the two modules and in order to compare the two battery packs that they form, the two packs need to have similar voltage, capacity and energy levels. Since that in the battery configuration employing the U27-36XP module the nominal voltage is 307.2 V – achieve by connecting 8 modules in-series – this value needs to be achieved approximately in the case of the Titanate 35 module, too. For that to happen, 6 modules were connected in-series, resulting in a nominal battery pack voltage of 324 V. Regarding the capacity and energy of the SPBES pack, the number of parallel-connected modules was estimated in a similar way, Table 6.26. In

this table, the "aimed" capacity and energy is shown, that of the U27-36XP pack. The $n_{parallel,C}$ and the $n_{parallel,E}$ are the number of parallel-connected Titanate 35 modules that are required to reach the capacity and energy, respectively, of the U27-36XP battery pack. Due to rounding of the $n_{parallel,C}$ and $n_{parallel,E}$ values the "achieved" SPBES pack capacity and energy slightly differ from those of the U27-36XP pack.

Table 6.26: The estimation of the corresponding $n_{parallel}$ values for the SPBES battery pack

U27-36XP Capacity (Ah)	$n_{parallel,C}$	Titanate 35 Capacity (Ah)	U27-36XP Energy (kWh)	$n_{parallel,E}$	Titanate 35 Energy (kWh)
1500	22	1540	461	21	476
2500	36	2520	768	34	771
5000	72	5040	1536	68	1542
7500	108	7560	2304	102	2313
10000	143	10010	3072	136	3084
15000	215	15050	4608	204	4627
20000	286	20020	6144	271	6146

Since the capacity of the pack is used in the battery model that was utilized, the number of parallel-connected modules for the SPBES pack was taken equal to $n_{parallel,C}$ and the energy of the pack was calculated using these values, Table 6.27. As expected, due to the higher capacity of the Titanate 35 module fewer modules are required compared with the U27-36XP, to reach the same pack capacity. Also, the weight and volume of the SPBES pack are much higher, but even the largest configuration with the 286 parallel-connected modules can probably be placed in the location of the replaced diesel generator, Table 6.28. Alternatively, it can be located in the deck, utilizing the containerized solution that SPBES offers.

Table 6.27: The number of parallel-connected modules, the capacity and the energy of the SPBES battery pack

$n_{parallel}$	Capacity (Ah)	Energy (kWh)
22	1540	499
36	2520	816
72	5040	1633
108	7560	2449
143	10010	3243
215	15050	4876
286	20020	6486

Table 6.28: The weight and volume of the SPBES pack depending on $n_{parallel}$

$n_{parallel}$	22	36	72	108	143	215	286
Weight (t)	2.52	3.78	7.02	10.26	13.41	19.89	26.28
Volume (m3)	2.0	3.0	5.5	8.0	10.5	15.6	20.6

The above calculations result in a battery pack composed of SPBES Titanate 35 modules, that has similar voltage, capacity and energy characteristics with the studied U27-36XP pack. In order to examine the economic feasibility of an HPS that employs the SPBES

pack, its behavior was supposed to be the same as the behavior of the U27-36XP pack. The fuel savings, the decrease in the operating hours of the gensets and the cycles found during the simulations of the HPS utilizing the U27-36XP pack, were considered to be the same for the corresponding capacity sizes. In fact, due to the much higher efficiency of the Titanate 35 module, an HPS utilizing this module would demonstrate even greater reductions.

Since the cycle life of the Titanate 35 module at 80% DOD is 22.5 times greater than the U27-36XP's and no cycle life value is provided for the 70% DOD, it was supposed to be 22.5 times greater the cycle life of the U27-36XP at the corresponding DOD value, i.e. 225000 cycles. The total cycles throughout the lifetime of the vessel were calculated using Table 6.24 and found equal to 73099, meaning there is no need for replacement when the Titanate 35 module is utilized. The details of the feasibility study conducted for the SPBES pack, when the 30 modules are connected in-parallel and when SOC_{min} = 30% are illustrated in Table 6.29. This time there is only one purchase of a battery pack and the proposed hybrid solution is an attractive investment, as the NPV is equal to $444,463. The replacement of the No. 2 diesel generator with the SPBES battery pack would provide savings equal to $53,050/year on average for 17 years, while the only cost during that period would be the initial purchase of the battery pack, which costs $230,400. As a result, the payback period of the investment is 4.3 years.

Table 6.29: The Net Present Value method for the SPBES battery pack, when $n_{parallel}$ = 30 and SOC_{min} = 30%

Year	Voyages	Cycles	DGs runtime decrease (h)	Fuel consumption decrease (t)	Maintenance savings ($)	Fuel savings ($)	Total savings ($)	Battery cost ($)	Net cash flow ($)	Present value ($)
2020	18.64	4381	2793.4	27.92	27,934	18,983	46,917	230,400	-183,483	-177,424
2021	17.92	4211	2685.2	26.84	26,852	19,107	45,959		45,959	42,974
2022	18.61	4374	2789.6	27.88	27,896	20,741	48,637		48,637	43,976
2023	18.61	4374	2789.6	27.88	27,896	21,633	49,529		49,529	43,304
2024	18.56	4362	2781.8	27.80	27,818	22,463	50,281		50,281	42,510
2025	18.61	4374	2789.6	27.88	27,896	23,417	51,313		51,313	41,950
2026	17.74	4168	2658.2	26.56	26,582	23,165	49,747		49,747	39,327
2027	18.59	4368	2785.7	27.84	27,857	25,167	53,023		53,023	40,533
2028	18.59	4368	2785.7	27.84	27,857	26,057	53,914		53,914	39,853
2029	17.56	4126	2631.1	26.29	26,311	25,453	51,765		51,765	37,001
2030	18.59	4368	2785.7	27.84	27,857	27,839	55,696		55,696	38,497
2031	17.45	4102	2615.7	26.14	26,157	26,977	53,134		53,134	35,513
2032	18.56	4362	2781.8	27.80	27,818	29,580	57,398		57,398	37,096
2033	18.56	4362	2781.8	27.80	27,818	30,469	58,288		58,288	36,427
2034	17.33	4072	2596.4	25.95	25,964	29,268	55,232		55,232	33,378
2035	18.56	4362	2781.8	27.80	27,818	32,249	60,067		60,067	35,101
2036	18.56	4362	2781.8	27.80	27,818	33,138	60,957		60,957	34,445
									NPV	444,463

6.5 Battery operation during port stay

Hybrid power systems often offer the significant advantage of zero-emission operation during port stay, utilizing power sources like batteries and fuel cells. Apart from the elimination of harmful substances close to residential areas, noise pollution reduction and lower port fees are also achieved. To examine the battery operation potential for this particular case, the energy consumed during the port stays of the Voyages A, B and C were estimated, Table 6.30. It was found that, in order to shut down completely the diesel generators during a port stay and cover the load demand exclusively by discharging the battery, a huge battery pack would be required. As shown earlier that would result in a very expensive and not viable solution.

Table 6.30: The energy consumed during the port stays of the studied voyages

	Voyage A		**Voyage B**		**Voyage C**	
	Port A1	**Port A2**	**Port B1**	**Port B2**	**Port C1**	**Port C2**
Energy (kWh)	12,950	23,347	23,347	41,198	29,097	55,380
Days	1.29	1.42	1.42	3.61	1.77	4.63
Energy/day (kWh/d)	10,068	16,482	16,482	11,399	16,443	11,964

7 Conclusions & Future Work

In this study, the concept of replacing one of the three diesel generators installed on board a 171,000 DWT bulk carrier with a lithium-ion battery pack was investigated. Li-ion technologies prevail in industrial applications and they are the most common choice for marine hybrid systems, due to their high energy and power density characteristics.

The dynamic behavior of the battery was represented using an equivalent circuit model and a battery module was selected, for which the discharge curves were available. These curves were essential for the realistic modeling of the battery and their availability was a limitation during the module selection process. Furthermore, an Energy Management System (EMS) was developed to control the parts of the hybrid arrangement. The basic principles of the EMS were the operation of the two remaining gensets exclusively in their optimum loading condition and as evenly as possible and the confinement of the battery operation between a SOC_{min} and a SOC_{max} value, to extend its lifetime. The optimum loading condition was found to be at 80% of the MCR and the No. 2 generator exhibited higher consumption at this point, thus it was the one that gave its place to the battery.

An examination of the performance of the proposed hybrid power system was conducted via 42 simulations, utilizing power output measurements of the three originally installed diesel generators. Seven battery pack configurations were studied, with the parallel-connected modules ranging from 30 to 400 and the pack's energy from 461 kWh to 6144 kWh. Also, two SOC_{min} values were tested, namely 20% and 30%, in simulations of three 20-day voyages, to obtain a more comprehensive overview of the system's behavior and to estimate average values.

The hybrid system was compared with the original power plant in terms of fuel burnt, emissions and run time of the diesel generators and displayed significant reductions in these parameters. More specifically, the fuel consumption and emissions decrease were between 1.63% and 5.91% and the operating hours of the gensets exhibited a drop between 24.68% and 33.91%, depending on the size of the battery. The simulations of the 461 kWh battery pack resulted in reductions similar to those of another study, which was undertaken jointly by MAN, DNV GL and Corvus Energy and researched the implementation of a 500 kWh pack in a container feeder's electricity generation system. Moreover, it was found that by upsizing the battery pack the decrease percentages were increased almost linearly, while by applying a lower SOC_{min} value, an 8.49% reduction on average in the battery cycles per voyage and a slightly better fuel efficiency were achieved.

At the end of this work, a feasibility study was conducted, specifying the exact amounts of savings and costs of the proposed hybrid system, throughout the remaining life of the bulk carrier. Taking into consideration the projected fuel and battery prices and the annual downtime of the vessel, several conclusions were made. Firstly, annual savings of $53,050 were achieved, due to the less required maintenance and lower fuel consumption. Secondly, the limited cycle life of the selected battery module resulted in frequent replacements of the pack, especially when the SOC_{min} was equal to 20%, making the investment not viable. For this reason, a battery module that has longer cycle life – but its discharge curves weren't available – was considered, resulting in an NPV equal to $444,463. Lastly, it was found that the smaller the size of the battery is the more appealing the hybrid solution becomes; both the savings and the battery cost are increasing as the battery size rises, though the latter increases with a higher rate.

Regarding topics of future research, the employment of a battery model that takes into account the aging of the battery and the Peurkert effect would be an idea worth investigating. Also, the development of a different EMS, the utilization of shore supply for charging the battery during port stays and a comparison between the results of the current study and a similar one that uses direct current instead of AC are interesting topics.

References

[1] International Maritime Organization, Third IMO Greenhouse Gas Study 2014, 2014.

[2] Concawe, Marine Fuel Facts, 2017.

[3] The International Council on Combustion Engines, Guide to Diesel Exhaust Emissions Control of NOx, SOx, Particulates, Smoke and CO2, 2008.

[4] International Maritime Organization, Energy Efficiency Measures. [Online]. Available: www.imo.org.

[5] H. O. Kristensen, Energy Demand And Exhaust Gas Emissions of Marine Engines, 2015.

[6] International Maritime Organization, Nitrogen oxides (NOx) – Regulation 13. [Online]. Available: www.imo.org.

[7] Wärtsilä Encyclopedia of Ship Technology, Selective Catalytic Reduction (SCR).

[8] M. Agarwal, Understanding Various Components of Exhaust Gas Emissions from Ships, 2019. [Online]. Available: www.marineinsight.com.

[9] J. J. Corbett and H. W. Koehler, Updated emissions from ocean shipping, *J. Geophys. Res.*, vol. 108, no. D20, 2003, doi: 10.1029/2003jd003751.

[10] S. Song, Ship emissions inventory, social cost and eco-efficiency in Shanghai Yangshan port, *Atmos. Environ.*, vol. 82, no. x, pp. 288–297, 2014, doi: 10.1016/j.atmosenv.2013.10.006.

[11] Entac Defra UK Ship Emissions Inventory, 2010.

[12] R. D. Geertsma, R. R. Negenborn, K. Visser, and J. J. Hopman, Design and control of hybrid power and propulsion systems for smart ships: A review of developments, *Appl. Energy*, vol. 194, pp. 30–54, 2017, doi: 10.1016/j.apenergy.2017.02.060.

[13] MAN Energy Solutions, Batteries on board ocean-going vessels, 2019.

[14] ABB Energy Storage Solutions, EssPro™ energy storage Power Conversion System (PCS) - The power to control energy brochure, 2017.

[15] S&P Global Platts, Specifications guide global bunker fuels, 2019.

[16] A. K. Ådnanes, Maritime electrical installations and diesel electric propulsion, *ABB AS Mar.*, 2003.

[17] D. Linden, *Linden's Handbook of Batteries*, Fourth. McGraw-Hill, 2011.

[18] M. R. Jongerden and B. R. Haverkort, Battery modeling, *Electrochem. Soc. Interface*, vol. 14, no. 4, pp. 39–42, 2005, doi: 10.1002/9781118970553.ch12.

[19] MIT Electric Vehicle Team, A Guide to Understanding Battery Specifications, *Current*, no. December, pp. 1–3, 2008.

[20] C. Bloch, J. Newcomb, S. Shiledar, and M. Tyson, Breakthrough Batteries: Powering the Era of Clean Electrification.

[21] M. Kalikatzarakis, R. D. Geertsma, E. J. Boonen, K. Visser, and R. R. Negenborn, Ship energy management for hybrid propulsion and power supply with shore charging, *Control Eng. Pract.*, vol. 76, no. November 2017, pp. 133–154, 2018, doi: 10.1016/j.conengprac.2018.04.009.

[22] C. Capasso and O. Veneri, Experimental analysis on the performance of lithium-based batteries for road full electric and hybrid vehicles, *Appl. Energy*, vol. 136, pp. 921–930, 2014, doi: 10.1016/j.apenergy.2014.04.013.

[23] Wärtsilä Marine Solutions, Hybrid propulsion is part of the future for RoPax ferries, pp. 1–10.

[24] N. Mjøs *et al.*, DNV GL Handbook for Maritime and Offshore Battery Systems, 2016.

[25] M. D. A. Al-Falahi, K. S. Nimma, S. D. G. Jayasinghe, H. Enshaei, and J. M. Guerrero, Power management optimization of hybrid power systems in electric ferries, *Energy Convers. Manag.*, vol. 172, no. June, pp. 50–66, 2018, doi: 10.1016/j.enconman.2018.07.012.

[26] Y. Yuan, J. Wang, X. Yan, Q. Li, and T. Long, A design and experimental investigation of a large-scale solar energy/diesel generator powered hybrid ship, *Energy*, vol. 165, pp. 965–978, 2018, doi: 10.1016/j.energy.2018.09.085.
[27] H. Lan, S. Wen, Y. Y. Hong, D. C. Yu, and L. Zhang, Optimal sizing of hybrid PV/diesel/battery in ship power system, *Appl. Energy*, vol. 158, pp. 26–34, 2015, doi: 10.1016/j.apenergy.2015.08.031.
[28] DNV GL, In Focus - The Future is Hybrid, 2015.
[29] G. Brown, Practical application of energy storage in hybrid commercial vessels, *J. Ocean Technol.*, vol. 13, no. 2, pp. 15–25, 2018.
[30] BU-205: Types of Lithium-ion. [Online]. Available: www.batteryuniversity.com.
[31] DNV GL, Technology Outlook 2030, 2019.
[32] Generic battery model. [Online]. Available: www.mathworks.com.
[33] MathWorks, Developing Battery Management Systems with Simulink and Model-Based Design, 2018.
[34] DNV GL, Rules for Classification of Ships, Part 6, Chapter 2, Section 1 Battery power.
[35] DNV GL, Rules for Classification of Ships, Part 1, Chapter 1, Section 1 General regulations.
[36] DNV GL, Rules for Classification of Ships, Part 4, Chapter 1 Machinery systems, general.
[37] D. R. Baker, Battery reality: There's nothing better than Lithium-Ion coming soon, 2019. [Online]. Available: www.bloomberg.com.
[38] I. Penn, How Zinc Batteries Could Change Energy Storage, 2018. [Online]. Available: www.nytimes.com.
[39] S. Boukhalfa and N. Kaul, 10 disruptive battery technologies trying to compete with lithium-ion batteries, 2019. [Online]. Available: www.solarpowerworldonline.com.
[40] N. Kobie, What is a solid-state battery and why is James Dyson so excited about it?, 2018. [Online]. Available: www.alphr.com.
[41] J. Temple, Why lithium-ion may rule batteries for a long time to come, 2018. [Online]. Available: www.technologyreview.com.
[42] R. Soat, Is 2020 the Year of Solid-State Batteries for EVs?, 2019. [Online]. Available: https://www.navigantresearch.com/.
[43] P. Bernard, Three battery technologies that could power the future, 2018. [Online]. Available: www.saftbatteries.com.
[44] L. Goldie-Scot, A Behind the Scenes Take on Lithium-ion Battery Prices, 2019. [Online]. Available: www.bnef.com.
[45] J. Leone, Lithium vs. Lithium-Ion Batteries, 2018. [Online]. Available: www.sciencing.com.
[46] Y. He *et al.*, Origin of lithium whisker formation and growth under stress, *Nat. Nanotechnol.*, vol. 14, no. October 2019, pp. 1042–1047, 2019.
[47] M. Shaibani, Batteries made with sulfur could be cheaper, greener and hold more energy, 2020. [Online]. Available: www.theconversation.com.
[48] R. F. Service, New generation of "flow batteries" could eventually sustain a grid powered by the sun and wind, *Science*, 2018.
[49] S. Davis, New Energy Storage Battery Technology Answers the Need for Li-Ion Replacement, 2018. [Online]. Available: www.powerelectronics.com.
[50] J. Daggett, Can Flow Batteries compete with Li-ion?, 2019. [Online]. Available: www.dnvgl.com.
[51] T. Connor, Gates, Bezos bet on flow battery technology, a potential rival to big bets on lithium-ion, 2019. [Online]. Available: www.cnbc.com.
[52] E. Wesoff, Battery roundup: funding for zinc-based storage, improved lithium-ion, new solid-state batteries, 2020. [Online]. Available: www.pv-magazine-usa.com.
[53] Technology Review, Zinc-Air Batteries, *MIT Technology Review*, 2001.

[54] V. Palomares, P. Serras, I. Villaluenga, K. B. Hueso, J. Carretero-González, and T. Rojo, Na-ion batteries, recent advances and present challenges to become low-cost energy storage systems, *Energy Environ. Sci.*, vol. 5, no. 3, pp. 5884–5901, 2012, doi: 10.1039/c2ee02781j.
[55] R. F. Service, Sodium batteries are one step closer to saving you from a mobile phone fire, *Science*, 2019.
[56] S. Hanley, Sodium-Ion Battery Research Shows Promising Results, 2019. [Online]. Available: www.cleantechnica.com.
[57] DNV GL, Alternative Fuels Insight. [Online]. Available: www.afi.dnvgl.com.
[58] I. Filks, Batteries included: Sweden's emissions-free ferries lead the charge, 2019. [Online]. Available: www.reuters.com.
[59] The maritime executive, ForSea Converts World's Largest Battery Ferries, Powered by ABB, 2018. [Online]. Available: www.maritime-executive.com.
[60] M. Louagie, Color Hybrid, the world's largest plug-in hybrid ferry, built by Ulstein Verft, 2019. [Online]. Available: www.ferryshippingnews.com.
[61] M. Schuler, Viking Lady Going Full Hybrid as FellowSHIP Fuel Cell Project Enters Phase III, 2012. [Online]. Available: www.gcaptain.com.
[62] Viking Lady - Safe as well as green, 2014. [Online]. Available: www.motorship.com.
[63] R. Orange, Princess Hybrid, 2020. [Online]. Available: www.wartsila.com.
[64] G. Lipsith, Batteries included – has the time come for hybrid tankers ?, 2019. [Online]. Available: www.rivieramm.com.
[65] Corvus Energy wins contract to supply energy storage for first hybrid chemical tanker, 2017. [Online]. Available: www.corvusenergy.com.
[66] AMPERE The world's first all-electric car ferry. [Online]. Available: www.corvusenergy.com.
[67] N. Mikkola, L. Randall, and A. Hagberg, *Green Growth in Nordic Regions*. 2016.
[68] Elektra Hybrid Electric Ferry. [Online]. Available: www.spbes.com.
[69] O. Tremblay, L. A. Dessaint, and A. I. Dekkiche, A generic battery model for the dynamic simulation of hybrid electric vehicles, *VPPC 2007 - Proc. 2007 IEEE Veh. Power Propuls. Conf.*, no. V, pp. 284–289, 2007, doi: 10.1109/VPPC.2007.4544139.
[70] aimtec, Connecting AC-DC and DC-DC Power Converters in Parallel, 2012.
[71] J. Hou, J. Sun, and H. Hofmann, Control development and performance evaluation for battery/flywheel hybrid energy storage solutions to mitigate load fluctuations in all-electric ship propulsion systems, *Appl. Energy*, vol. 212, no. October 2017, pp. 919–930, 2018, doi: 10.1016/j.apenergy.2017.12.098.
[72] HYUNDAI-HiMSEN, Marine & Offshore GenSets.
[73] MAN Energy Solutions, DNV GL, and C. Energy, HYCAS: Joint study to explore new cost-effective applications of hybrid power generation on larger ocean-going cargo ships, 2019.
[74] Global 20 Ports Average. [Online]. Available: www.shipandbunker.com.
[75] International Association of Classification Societies (IACS), Requirements concerning Survey and Certification, 2017.
[76] W. Kenton, Net Present Value (NPV), 2019. [Online]. Available: www.investopedia.com.
[77] O. Jan, NPV and Inflation, 2019. [Online]. Available: www.xplaind.com.